6-23-2015

Communication-Theoretic Foundations for Optical Receivers Using Dynamically Biased Avalanche Photodiodes

Georges El-Howayek

Georges El-Howayek

Candidate

Electrical and Computer Engineering

Department

This dissertation is approved, and it is acceptable in quality and form for publication:

Approved by the Dissertation Committee:

Dr. Majeed M Hayat , Chairperson

Dr. Sanjay Krishna

Dr. Balu Santhanam

Dr. Payman Zarkesh-Ha

Dr. Guoyi Zhang

Communication-Theoretic Foundations for Optical Receivers Using Dynamically Biased Avalanche Photodiodes

by

Georges El-Howayek

M.S., Electrical Engineering, University of New Mexico, 2010
B.E., Electrical Engineering, Lebanese American University, 2008

DISSERTATION

Doctor of Philosophy
Engineering

The University of New Mexico

Albuquerque, New Mexico

May, 2015

Submitted by: Georges El-Howayek

Supervisor: Dr. Majeed M Hayat
Department of Electrical and Computer Engineering
University of New Mexico

Committee Members: Dr. Sanjay Krishna
Department of Electrical and Computer Engineering
University of New Mexico

Dr. Balu Santhanam
Department of Electrical and Computer Engineering
University of New Mexico

Dr. Payman Zarkesh-Ha
Department of Electrical and Computer Engineering
University of New Mexico

Dr. Guoyi Zhang
Department of Mathematics and Statistics
University of New Mexico

Dedication

To my wife, my beloved parents, and my wonderful siblings.

"The greatest enemy of knowledge is not ignorance, it is the illusion of knowledge"
– Daniel J. Boorstin

Acknowledgments

This work is the result of invaluable support and guidance of many, some of whom are acknowledged below. First, I would like to express my greatest gratitude to my advisor Professor Majeed M. Hayat for his valuable support, kindness and encouragement over the past years at UNM. His valuable advice, guidance and assistance were essential in achieving this work and helping me to develop my research career. Working with Professor Hayat has been a great learning experience for me. I would also like to thank my committee members Dr. Sanjay Krishna, Dr. Balu Santhanam, Dr. Payman Zarkesh-Ha and Dr. Guoyi Zhang for their valuable suggestions and help. I am very thankful for them serving as my committee members. I would like to also thank all the members of our research groups, in particular Dr. Daivd Ramirez, for their collaboration and the time we spent together throughout our journey at UNM.

I would also like to express my gratitude to my professors from my undergraduate university, the Lebanese American University (LAU), especially Professor Chadi Abou-Rjeily and Professor Samer S. Saab who have been very encouraging and supportive to pursue my graduate studies.

Last, but not least, I would like to thank my beloved wife Julie-May, my parents Rouphaiel and Therese, my siblings, Alain and Krystel and my entire family for their love, sacrifice and infinite support. I want also to thank all my friends who have been a great support for me during my stay in Albuquerque.

This work has been supported by Prof. Majeed M. Hayat's projects supported in part by the Science and Technology Corporation (STC.UNM) GAP Funding and in part by the National Science Foundation under the Smart Lighting ERC.

Communication-Theoretic Foundations for Optical Receivers Using Dynamically Biased Avalanche Photodiodes

by

Georges El-Howayek

M.S., Electrical Engineering, University of New Mexico, 2010
B.E., Electrical Engineering, Lebanese American University, 2008

Ph.D., Engineering, University of New Mexico, 2015

Abstract

To meet the demands of the exponential growth in video, voice, data and mobile device traffic over the internet, the telecommunication industry has been moving toward higher speed protocols such as 40-Gb/s and 100-Gb/s [1]. Operations at such high speeds require detectors with optimized internal gain (leading to high sensitivity) to reduce cost [2]. Avalanche photodiodes (APDs) are commonly used photodetectors in many high-speed optical receivers due to their internal optoelectronic gain, which allows the photogenerated current to dominate the thermal noise without the need for optical pre-amplification of the received optical signal. However, the long avalanche buildup time associated with APDs, namely the time needed for all the impact ionizations to settle, has limited their speed and stopped them from meeting the expectations of 40-Gb/s systems. A new approach was proposed recently for operating APDs employing bit-synchronous and periodic dynamic biasing that is expected to reduce the buildup time dramatically [3].

In this dissertation, we present an extensive theoretical modeling and analysis for the novel approach of dynamically biased APD. We develop the first theory for the joint buildup-time and gain statistics for avalanche multiplication under dynamic electric fields. We also develop a theory for filtered shot noise under dynamic biasing, which addresses rigorously the statistic of the dynamically biased APD photocurrent, such as the mean, variance, autocorrelation function, etc. This is used, in turn, to derive analytical expressions for the statistics of the output of the integrate-and-dump optical receiver output. The study is characterized by its ability to predict the performance of a dynamically biased APD-based receiver and to optimize the system parameters to achieve an optimal receiver performance. The exact expressions for the receiver bit-error rate and sensitivity in an on-off keying setting will be extracted using the photocurrent statistics. The sensitivity analysis of the dynamically biased APD-based receiver will specifically capture intersymbol interference (ISI) and dark current, as well as Johnson noise from the trans-impedance amplifier used in the pre-amplification stage of receivers. The results show that operating the APD under dynamic biasing improves the receiver performance beyond its traditional limits operating under static biasing.

Publications

In the following, we present a list of journal and conference publications that have resulted from the work in this dissertation.

Patents

"Method for sensitivity optimization of optical receivers using avalanche photodiodes operating under a dynamic reverse bias" (with M. M. Hayat, P. Zarkesh-Ha, and G. El-Howayek) United States Patent No. 1863.139PRV

Journal Publications

1. G. El-Howayek and M. M. Hayat, "Optimization of InP APDs for dynamically biased avalanche photodiodes," 2015. [In preparation]

2. G. El-Howayek and M. M. Hayat, "Error probabilities for optical receivers that employ dynamically biased avalanche photodiodes," *IEEE Transactions on Communications,* Dec. 2014. [In review]

3. G. El-Howayek, C. Zhang, Y. Li, J. S. Ng, J. P. R. David and M. M. Hayat, "On the use of gaussian approximation in analyzing the performance of optical

receivers," *IEEE Photonics Journal*, vol.6, no.1, pp.1-8, Feb. 2014.

Conference Publications

1. M. M. Hayat, P. Zarkesh-Ha, X. Zheng, G. El-Howayek and R. Efroymson, "First demonstration of dynamically biased APDs for improved high-speed direct-detection communication, in *Optical Fiber Communication Conference and Exhibit*, Los Angeles, CA, March 2015.

2. G. El-Howayek and M. M. Hayat, "Method for Performance Analysis and Optimization of APD Optical Receivers Operating Under Dynamic Reverse Bias," *IEEE Photonics Conference (IPC 2013)*, Bellevue, WA, Sep. 2013.

Contents

List of Figures

List of Tables

Glossary

APD	Avalanche photodiode
BER	Bit Error Rate
CDF	cumulitive distribution function
DSMT	Dead-Space-Multiplication Theory
EDFA	Erbium Doped Fiber Amplifier
GBP	Gain-Bandwidth Product
Ge	Germanium
InP	Indium-Phosphide
ISI	Intersymbol Interference
MGF	Moment Generating Function
NRZ	Non-Return-to-zero
OC	Optical Carrier
OOK	On-Off-Keying
PD	Bit-Pattern–Dependent

PDF	Probability Destribution Function
PMF	Probability Mass Function
PI	Bit-Pattern–Independent
RD	Random Duration
RD-R	Rectangular Random-Duration
SNR	Signal to Noise Ratio
SONET	Synchronous Optical Network
TIA	Trans-Impedance Amplifier
SAM	Separate Absorption and Multiplication
Si	Silicon

Chapter 1

Introduction

1.1 Overview and motivation

The exponential growth of the Internet use has increased the demand for highly sensitive optical detectors for high-bit-rate optical fiber communication systems [1]. The Synchronous Optical Network (SONET) standards, optical carrier (OC) level 48 and OC-192, specify the data rates in optical networks as 2.5Gb/s [9] and 10Gb/s [10] respectively, but these are increasing to 40Gb/s and 100Gb/s, such as OC-768. The intrinsic InGaAs pin photodetectors have been used extensively in optical communications due to their good electron transport properties and their ability to absorb radiation in $1.0 - 1.7$ μm wavelength region efficiently [11]. Several proposed structures for pin diodes meet with the requirements of the OC-192 [12, 13] and OC-768 [14,15] standards. The PIN diodes have been the perfected choice for most optical communication. Presently, the only viable option for direct detection of 40-G/s bit streams is InGaAs PIN photodiodes since very high bandwidths can be achieved with them [16]. However, PIN photodiodes have low sensitivity since can they generate only one electron-hole pair per incident photon. Therefore, a pre-amplifier is needed

for low power level detection. Erbium doped fiber amplifiers (EDFAs) are used to pre-amplify the signals optically before their detection by the PIN photodiode [17]. The resulting EDFA-PIN receiver can exhibit very high sensitivity, due to EDFA's high optical gain and low noise, as well as high speed, which is due to the high bandwidth of the PIN photodiode. However, these receivers can be bulky and expensive. An EDFA requires the use of meters of fiber (coiled in a fairly sizeable disk), and more importantly, it requires the use of a pump laser, which provides the optical amplification. The EDFA-PIN approach is expensive [18, 19].

This limitation can be overcome by using avalanche photodiodes (APDs), in which each detected photon is converted into a cascade moving carrier pairs. This will offer an internal gain that improves the receivers' sensitivity as it amplifies the photocurrent without the need for optical pre-amplification of the received optical signal. It is well known that the internal gain of APDs provides a higher sensitivity in optical receivers than PIN photodiodes [20–22]. The APD is a reverse-biased photodiode in which the electric field inside the depletion region is large enough to excite new carries; this process is known as impact ionization. The APD reduces the relative effect of Johnson noise in the preamplifier stage of an optical receiver and improves the receiver's sensitivity [2]. In addition to their high sensitivity, APD-based receivers are highly cost effective compared to EDFA receivers. However, since the impact ionization is random, the uncertainty in the multiplication factor or gain, G, produces excess avalanche noise, known by the excess noise factor F. Nonetheless, at high frequencies the associated noise may still be less than that of a pre-amplifier. Thus the signal to noise ratio (SNR) of an optimized low noise APD can outperform receivers that employ a combination of optical pre-amplification and a pin photodetector.

Moreover, the APD's avalanche buildup time, which is the stochastic time required for the cascade of impact ionizations to complete per incident photon, can

further limit the receiver gain-bandwidth product by causing intersymbol interference (ISI) in optical receivers [23, 24]. This effect becomes more important when the transmission speed is very high as in the OC-192 standard, where ISI can limit the receiver performance. The buildup time has heretofore been the factor that limits the use of APDs in 40-Gb/s systems. Hayat *et al.* [3, 25] introduced a novel approach for operating APDs in the linear mode employing bit-synchronous and periodic dynamic biasing that reduces the buildup time dramatically. It is predicted that the new approach projects substantial improvements in the APDs gain-bandwidth products (GBPs).

In this dissertation, we rigorously analyze and theoretically model the APD's performance under dynamic biasing APD. We develop the theory for the joint statistics of the stochastic gain and stochastic buildup time in dynamically biased APDs for the first time, which is a major expansion of the recursive equations developed in [23] under the assumption of static electric fields. We also develop a theory for filtered shot noise under dynamic biasing, which addresses rigorously the statistic of the dynamically biased APD photocurrent, such as the mean, variance, autocorrelation function, etc. We incorporate these statistics in deriving analytical expressions for the statistics of the photocurrent of dynamically biased APDs. The proposed study is characterized by its ability to predict the performance of a dynamically biased APD-based receivers and to optimize the system parameters to achieve an optimal receiver performance. We also provide an approximation method for calculating the statistics of the impulse-response function of the APD-based receivers operating under dynamic biasing using the joint statistics of the stochastic gain and buildup time. The exact expressions for the receiver bit-error rate and sensitivity in an on-off keying setting will be extracted using the photocurrent statistics. The sensitivity analysis of the dynamically biased APD-based receiver will incorporate ISI and dark current as well as trans-impedance amplifier (TIA) noise used in the pre-amplification stage of receivers. The results show that operating under dynamic

biasing improves the receiver performance beyond its traditional limits operating under static biasing. Moreover, the analysis show that dynamically biased APD relax the stringent requirements of the width of the multiplication region, as normally done thin-APD to enhance its speed.

1.2 Literature review

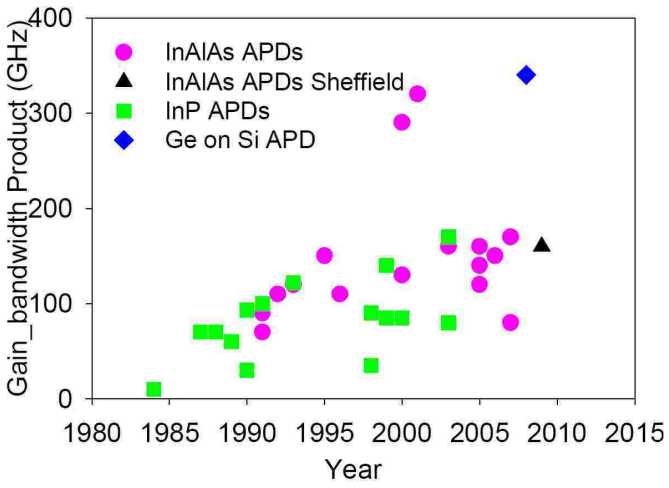

Figure 1.1: Trend in the gain-bandwidth products of InAlAs, InP and Ge-on-Si APDs reported in the past three decades [1].

There have been numerous efforts in the past two decades to increase the quantum efficiency and the avalanche gain or GBP APDs while maintaining a minimum noise level. The first generation optical-fiber communication systems have been developed in 1978 using a silicon APD [26]. The developed APD has been optimized for optical wavelength of 800 to 850 nm and exhibits a quantum efficiency greater than 90 %. To increase quantum efficiency without sacrificing in the avalanche gain performance, separate absorption and multiplication (SAM) structure APDs became the photodiodes of choice [27]. Due to the low loss wavelength of 1550 nm, current commercial SAM APDs with an InP multiplication layer and InGaAs absorption layer,

have been the perfect chose to use with the 2.5 Gb/s [28–30] and 10 Gb/s [31, 32] standards. Figure 1.1 shows the general trend in the experimental APD GBPs from 1984 to present. The performance is optimized by properly controlling the thickness of the multiplication layers to achieve a good avalanche gain while keeping the field low enough to minimize the tunneling. Thin multiplication region have been demonstrated to be an effective method for reducing multiplication noise, due to the dead-space effect, and increasing GBPs [33–37].

The SNR of an APD in the presence of Johnson noise and dark current can be found as follows [16]:

$$\text{SNR} = \frac{(\eta\Phi g)^2}{2\eta\Phi B g^2 F + \sigma_J^2 + \sigma_{\text{tunn}}^2}, \tag{1.1}$$

where Φ is the photon incident rate on the APD, η is the APD's quantum efficiency, i.e., the probability that a single photon incident on the device generates a photo-carrier pair that contributes to the detectors currents, B is the 3-dB bandwidth, σ_J^2 is the variance of the Johnson noise and σ_{tunn}^2 is the variance of the dark current dominated by tunneling. It is clear from (1.1) how the SNR increases with the average avalanche gain, $g = \mathsf{E}[G]$. This advantage poses a drawback as the excess noise factor F increases with the average gain g. However, there exist an optimal operating gain where the avalanche benefits outweighs the associated noise. Figure 1.2 shows the excess noise figure versus the avalanche gain for GaAs APDs with multiplication region width varies from 0.1 to 0.8 μm [4]. For a specific gain, it is clear that the excess noise decreases significantly with decreasing the width. In 2003, an APD with a thin multiplication layer of 80 nm was fabricated to achieve the highest value of a commercial InGaAs/InP APD GBP of 170 GHz [33]. However, such thin multiplication layer is likely to contribute significant band-to-band tunneling current which causes an increase in dark currents.

One of the InP based APDs limitation is the small (close to unity) electron-to-hole ionization coefficient ratio, k, reported to be 2.5-4 [8]. Therefore an alternative

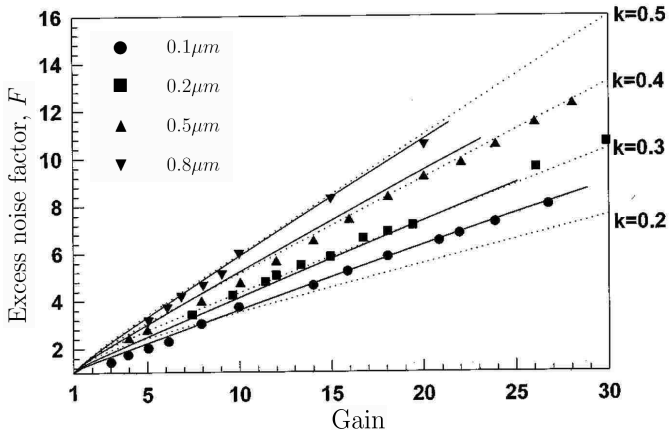

Figure 1.2: Calculated excess noise curves (solid lines) with experimental data of GaAs homojunction APDs for different multiplication widths [4].

material for the multiplication region was InAlAs which has an ionization coefficient ratio farther from unity (k between 4 and 6.7 [38]) than that for InP, hence giving it an edge over InP in terms of noise and GBP. The highest gain bandwidth products of InAlAs based APDs were reported by a group at University of Texas at Austin with values of 290 GHz in 2000 [37] and 320 GHz in 2001 [39], as shown in Fig. 1.1.

While InP/InGaAs SAM APDs have achieved excellent receiver sensitivities for 2.5 Gb/s [40] and 10 Gb/s [41], they cannot sustain higher bit rates due to their long avalanche buildup time. Much of the recent work on APDs has focused on developing new structures and incorporating alternative materials that will yield lower noise and higher speed while maintaining optimal gain levels. The first demonstration at 40 Gb/s using the APD receiver was demonstrated in [42]. The minimum received power is -19.6 dBm at 10^{-9} bit error rate (BER) and -19.0 dBm at 10^{-10} BER. This was achieved by adding a GaAs-based TIA. Due to the TIA boost, the receiver had a nominal GBP of 270 GHz at a gain of 10, whereas the GBP of the APD chip alone was 140 GHz at a gain of 3.

Due to the large asymmetry of electron and hole ionization coefficients in silicon

(Si) ($k < 0.1$), this material has been studied for several decades. However, Si is not appropriate to absorb at the telecommunication wavelengths, which require the use of smaller bandgap materials such as germanium (Ge). As a result, APDs with a Ge absorption layer and a Si multiplication layer can achieve very good performance with high quantum efficiency and low noise. In 2009, a monolithically grown germanium/silicon avalanche photodetector was demonstrated to have a GBP of 340 GHz and a sensitivity of -28 dBm at 10 Gb/s [43]. Later that year, Zaoui *et al.* [44] reported a SAM Ge/Si APD with a GBP of 840 GHz operating at 1310nm.

1.3 Review of the dynamic-biasing approach

In traditional linear-mode setting, an APD is operated under a constant reverse bias, which is selected to yield the optimal multiplication factor that maximizes the receiver sensitivity [25] by finding the optimal tradeoff between speed (buildup time), avalanche gain and the receiver noise (including the excess noise resulting from the impact ionization uncertainty). At high speed communication, the APD performance is limited by the avalanche buildup time. It is well know that the APD's avalanche amplification is correlated with the buildup time [23, 45]. Moreover, the buildup time increases at higher realizations of the gain. However if a dynamic biasing is considered instead of the traditional constant bias, then the buildup time can be controlled to improve the GBP and achieve higher transmission rates.

We would like to mention that while a sinusoidal-gating approach has been proposed for Geiger-mode APDs in the context of gated photon counting [46–48] its rationale is totally different from that associated with the novel linear-mode dynamic biasing approach presented here. The purpose there is to force quenching of the avalanche pulse after each detection-gate (high cycle of the sinusoidal bias) and therefore minimize the total number of multiplications, which, in turn, would

reduce after-pulsing. Specifically, photon counting with sinusoidal-gating is a binary detection problem: the APD is responsive to only one photon each gate. In contrast, in the proposed linear-mode dynamic biasing approach each and every photon in the optical pulse that is absorbed by the photodetector contributes to the analog photocurrent. Thus, unlike linear-mode operation, ISI is not a concern in Geiger-mode operation.

We illustrate the new approach proposed in [3] by exploring a simple, idealistic idea that can eliminate the buildup time problem. Consider an On-Off-Keying (OOK) optical receiver system with a sinusoidal reversed biased APD synchronized with the optical bit stream as shown in Fig. 1.3(a). The photoncurrent generated as a result of such dynamic biasing has the following properties. The photons that are absorbed early in the optical pulse under dynamic biasing experience a period of high electric field in the multiplication region of the APD. This phenomenon generates a strong photocurrent as shown in the schematic plot of Fig. 1.3(c). Next, as a low electric field follows the high field-phase, the carries in the multiplication region face a weaker impact ionization process, which causes a sudden drop in the impulse response and a cutoff in the buildup time. Thus, the impulse response of an early photon is distinguished by its high avalanche gain and its quenched tail at the end of the bit period to avoid interference with the next incoming bit. On the other hand, the *late* photons (the photons absorbed at the end of the bit period) experience a low electric field when they first enter the multiplication region. This will make the parent carrier to travel the multiplication region with a very low probability to ionize. Therefore, the resulting impulse response will have a low avalanche gain and a very short buildup time duration as shown in Fig. 1.3(c). Unlike the static bias case shown in Fig. 1.3(b), the impulse response of a photon in a dynamic bias APD receiver is age-dependent. The statistical properties of the avalanche gain and buildup time depends on the arrival time of the carrier to the multiplication region in each optical pulse. Whereas in the constant bias case scenario, all absorbed photon has

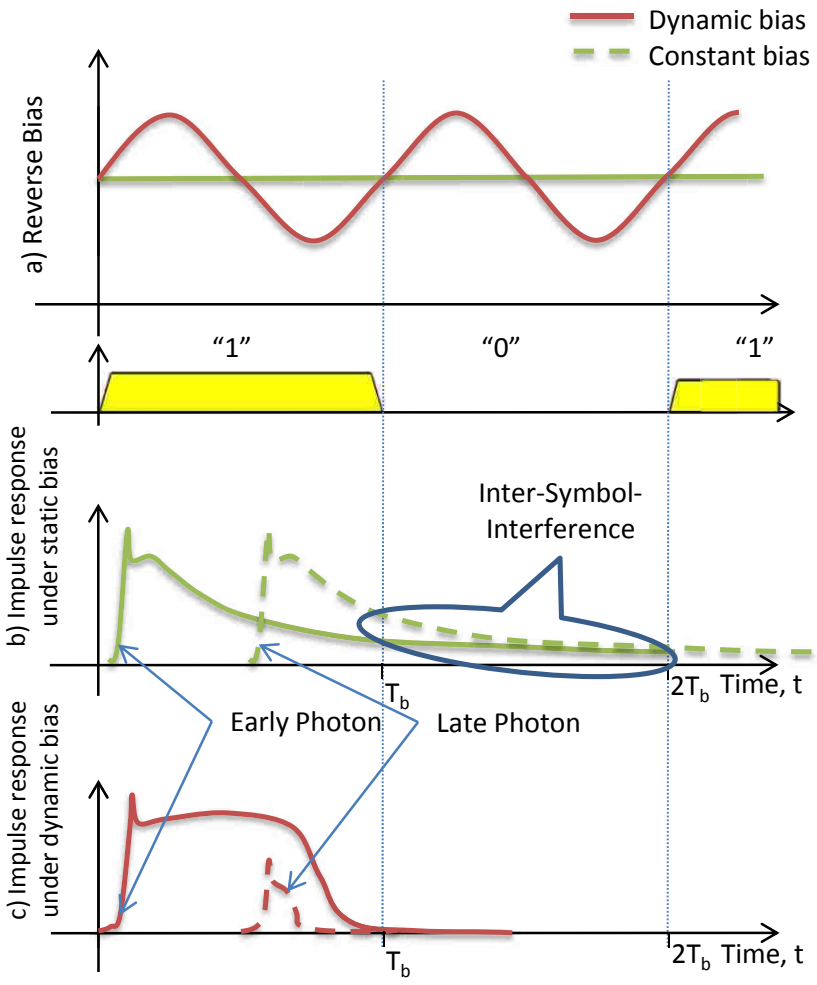

Figure 1.3: Schematic of the proposed dynamic biasing approach (red curves) compared with the traditional static biasing approach (green curves). The periodic change in the reverse bias within the optical-pulse period causes (1) photons that arrive early in the pulse window (c- solid line) to trigger high avalanche gains but limited avalanche duration, and (2) late photons (c- dashed line) to trigger avalanches with low gains and limited buildup times.

an identical independent distribution regardless of its arrival time.

1.3.1 Dynamic biasing in digital optical communication

Although the optoelectronic gain offered by the dynamically biased APD is dependent periodically upon the arrival instant of the photon within each information bit, the total charge accumulated in each bit in an integrate-and-dump receiver is not affected by the time-variant nature of the gain. More precisely, since the photocurrent is integrated over each bit in the receiver, the total charge is simply proportional to the product of the average mean gain (averaged over all arrival times) and the total number of photons in the optical pulse in each bit. In other words, the charge produced in each bit remains proportional to the energy in the optical pulse in each bit. Thus, the dynamically biased APD is linear as far as the receiver output is concerned and hence it is a perfect fit to digital optical communications.

1.3.2 The potential impact of dynamic-biasing on communication systems

While sinusoidal biasing has been reported by Herbert and Chidley [49] as a way to reduce excess noise in APDs, to the best of our knowledge, the dynamic-biasing approach has not been explored for linear-mode APDs operation as a way to improve bandwidth [25]. It introduces a totally new paradigm for APD design and adds a new dimension to the traditional material- and structure-based approaches. Another feature of our approach is that it is essentially APD-agnostic; that is, it can be used to improve the GBP of any APD that has a poor buildup-time performance. An added advantage of the dynamically biased APD approach is that with the dynamic biasing scheme we can actually relax the stringent requirements of the width of the multiplication region, as normally done to enhance the APD speed. This, in turn, reduces the electric field in the multiplication region, which reduces tunneling current, as it is shown in Chapter 7. With such attractive performance and cost effectiveness,

we anticipate the dynamically biased APD solution to digital receivers to have a huge immediate impact on next-generation long-haul and metro networks. In addition to telecom, free-space communication may too benefit from ultrafast APD-based receivers include free-space communication. As free-space communication moves to speeds beyond 10 Gb/s and longer ranges (without repeaters), there is a need for fast detectors with larger areas (larger collection efficiency). To benefit from an APD receiver, the avalanche multiplication region of the APD must be scaled up to offset the larger cross section required to achieve high collection efficiency in order to prevent large junction capacitances. Now a larger multiplication region for the APD causes the buildup time to increase, rendering the APD approach ineffective at higher speeds. However, the proposed dynamic biasing approach can be used to shrink the buildup time back to levels to much shorter multiplication regions without sacrificing collection efficiency. Another potential arena for the proposed dynamically biased APD-based receiver is data centers, where systems have a very tight power budget, requiring high speed detection and high sensitivity.

1.4 Contributions of this dissertation

A key aspect of this dissertation is theoretical model and analysis of the dynamically biased APD and the rigorous prediction of the sensitivity of a dynamically biased APD-based receiver. In this dissertation, we characterize, predict and analyze the reliability and performance of the proposed dynamically biased APD. Here we develop the first theory for the joint buildup-time and gain statistics for avalanche multiplication under dynamic electric fields. This is a major expansion of the APD theory beyond models for static fields [6, 23, 50–58] and the initial work on dynamically biased impact ionization developed in [25]. We also develop a theory for filtered shot noise under dynamic biasing, which addresses rigorously the statistics of the dynami-

cally biased APD photocurrent (mean, variance, autocorrelation function, etc.). This is used in turn to derive analytical expressions for the statistics of the photocurrent of dynamically based APDs. The exact expressions for the receiver bit-error rate and sensitivity in an on-off keying setting is extracted using the photocurrent statistics. The sensitivity analysis of the dynamically biased APD-based receiver specifically capture ISI and dark current as well as TIA noise used in the pre-amplification stage of receivers.

In the following, we summarize the main contributions of this dissertation.

1.4.1 Statistical properties of gain and buildup time in APDs

The APD's impulse-response function is a stochastic process, with a random duration (RD), representing the avalanche buildup time, and a random area, representing the multiplication factor or gain. Moreover, the stochastic gain and stochastic buildup time are statistically correlated [23]. The exact calculation of the joint probability distribution function (PDF) of the gain and buildup time is essential to predict the receiver performance. It is accomplished by developing a novel recursive theory that generalizes the existing recursive techniques for computing the joint PDFs of the gain and the buildup time under the assumption of a constant electric field in the multiplication region [23, 45].

To investigate the receiver performance of the APD in dynamic bias, we generalized the recursive theory that computes the joint PDF of the gain and the buildup time, to accommodate the dynamic behavior of the reverse bias. The dynamic-field scenario brings about a new element to the analysis of impact ionization. This element is the age (or time stamp) of a carrier measured from the point in time when the dynamic bias is launched. The novel recursive theory was modeled while taking the carrier's age into account. For a linear-mode operation of the APD, the cascade

of impact ionizations resulting from a photon arrived at age s, terminate at some finite random duration, $T(s)$, yielding a net random gain $G(s)$. The recursive theory determines the joint PDF, $f_{G,T}(g,t;s) = P\{G(s) = g, T(s) \leq t\}$, where g is the number of electron-hole pairs involved in the avalanche buildup, and t is the time by which the avalanche buildup is completed [59].

1.4.2 Novel theory for photocurrent generated by dynamically biased APDs

Existing mathematical theory for photocurrent statistics, also termed filtered point process [60], assumes that the detector's behavior is statistically stationary. This assumption was critical in deriving analytical expressions for the mean and the variance of the photocurrent generated by an APD [11, 61, 62], which are key enablers of the modeling of APD-based receivers. However, this hypothesis is not valid when the APD is dynamically biased: a new theory for shot noise must be developed to accommodate the dynamic nature of the APD's behavior as the bias is periodically varied. In our work, we derive the statistical properties of the photocurrent produced by a dynamically biased APD when illuminated by random bit patterns of arbitrary pulse shape. Unlike the static case, the statistics of the shot noise of an APD operating under dynamic reverse bias will vary cyclically with time with a period equal to the dynamic field period. Such cyclostationary stochastic photocurrent will play a key role in the analysis of the receiver performance.

The approach for determining the statistical properties of the photocurrent is based on the mathematical theory for filtered point processes [60, 63]. Specially, for the underlying point process, which represents the photon stream, we will consider a doubly stochastic Poisson point process, where the stochastic intensity is proportional to the instantaneous optical power of the received light at the receiver.

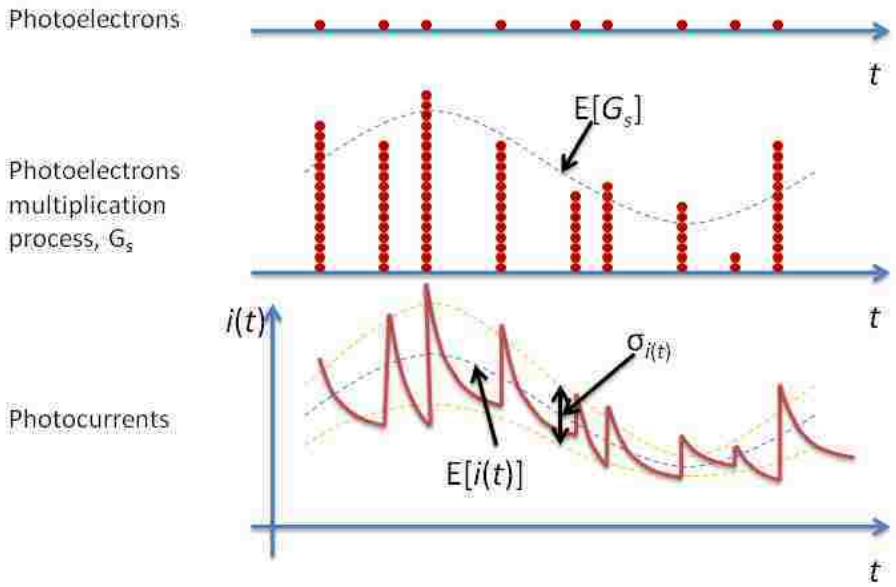

Figure 1.4: Each photoelectron in APD generates random number G_s of electron-hole pairs following a cyclostarionary random process, each of which produces an impulse response. The total photocurrent of the receiver output is the superposition of these impulse responses.

The arrival of each photon produces a stochastic pulse (see Fig. 1.4), which is the stochastic impulse response of the APD, which is dependent on the arrival time of the photon with respect to the dynamic electric field (or equivalently with respect to its position relative to the start of the bit). The photocurrent produced by the APD is simply the superposition of all such stochastic pulses. This photocurrent is then integrated over each bit period to produce the stochastic integrated charge per bit, including the contributions from the present and all the past bits. From the stochastic integrated charge, an optimal decision is made, with some statistical certainty, whether the present bit has been a one or zero. A key component in determining the statistical properties of the cyclostationary photocurrent is the determination of the joint statistics of the gain and buildup time.

1.4.3 Formulating and computing the evolution of the impulse response

The recurrence theory for the avalanche multiplication, including the statistics of the gain and impulse-response function, under non-uniform, static electric fields was originally formulated by Hayat *et al.* in [50, 52, 54] and later extended to accommodate stochastic carrier velocity by Tan *et al.* [64]. The impulse response statistics has been generalized for the dynamic electric fields in [25] by considering the age of the absorbed photon.

To calculate the statics of the photocurrent, such as the mean and the variance, knowledge of the first and second moment of the impulse-response function is required. Further, in order to calculate the variance of the receiver output, as required when assessing the BER, the autocorrelation function of the impulse response is also necessary. Therefore we determine the asymptotic behavior, and particularly the decay rate, of the mean and variance of the impulse response function of the dynamically biased APD.

1.4.4 Gaussian approximation in analyzing the performance of optical receivers

In many cases, a closed-form expression for the BER is required to understand, predict and provide analytical insight for the receiver performance. A closed-form expression for the BER can be found by first conditioning on the past bit pattern; then the BER is calculated by averaging the conditional BER over all possible past bit patterns. This approach, denoted here by the bit-pattern–dependent (PD) approach, was adopted by Ong *et al.* [58, 65] in which the receiver output, conditional on the present and all the past bits, is approximated by a Gaussian random variable.

The Gaussian approximation is known to give a good estimate of the BER [66]. On the other hand, to simplify the analysis, another method has been commonly used by conditioning on the current bit while considering the *average* of all possible bit patterns (in place of the individual realizations of bit patterns) to generate the Gaussian distribution of the output [23, 67, 68]. Hence, the receiver output in this approach is bit-pattern–independent (PI), as it depends only on the average past bit pattern. Due to its simplicity, the PI method has been used to evaluate the APD performance and to give analytical insight for the system behavior in low speed applications. However, the benefit from the simplification comes at the expense of inaccuracy in the BER when ISI is dominant, i.e., when transmission speed is very high as in the OC-192 standard [69].

We analyze the closed-form expressions of the BER found using the PI and PD methods and study their accuracy. It is found that at high transmission speeds, the PD method can give a much more accurate approximation of the BER than that offered by the PI method. Therefore to estimate the APD performance under dynamic biasing, we consider the PD method to find a closed-form expression for the BER.

1.4.5 Performance analysis of a dynamically biased APD

We will use the theoretical model described earlier to analyze the receiver performance. Knowing the ionization parameters for the APD with using the joint distribution function of the gain and buildup time, we are able to compute the BER, GBP and the pulse response. The analysis conducted in this dissertation includes well-defined parameters that capture ISI, detector speed relative to the transmission speed, and the complex correlation between the APD's gain and buildup time. These results are optimized by the peak-to-peak voltage, phase offset and DC value

of the sinusoidal dynamic bias to achieve the optimal receiver sensitivity, defined as the minimum optical power needed to achieve a BER of 10^{-12}. It is also important to understand the sensitivity of the GBP enhancement to errors and perturbations resulting from the implementation of the sinusoidal bias. To this end, we will systematically study the effects of non-ideal factors such as fluctuations in the amplitude, DC and phase of the dynamic bias, clock-synchronization errors.

1.4.6 Generalization of the analysis to include dark current and realistic Johnson noise for an InP APD

We generalize the BER analysis to include dark current and realistic Johnson noise for an InP-based APD. The generalized model enable us to identify the optimal dynamic reverse bias voltage for InP-based APD for use at a prescribed digital transmission speed. There are three main competing factors that govern the sensitivity of APD-based optical receivers at high speeds. First, the avalanche noise of the APD which governs the penalty brought about by the stochastic nature of the impact-ionization process. Second, the stochastic avalanche duration (or buildup time), which governs the APD's speed and ultimately the level of ISI. With the dynamic reverse bias, this effect is expected to be dramatically reduced and eventually improving the receiver sensitivity. Last but not least, the APD's dark current, which is typically dominated by tunneling in the avalanche region, reduces the benefits of the dynamic biasing in thin APDs. Our generalized model considers all the three effects in the calculation. It turns out that with the dynamic biasing scheme we can relax the stringent requirements of the width of the multiplication region, as normally done to enhance the APD speed. This, in turn, reduces the electric field in the multiplication region, which reduces tunneling current. The sensitivity formulation can be used as a guide in designing dynamically biased APD-based receivers for specific system performance requirements well beyond the limits previously known under the

traditional constant-bias setting.

1.5 Organization of the dissertation

For the convenience of the reader, the chapters provide brief review of related background information, as well as brief summary and our conclusions at the end of each chapter.

The remainder of this dissertation is organized as follows.

Chapter 2 introduces the dynamic biasing approach proposed by Hayat *et al.* [3]. The potential benefits of dynamic biasing in improving the GBP is described qualitatively. The effect of the dynamic bias on the APD characteristics is also analyzed. In Chapter 3, we derive recursive equations that describes the joint distribution of the stochastic gain and buildup time. The joint PDF shows the correlation between the gain and buildup time as in the static case. It also shows the dependence of the carrier age, s, on the buildup time. Chapter 4 analyzes the impulse response shape and approximates it by a simplified model. These simplifications are used in deriving closed expressions for the BER. We also show the pulse response of a dynamically biased APD and compare it to the static case. The expected eye diagram of an InP-APD was found to show the potential benefits of dynamic biasing in improving the BER. In Chapter 5, analytical comparison between two methods to approximate the integrate-and-dump receiver output is conducted. In the analysis, we carefully consider the ISI since it is a crucial factor in the optical receivers at high speed communications. Numerical calculations were used to compare the two methods. In Chapter 6, the closed form expressions for the BER of a dynamically biased APD optical receiver were formulated as function of the receiver statistics. The BER expressions include the ISI and Johnson noise effect. Numerical calculations is also presented to show the dynamic biasing enhancements over the conventional

static bias. In addition to that, we study the effects of non-ideal factors such as DC and phase of the dynamic bias and clock-synchronization errors on the receiver performance. In Chapter 7, we have generalized the dynamically biased APD-based receiver model to include tunneling current and used it for the purpose of optimization by the peak-to-peak voltage, phase offset and DC value of the sinusoidal dynamic bias for best receiver sensitivity for an arbitrarily prescribed transmission speed. The model offers compact analytical expressions for the mean and the variance of the output of the integrate-and-dump APD-based receiver that capture the dark current, the effects of ISI and the stochastic correlation between the APD's gain and bandwidth. Finally, Chapter 8 concludes the dissertation and discusses possible new research lines for future work.

Chapter 2

Basics of Avalanche Multiplication Theory under Dynamic Biasing

For its relevance to the work of this dissertation, we review in this chapter the dynamic biasing approach proposed by Hayat *et al.* [3]. In Section 2.1, we review the APD characteristics and define some important variables. In Section 2.2, we give a qualitative description of the potential benefits of dynamic biasing in improving the GBP. Some preliminary results found in [25] for the impact ionization under dynamic biasing is presented in Section 2.3. These results will make starting points for receiver performance analysis.

2.1 Conventional avalanche multiplication theory: Constant biasing

In the traditional linear-mode setting, an APD, which is essentially a strongly reverse-biased PIN photodiode, is operated under a constant (static) reverse bias, which

creates a high-field condition that is amenable to impact ionizations in the multiplication region. The ionization process is described in the schematic of Fig. 2.1. A photon is absorbed at location x_2, creating an electron-hole pair. The electron accelerates under the effect of the strong electric field and reaches its saturation velocity. While the electron traveling in the multiplication region and after acquiring enough energy ($> E_g$), with a certain probability, it may generate a second electron-hole pair by impact ionization as shown at location x_3. The two electrons then will follow the same process and each of them may ionize independently. Similarly the holes generated also accelerate while moving left and by acquiring enough energy they may be the source for a further impact ionization (as shown at location x_1).

2.1.1 Impact ionization coefficient

The ability of electrons and holes to impact ionize is characterized by the ionization coefficients α and β, respectively. These quantities represent rates of ionization per unit length. An important parameter for characterizing the performance of an APD is the ionization coefficient ratio $k = \beta/\alpha$. As it is mentioned earlier, it is always desirable to fabricate APDs from materials that have an ionization ratio far from unity. In that case, the avalanche process proceeds principally in one direction (either electron or hole). This will reduce the avalanche noise and the avalanche buildup time. The dependence of the ionization coefficients on the electric field E can be modeled from the non-localized model [6] by the equations

$$\alpha(E) = A_e \exp\left[-\left(\frac{B_e}{E}\right)^{m_e}\right] \tag{2.1a}$$

and

$$\beta(E) = A_h \exp\left[-\left(\frac{B_h}{E}\right)^{m_h}\right], \tag{2.1b}$$

where A, B and m are material-dependent parameters chosen by fitting measured gain-noise data. Table 2.1 shows the sets of width-independent parameters for several

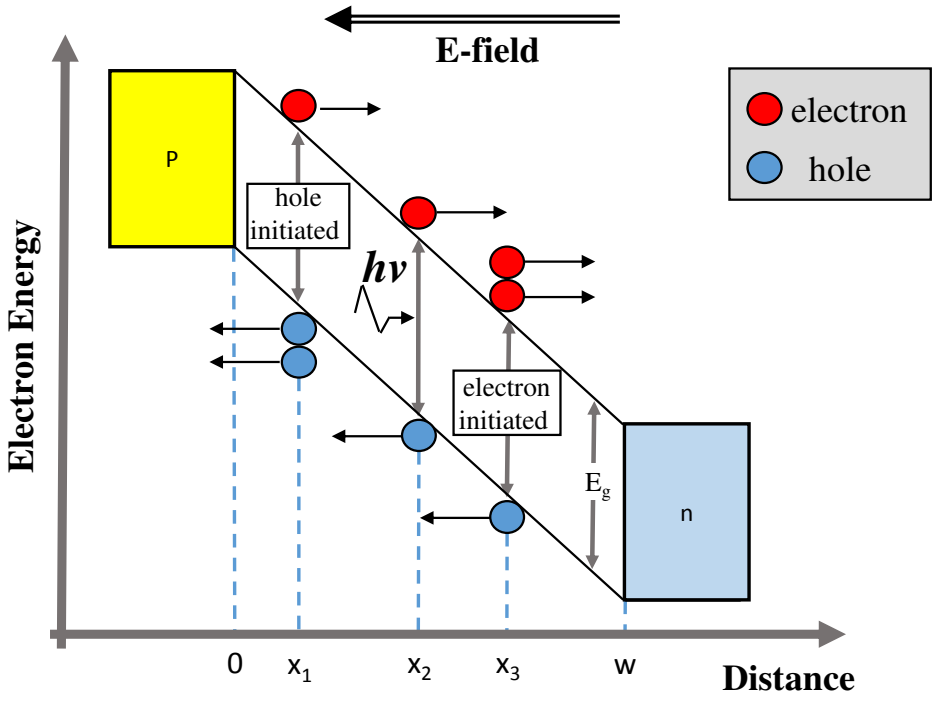

Figure 2.1: Schematic representation of the process of the multiplication process in APDs. The diagram shows the change in the electron energy as it travels the high electric field in the multiplication region spanning from $x = 0$ to w. E_g is the material bandgap energy. x_1 and x_3 are the location of a hole and an electron impact ionization, respectively.

III-V semiconductor materials [8, 53, 70].

2.1.2 Dead space

The first mathematical model to characterize the mean gain and excess noise factor of APDs was first introduced by McIntyre [57]. He models the excess noise factor as function of the mean gain and the ionization coefficients for electrons and holes ignoring the multiplication region width. It turns out that McIntyre's original model

	$Al_{0.2}Ga_{0.8}As$	$In_{0.52}Al_{0.48}As$	InP
A_e	5.39×10^6	4.17×10^6	1.41×10^6
B_e	2.71×10^6	2.09×10^6	1.69×10^6
m_e	0.94	1.2	1.23
A_h	1.28×10^6	2.65×10^6	2.11×10^6
B_h	2.06×10^6	2.79×10^6	1.77×10^6
m_h	0.95	1.07	1.15
	Si	GaAs	InGaAs
A_e	7.03×10^5	6.01×10^6	1.8×10^7
B_e	1.231×10^6	2.39×10^6	1.95×10^6
m_e	1.0	0.92	1.0
A_h	6.71×10^5	3.59×10^6	2.56×10^7
B_h	1.693×10^6	2.26×10^6	2.2×10^6
m_h	1.0	0.92	1.0

Table 2.1: Material-dependent parameters, A, B and m, for different III-V semiconductor materials.

fails in correctly predicting the excess noise factor in thin APDs (e.g., < 400 nm). It has been demonstrated that the excess noise factor and the avalanche buildup time are reduced by using thin multiplication layers [4, 6, 50, 52, 71–76]. This reduction was found to be due to the effect of a carrier's past-history on its ability to create a new carrier pair via impact ionization. The newly generated carriers are incapable of immediately causing impact ionizations. They must first travel a finite distance, called dead space, in order to acquire sufficient kinetic energy to become capable of ionization. This means that the ionization probability is negligible for a certain distance, the dead space. The reduction of the excess noise factor and the avalanche buildup time is a consequence of the dead space in thin devices.

Models that include the dead space effect have been developed. The effect of dead space on the gain and excess noise factor has been extensively studied and multiplication models that take carrier history into account have been developed and tested against experimental measurements [50, 52, 53, 72, 75, 77, 78]. Hayat *et al.* [50,52,72] formulated a dead-space-multiplication theory (DSMT) that permitted

the gain, excess noise factor in the presence of dead space. According to the DSMT model, the impact ionization probability density function is equal to zero when the distance traveled by the carrier is less than the dead space distance. The kinetic energy gained acquired by the moving carrier is equated to the ionization threshold energy of the carrier. Thus, the electron, $d_e(x)$, and holes, $d_h(x)$, dead spaces can be obtained numerically as follows:

$$q\int_{x}^{x+d_e(x)} E(\tilde{x})\,\mathrm{d}\tilde{x} = E_{th_e} \tag{2.2a}$$

and

$$q\int_{x-d_h(x)}^{x} E(\tilde{x})\,\mathrm{d}\tilde{x} = E_{th_h}, \tag{2.2b}$$

where q is the electron charge and E_{th_e} and E_{th_h} are the ionization threshold energy of the electron and the hole, respectively. The values of E_{th} for several III-V semiconductor materials are summarized in Table 2.2 [8, 53, 70].

	$Al_{0.2}Ga_{0.8}As$	$In_{0.52}Al_{0.48}As$	InP
E_{th_e}	2.04	2.15	2.80
E_{th_h}	2.15	2.30	3.00
	Si	GaAs	InGaAs
E_{th_e}	1.20	1.70	1.20
E_{th_h}	1.00	1.40	1.00

Table 2.2: Ionization threshold energy, E_{th_e} and E_{th_h}, for different III-V semiconductor materials.

Table 2.3 extracted from [6] shows an example of the relative dead space, defined as the ratio of the dead-space to the multiplication-region width, w, for four different GaAs APD devices. The relative dead-space in Table 2.3 is seen to increase as the multiplication-region width is reduced. This result emphasis the effect of dead space on thin APD devices.

Multiplication Width(nm)	Electric Field ($\times 10^5$ V/cm)	Mean Gain	d_e/w (%)	d_h/w (%)
100	6.3 − 6.8	8 − 29	25 − 27	21 − 22
200	4.7 − 5.0	6 − 30	17 − 15	14 − 15
500	3.5 − 3.7	4 − 28	9.2 − 9.8	7.6 − 8.0
800	3.2 − 3.3	5 − 20	6.4 − 6.6	5.3 − 5.8

Table 2.3: An example of the relative dead space, defined as the ratio of the dead-space to the multiplication-region width, w, for four different GaAs APDs. The lower and upper limits of the electric field produce the lower and upper limits, respectively, of the mean gain and the relative dead space [6].

2.1.3 Gain and buildup time

The time response of an APD to an individual photon has a finite width, called the buildup time. The cascade of impact ionizations and the associated buildup time in a simple multiplication region is illustrated in Fig. 2.2. A parent carrier is generated in the absorption layer and injected in the multiplication region. The photo-generated parent electron starts the ionization process. While drifting in the high-filed intrinsic layer, the parent electron acquire enough energy to ionize at any location to produce another electron and hole. The newly generated carries will follow the same process to produce more electrons and holes. A first wave of impact ionizations takes place while the photo-generated electron is still in the multiplication region. Next as the offspring electrons drift together and reach the end of the multiplication region, the offspring holes, which are still present in the multiplication region, move in the opposite direction, as shown in the figure, causing a second-wave of impact ionizations that lasts for one hole-transit time. As the second wave ends, a third wave is launched lasting for one electron transit time, and so on. This process terminates when all the carries exit the multiplication layer.

Under a fixed reverse bias, each absorbed photon from the received optical pulse will trigger an avalanche that takes a finite time, known as the buildup time. More-

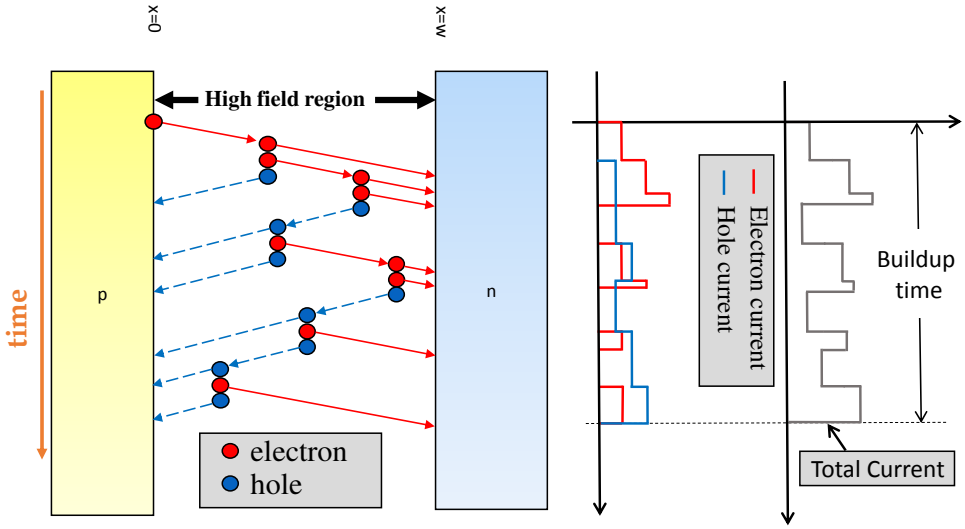

Figure 2.2: Schematic representation of the impact ionization and the associated buildup time process in a simple multiplication region.

over, the buildup time can be controlled by changing the reverse bias voltage. Due to the correlation between the gain and the buildup time [23], as we increase the mean gain of the APD to overcome receiver noise, the tails of the individual responses from the photons, add up to interfere to the photocurrent of the next bit as shown in Fig. 1.3(b). This interference, known as the ISI, reduces the APD performance. The buildup time limited bandwidth of an APD begins to dominate RC effects at reasonable operation gains (> 10) and ultimately limits the operability of ADPs at high bit rates [51]. The bias is typically optimized to maximize the receiver sensitivity [16] by providing just enough gain to overcome Johnson noise while maintaining a low excess noise factor and acceptably low buildup time.

2.2 Dynamic biasing approach: minimizing the buildup time

The use of a practical, bit-synchronous and periodic dynamic biasing of an APD, in lieu of traditional static bias, to dynamically control the impact ionization process for linear-mode operation was first introduced by Hayat and *et al.* [3, 25]. It was shown theoretically that the scheme can offer substantial reduction in the duration of the APDs pulse response, thereby minimizing ISI without sacrificing avalanche gain. Due to the coupling between the buildup time and the reverse bias, we can reduce the interference to the next bit by abruptly reducing the reverse bias of the APD near the end of the optical pulse to stop (or reduce) all the impact ionization. As a result, the pulse response will be quenched at the end of each bit period in preparation for the next incoming optical pulse. Note that the losses in the gain due to the quenching effect can be compensated by increasing the reverse voltage at the beginning of the optical pulse. This idealistic approach can limit the pulse response to the optical pulse duration without reducing the APD's gain. As a result, the GBP can increase indefinitely by simply increasing the gain.

We show theoretically in this dissertation that such novel scheme can achieve substantial reduction in the duration of the APD's pulse response, thereby minimizing ISI without sacrificing avalanche gain while improving the BER.

To achieve a realistic model for such periodic, abrupt transitions in the bias, we select a sinusoidal biasing scheme that can approximate the active quenching phenomenon described earlier (as shown in Fig. 1.3(a)). The reverse bias is frequency-matched and synchronized with the optical bit stream. The success of such approach would rely on our ability to discover the optimized parameters of the sinusoidal dynamic bias that yield the lowest receiver sensitivity possible. Meeting these challenges is at the heart of this dissertation.

2.3 The impact ionization under dynamic biasing

Consider a typical InP–InGaAs APD with a multiplication region extending from $x = 0$ to $x = w$, as shown in Fig. 2.3. When a photon get absorbed in the InGaAs absorption layer, a parent photo-generated carrier (a hold in this case) is generated and sweep out to the multiplication region (InP layer) at $x = w$ due to the relative low electric field.

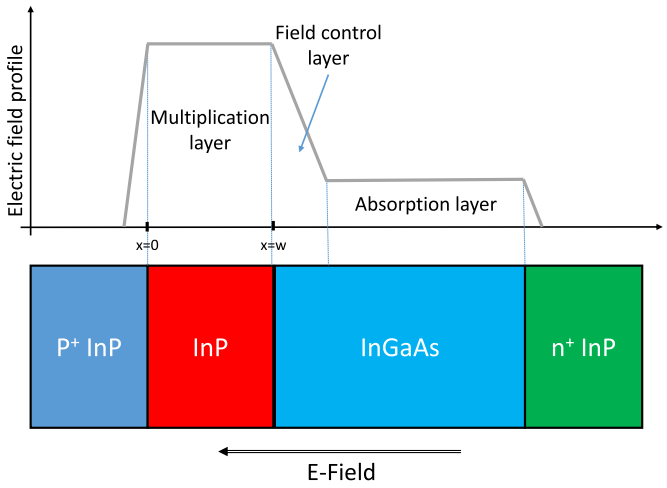

Figure 2.3: Schematic of the SAM layer structure of typical InP-nGaAs APD (not to scale). Also shown is the electric field profile under normal reverse bias operation [5]. Note that, the electric field shown here is at a specific time t.

2.3.1 The ionization coefficient under dynamic biasing

Suppose that a time-varying bias, $V_b(t)$, is applied to an APD. Let $E(x,t)$ denote a casual and spatially nonuniform dynamic electric field in the multiplication region at position x and at time t. The electron and hole time-varying non-localized ionization coefficients associated with caries at location x in the multiplication region at time t are defined to be $\alpha(x,t)$ and $\beta(x,t)$, respectively. By replacing the static field in

non-localized model shown in (2.1), the dynamic coefficients are given by [25]

$$\alpha(x,t) = A_e \exp\left[-\left(\frac{B_e}{E(x,t)}\right)^{m_e}\right] \tag{2.3a}$$

and

$$\beta(x,t) = A_h \exp\left[-\left(\frac{B_h}{E(x,t)}\right)^{m_h}\right], \tag{2.3b}$$

where the material specific constants A, B and m are listed in Table 2.1 for various III-V materials. These coefficients are used in turn to derive analytical expressions for the probability density function of a carrier to ionize in dynamic-field scenario.

2.3.2 The probability density function of the carrier path in dynamically biased APD

The probability density function of the carrier's free path before the first impact ionization in a dynamic-field scenario depends on the starting location of the parent carrier as well as its age s relative to the launch instant of the dynamic electric field [25]. Suppose that a parent hole or electron is created at an arbitrary location x in the multiplication region of the APD and with an age s (i.e., at time $t = s$), and assume that the field is sufficiently high so as conduction-band electrons and valence-band holes travel at their material-specific saturation velocities, v_e and v_h, respectively.

let X_h and X_e be the stochastic free-path distances the holes and electrons, respectively, travel before the impact ionization. As the carrier travels the multiplication region, it can ionize at stochastic location, denoted by ξ. More precisely, we define $h_e(\xi; x, s)$ and $h_e(\xi; x, s)$ as the dynamic probability density functions of the free-path-distances, X_e and X_h, of the first ionization position due to an electron and hole, respectively, portioned in the multiplication region at location x, and of age

s. The age-dependent probability density function of the free paths, $h_h(\xi_2;\xi_1,s)$ and $h_e(\xi_2;\xi_1,s)$, were defined in [25] according to the dead-space multiplication theory (DSMT). Under a dynamic electric field, the probability density function of the first ionization by a parent carrier of age s and at location ξ_1 is zero before the dead space is traveled and exponential with a nonuniform rate after the dead space.

$$h_e(\xi;x,s)=\begin{cases}\alpha\left(\xi,s+\frac{\xi-x}{v_e}\right)e^{-\int_{x+d_e(x,s)}^{\xi}\alpha\left(\sigma,s+\frac{\sigma-x}{v_e}\right)\mathrm{d}\sigma}, & \xi\geq x+d_e(x,s)\\ 0, & \text{otherwise}\end{cases} \tag{2.4a}$$

and

$$h_h(\xi;x,s)=\begin{cases}\beta\left(\xi,s+\frac{x-\xi}{v_h}\right)e^{-\int_{\xi}^{x-d_h(x,s)}\beta\left(\sigma,s+\frac{x-\sigma}{v_h}\right)\mathrm{d}\sigma}, & \xi\leq x-d_h(x,s)\\ 0, & \text{otherwise,}\end{cases} \tag{2.4b}$$

where $d_e(x,s)$ and $d_h(x,s)$ are the aged-dependent dead spaces for an electron and hole, respectively. From the static electric field model described in (2.2) and by replacing the static field with its dynamic value, the age-dependent dead space is the distance d that satisfies the equations

$$q\int_{x}^{x+d_e(x,s)}E(\tilde{x},s+(\tilde{x}-x)/v_e)\,\mathrm{d}\tilde{x}=E_{th_e} \tag{2.5a}$$

and

$$q\int_{x-d_h(x,s)}^{x}E(\tilde{x},s+(x-\tilde{x})/v_h))\,\mathrm{d}\tilde{x}=E_{th_h}, \tag{2.5b}$$

where E_{th} is the ionization threshold energy for the materials. In the above, $h_e(\xi;x,s)d\xi$ approximates the probability that an electron born at location x and of age s impact ionizes for the first time in the interval $[\xi,\xi+d\xi]$. These probability density functions will play a critical role in the derivation of the joint PDF of the gain and the buildup time.

2.4 Summary and conclusions

In this chapter, we briefly reviewed the impact ionization process in APDs. We also introduced the dynamic biasing approach for APD-based optical receivers. This approach is aimed to reduce the buildup time without sacrificing the avalanche gain. We showed the generalization of the impact ionization coefficients to include the dynamic nature of the electric field in the multiplication region. The probability density function for the random paths traveled by the carriers, electrons and holes, were defined according to the dead-space multiplication theory .

Chapter 3

Statistical Properties of Gain and Buildup Time in Dynamically Biased APDs

In this chapter, we develop the first theory for the joint probability distribution of the stochastic gain and stochastic buildup time in dynamically biased APDs [79]. This development constitutes a major expansion of (i) the recursive equations developed in [23] under the traditional assumption of a static bias, and (ii) the recursive technique characterizing the gain and buildup time individually [25]. As described earlier, the results will be incorporated in the performance analysis of APD-based receivers at high transmission speeds. The theory developed here includes the dead-space effect, which is essential to consider in thin APD's multiplication layers.

This theory will enable the analytical determination of the statistics of the APDs impulse response function as well as its autocorrelation function, which, in turn enables the determination of the statistics of the dynamically biased APD photocurrent as well as the output of the integrate-and-dump receiver that is built around it. Fol-

lowing [25], the dynamic-field scenario brings about a new element to the analysis of impact ionization. This element is the age (or time stamp) of a carrier measured from the point in time when the dynamic bias is launched. The age will play a key role in the statistical analysis of the avalanche multiplication process. Specifically, carriers born at different times will experience different dynamical electric fields ahead of them as they generate their own chains of impact ionizations. To take the age-factor into account in the analysis of the avalanche multiplication process, the usual ionization probability of a carrier is parameterized by the time at which the parent carrier is injected in the multiplication region. The key enabling idea in modeling the joint distribution for a dynamic reversed bias APD is to consider the age of the parent carrier relative to the launch of the dynamic bias as discussed next.

3.1 Definitions

Consider a multiplication region of the APD extending from $x = 0$ to $x = w$. Assume that a dynamic electric field, $E(t) = V(t)/w$, is present in the multiplication region, where $V(t)$ is the time-varying applied bias voltage. When a carrier enters the multiplication region with an age s relative to the launch time of the dynamic bias, an age-dependent avalanche process will be triggered. For a parent carrier entering the multiplication region with age s and triggering an avalanche multiplication process, let T_s be the stochastic time required for the avalanche process to terminate, and let G_s be the total number of electron-hole pairs generated by this process. Note that T_s is the stochastic duration of the APD's impulse-response function induced by an injected carrier in the multiplication region with age s. Meanwhile, G_s merely is proportional to the area under the stochastic impulse-response function.

The age-dependent joint probability distribution function (PDF) associated with G_s and T_s is the probability that a parent carrier entering the multiplication region

at age s generates m electron-hole pairs in a time less than or equal to t. Formally, we define the joint PDF as $f_{G_s,T_s}(m,t;s) = \mathsf{P}\{G_s = m, T_s \leq t\}$. Following the concept of the recursive approach [25], let the random variable $Z(x,s)$ be the total number of electrons and holes (including the parent carrier) initiated by a parent electron located at location x with age s. Similarly, let $Y(x,s)$ be the total number of electrons and holes (including the parent carrier) initiated by a parent hole located at location x with age s. Note that if we assume that the electric field is in the opposite direction of the x-axis and the multiplication region span the region from $x = 0$ to $x = w$, by convention $Z(w,s) = Y(0,s) = 1$, $s \geq 0$, since an electron (hole) generated at the right (left) edge of the multiplication region will exit the multiplication region without ionization.

Let X_h and X_e be the stochastic free-path distances the holes and electrons, respectively, travel before they effect an impact ionization. The age-dependent probability density function of the free paths X_h and X_e, denoted by $h_h(\xi_2;\xi_1,s)$ and $h_e(\xi_2;\xi_1,s)$, respectively, were defined in Sec.2.3.2 according to the dead-space multiplication theory (DSMT) under dynamic electric fields. For convenience they are reiterated here:

$$h_h(\xi_2;\xi_1,s) = \begin{cases} \beta(\xi_2, s+\tau_h) e^{-\int_{\xi_2}^{\xi_1 - d_h(\xi_1,s)} \beta(\sigma, s+\tau_h)\,\mathrm{d}\sigma}, & \xi_2 < \xi_1 - d_h(\xi_1,s) \\ 0, & \text{otherwise} \end{cases} \tag{3.1}$$

and

$$h_e(\xi_2;\xi_1,s) = \begin{cases} \alpha(\xi_2, s+\tau_e) e^{-\int_{\xi_1 + d_e(\xi_1,s)}^{\xi_2} \alpha(\sigma, s+\tau_e)\,\mathrm{d}\sigma}, & \xi_2 > \xi_1 + d_e(\xi_1,s) \\ 0, & \text{otherwise} \end{cases} \tag{3.2}$$

where $\beta(x,t)$ and $\alpha(x,t)$ are the position and age-dependent ionization coefficients, $d_h(x,s)$ and $d_e(x,s)$ represent the age-dependent dead spaces for a hole and electron, respectively, $\tau_e = (\xi - x)/v_e$ and $\tau_h = (x - \xi)/v_h$ is the electron and hole transport

time between x and ξ. Note that $h_e(\xi; x, s)d\xi$ approximates the probability that an electron born at location x and of age s impact ionizes for the first time in the interval $[\xi, \xi + d\xi]$.

Other intermediate quantities required in this formulation are the buildup times. As in [25], define $Z(x, s)$ $(Y(x, s))$ as the totality of electrons and holes due to avalanche processes triggered by a parent electron (hole) of age s relative to the launch instant of the electric field. Now let $T_Z(x, s)$ be the random time required for the $Z(x, s)$ electrons and holes to exit the multiplication region; similarly, $T_Y(x, s)$ is defined in the same way. It is worth to mention that T_Z (or T_Y) is always greater than the electron (or hole) transport time between x and w, which is the time needed for the parent electron (or hole) to exit the multiplication region. We define the joint PDFs of the pairs (Z, T_Z) and (Y, T_Y) as follows:

$$f_e(m, t; x, s) = \mathsf{P}\{Z(x, s) = m, T_Z(x, s) \leq t\}, \tag{3.3a}$$

and

$$f_h(m, t; x, s) = \mathsf{P}\{Y(x, s) = m, T_Y(x, s) \leq t\}. \tag{3.3b}$$

Note that with this notation, the stochastic buildup time T_s defined earlier becomes $T_s = T_Y(w, s)$, and its corresponding stochastic gain is $G_s = 0.5(Y(w, s) + 1)$. For example, for an InGaAs-InP APD in which photo-generated holes initiate avalanche processes in the InP multiplication region starting from $x = w$, we have $f_{G_s,T_s}(m, t, s) = f_h(2m - 1, t; w, s)$.

3.2 Recursive equations

The key observation needed in the formulation of a recursion for the PDFs defined above is that a parent electron born at location x and of age s generates a certain

number of offspring carriers ($Z(x,s) = m$, say) within a certain time ($T_Z(x,s) \leq t$, say) precisely when its two offspring electrons and offspring hole, born for example at location ξ, will collectively create the same intended number of carriers (m) albeit within a reduced time $t - \tau_e$. The age of the two offspring electrons and hole at birth is $s + \tau_e$.

With this regeneration concept in mind and by using the fact that all carries impact ionize independently of one another other, the conditional PDF of $f_e(m,t;x,s|\xi)$ conditioned on the first ionization location ξ can be written as

$$f_e(m,t;x,s|\xi) = f_e\left(m,t-\tau_e;\xi,s+\tau_e\right) * f_e\left(m,t-\tau_e;\xi,s+\tau_e\right) * f_h\left(m,t-\tau_e;\xi,s+\tau_e\right), \tag{3.4}$$

where $*$ denotes discrete convolution in the variable m and τ_e is the time needed for an electron to move from x to ξ (i.e., $\tau_e = \frac{\xi - x}{v_e}$). Similarly, if we start with a parent hole, the conditional PDF $f_h(m,t;x,s|\xi)$ recursive equation can be written as

$$f_h(m,t;x,s|\xi) = f_h\left(m,t-\tau_h;\xi,s+\tau_h\right) * f_h\left(m,t-\tau_h;\xi,s+\tau_h\right) * f_e\left(m,t-\tau_h;\xi,s+\tau_h\right), \tag{3.5}$$

The conditioning on the first impact ionization location can be removed by averaging over all passible locatiuons ξ in the interval $[x,w]$ of the first ionization of the parent electron (using the probability density function h_e), we obtain the following recursive equation:

$$f_e(m,t;x,s) = g_e(x,t,s)\delta_{m-1} + \int_x^w \left[f_e\left(m,t-\tau_e;\xi,s+\tau_e\right) * f_e\left(m,t-\tau_e;\xi,s+\tau_e\right) * f_h\left(m,t-\tau_e;\xi,s+\tau_e\right)\right] h_e(\xi;x,s)\,\mathrm{d}\xi, \tag{3.6}$$

where δ_i is the Kronecker delta function ($\delta_i = 1$ when $i = 0$ and zero otherwise) and $*$ denotes discrete convolution in the variable m. The function $g_e(x,t,s)$ represents

the probability that the parent electron does not ionize within time t (in this case $Z(x,s)=1$ and $T_Z(x,s)=(w-x)/v_e$) and it is given as:

$$g_e(x,t,s)=u\left(t-\frac{w-x}{v_e}\right)\int_w^\infty h_e(\xi;x,s)\,\mathrm{d}\xi, \tag{3.7}$$

where $u(x)$ is the unit step function. Similarly, the conditional PDF $f_h(m,t;x,s|\xi)$ recursive equation becomes

$$\begin{aligned} f_h(m,t;x,s)=g_h(x,t,s)\delta_{m-1}+\int_0^x &\left[f_h\left(m,t-\tau_h;\xi,s+\tau_h\right)*\right.\\ &\left.f_h\left(m,t-\tau_h;\xi,s+\tau_h\right)*f_e\left(m,t-\tau_h;\xi,s+\tau_h\right)\right]h_h(\xi;x,s)\,\mathrm{d}\xi, \end{aligned} \tag{3.8}$$

where $g_h(x,t,s)$ is the probability that the parent hole does not ionize at within time t, and it is given by

$$g_e(x,t,s)=u\left(t-\frac{w-x}{v_e}\right)\int_w^\infty h_e(\xi;x,s)\,\mathrm{d}\xi. \tag{3.9}$$

The coupled pair of recursive equations in (3.6) and (3.8), which fully characterize the PDFs f_e and f_h, can be solved numerically to determine the joint PDF $f_{G_s,T_s}(m,t,s)$. However, the discrete convolution under the integrals can be simplified to multiplication using the $z-$transform properties. Let $F_e(z,t;x,s)$ and $F_h(z,t;x,s)$ be the $z-$transforms of $f_e(m,t;x,s)$ and $f_e(m,t;x,s)$ with respect to the variable m. More precisely, if we define

$$F_e(z,t;x,s)=\sum_{k=0}^{\infty}f_e(k,t;x,s)z^k \tag{3.10a}$$

and

$$F_h(z,t;x,s)=\sum_{k=0}^{\infty}f_h(k,t;x,s)z^k, \tag{3.10b}$$

for all complex $|z|\leq 1$, then the discrete recursive equations defined in (3.6) and (3.8) can be simplified to

$$\begin{aligned} F_e(z,t;x,s)=g_e(x,t,s)z+\int_x^w &F_e^2\left(z,t-\tau_e;\xi,s+\tau_e\right)\\ &F_h\left(z,t-\tau_e;\xi,s+\tau_e\right)h_e(\xi;x,s)\,\mathrm{d}\xi, \end{aligned} \tag{3.11a}$$

and

$$F_h(z,t;x,s) = g_h(x,t,s)z + \int_0^x F_h^2\left(z,t-\tau_h;\xi,s+\tau_h\right) F_e\left(z,t-\tau_h;\xi,s+\tau_h\right) h_h(\xi;x,s)\,\mathrm{d}\xi. \tag{3.11b}$$

Let $F_{G_s,T_s}(z,t;s)$ be the $z-$transform of the joint distribution f_{G_s,T_s} of the random variables G_s and T_s with respect to m. After solving the coupled recursive equations numerically over $z = e^{-j\omega}$ $(-\pi < \omega \leq \pi)$, $t \geq 0$, $x \in [0,w]$ and $s \in [0,T_b]$, while using the time shifting and scaling properties of the $z-$transform and since $f_{G_s,T_s}(m,t,s) = f_h(2m-1,t;w,s)$ for an InP APD, we obtain

$$F_{G_s,T_s}(z,t;s) = \sqrt{z}F_h(\sqrt{z},t;w,s). \tag{3.12}$$

The joint PDF of the avalanche process initiated by a parent hole from the right, can then be found by using the inversion formula [80], i.e., by evaluating the $z-$transform on the unit circle and find its Fourier series coefficients

$$f_{G_s,T_s}(m,t;s) = \frac{1}{2\pi}\int_{-\pi}^{\pi} F_{G_s,T_s}(e^{j\omega},t;s)e^{-j\omega n}\,\mathrm{d}\omega. \tag{3.13}$$

Note that, for the case of an avalanche process initiated by an electron at $x = 0$ instead of a hole, the stochastic buildup time T_s becomes $T_s = T_Z(0,s)$, and its corresponding stochastic gain is $G_s = 0.5(Z(0,s)+1)$. Thus the age-dependent joint PDF of the stochastic gain and buildup time is $f_{G_s,T_s}(m,t,s) = f_e(2m-1,t;0,s)$ and its corresponding $z-$transform with respect to m becomes $F_{G_s,T_s}(z,t;s) = \sqrt{z}F_e(\sqrt{z},t;0,s)$.

3.3 Numerical analysis

In our calculations, we selected an InGaAs-InP APD receiver with a multiplication layer of width $w = 200$ nm. The APD is dynamically biased with a sinusoidal reverse

voltage of the form

$$V_B(t) = B + C\sin(2\pi f_b t + \psi) \tag{3.14}$$

where f_b is the bit transmission rate, i.e., $f_b = 1/T_b$ and T_b is the optical pulse window. The probability density function of the free path, $h_e(\xi_2;\xi_1,s)$ and $h_h(\xi_2;\xi_1,s)$, were calculated according to the deadspace multiplication theory (DSMT) as described in Chapter 2. The calculation of the free path's probability density functions require the knowledge of the ionization coefficients and ionization-threshold energies for the InP multiplication region, which can be extracted from Section 2.3. The quantities B, C and ψ are parameters that control the overall performance of the system. Our main goal is to optimize these parameters to achieve an optimal receiver performance. As an example, the peak-to-peak and the DC parameters of the sinusoidal-biasing parameters were selected as $B = 13$ V and $C = 6$ V. The sinusoidal-biasing period is equal to 5.5 transit times, which is equivalent to a data rate of $f_b = 60Gb/s$. For simplicity we assume a spatially uniform electric field, $E(t) = V_B(t)/w$. The electron and hole saturation velocity are approximated as $v_e = v_h = 0.67 \times 10^7$ cm/s.

We first solve numerically the coupled recursive equations (3.11) using a simple iterative method. Next, the joint PDF of the random gain and G_s and the random buildup time T_s were calculated from (3.13). Figure 3.1 shows examples of the age-dependent joint PDF $f_{G_s,T_s}(m,t,s)$ calculated for different values of the age variable, s ($s = 0$, $s = T_b/4$, $s = T_b/2$ and $s = 3T_b/4$). The hole transit time is simply $w/v_h = 3.0$ ps. The correlation between the gain and the buildup time is clear from the joint PDF plots in agreement with the behavior of the static bias case [23]. The numerical calculations show that the arrival time of the incident photon to the multiplication region, s, plays a key role in the distribution function, a property that is heavily exploited in reducing the buildup time for optical receivers by adjusting the arrival time, s, of the incident photon relative to dynamic-bias cycle. For instance, by examining the shape of the PDF, the age-dependent joint PDF of an avalanche

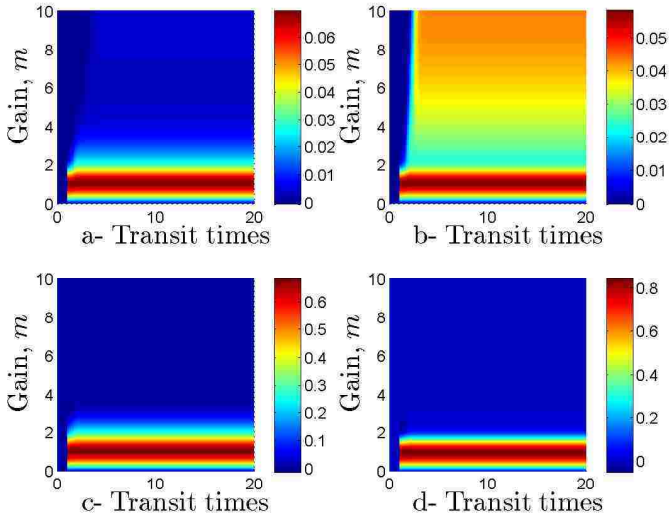

Figure 3.1: Joint PDF f_{G_s,T_s} of the stochastic gain G_s and the stochastic buildup time T_s for an InP APD with a 200-nm multiplication layer. Figures 3.1(a), (b), (c) and (d) correspond to different initiating parent hole of age $s = 0$, $s = 0.25T_b$, $s = 0.5T_b$ and $s = 0.75T_b$, respectively. The reverse dynamic voltage bias is of the form $V_b(t) = 13 + 6\sin(2\pi t/T_b)$, where T_b is the bit duration with $1/T_b \approx 60$ Gb/s.

triggered by a photon arrived at the beginning of the pulse ($s = 0$), is expected to have a higher mean gain ($\mathsf{E}[G_s]$) and longer mean buildup time ($\mathsf{E}[T_s]$) compared to a photon arrived at a later time (e.g., $s = 3T_b/4$).

In order to better understand the effect of the incident photon's arrival age, s, the probability mass function (PMF) of the stochastic gain G_s can be found by taking the limit of the joint PDF as t approaches infinity, i.e., $f_{G_s}(m, s) = \lim_{t\to\infty} f_{G_s,T_s}(m, t, s)$. The result is shown in Fig. 3.2. Furthermore, the cumulative distribution function (CDF) of the stochastic buildup time T_s (Fig. 3.3) as a function of the age, s can be found as follows: $F_{T_s}(t, s) = \sum_{m=1}^{\infty} f_{G_s,T_s}(m, t, s)$. Figure 3.2 shows a high mean for the gain (accompanied by a larger spread) at the beginning of the period (at $s = 0$) and decreases to unity when s is around 70% of the bit period T_b. Moreover, the CDF of the buildup time shows a similar behavior in Fig. 3.3, where the expected buildup approaches a unit of transit time when the age, s is around $0.7T_b$. Recall that the

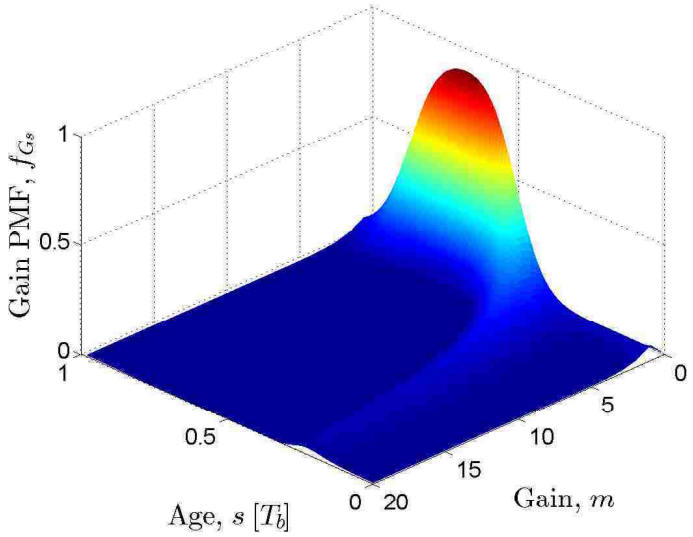

Figure 3.2: Marginal probability mass function of the stochastic gain, G_s, as a function of the initiating hole age (in bit duration, T_b).

minimum possible buildup time is the hole transit time w/v_h, i.e., $\mathsf{P}\{T_s \leq 1\} = 0$. This feature is observed in Figs. 3.1 and 3.3.

For this example, the average gain calculated by Hayat and Ramirez [25] for this particular receiver is 28. The marginal density function of the gain (obtained by integrating the joint PDF over the buildup time) yields the mean of 26.7, which is in good agreement with the previous results found in [25].

3.4 Summary and conclusions

In this chapter, we described a recursive method to compute the aged-dependent joint PDF of the stochastic gain, G_s, and the stochastic buildup time, T_s of an APD operating under dynamic reverse bias. This result will be used to calculate the statistical properties of the impulse-response function and investigate the effect of the

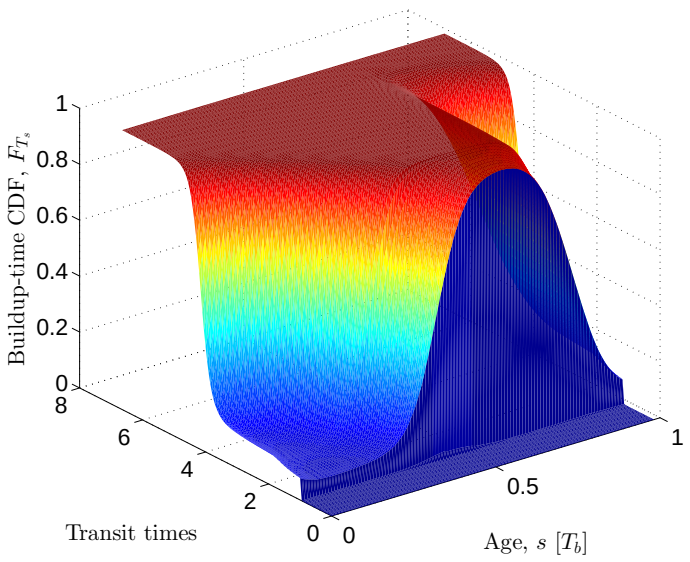

Figure 3.3: Marginal cumulative density function of the stochastic buildup time, T_s, as a function of the initiating hole age (in bit duration, T_b).

dynamic electric field on the receiver performance. It was clear from the numerical calculation the dependency of the joint PDF of G_s and T_s on the parent carrier age, s. In each illuminated transmitted bit, some of the arrived photons with a certain age have a long expected buildup time with high expected gain and the others have a short buildup time with a gain close to unity. The results showed that the photons arrive at 70% of the transmission bit window has a minimum expected buildup time, $\mathsf{E}[T_s]$ and small expected gain $\mathsf{E}[G_s]$.

Chapter 4

Dynamically Biased APD Impulse Response Statistics

In this chapter, we determine the asymptotic behavior, and particularly the decay rate, of the mean and variance of the impulse response function of the dynamically biased APD. These quantities are critical to our understanding and accurate assessment of ISI. To facilitate the calculation of these quantities, a stochastic model for the impulse-response function is required. Following the approach of [23], the rationale is to approximate the impulse response function by a specified shape parameterized by the age-dependent stochastic gain G_s and the age-dependent stochastic buildup time T_s. An example of such a shape is the rectangular random-duration (RD-R) with random height qG_s/T_s and random duration T_s, where q is the electrons charge. The randomness in the impulse-response functions area represents the gain uncertainty and the randomness in its duration represents the buildup time. This shape significantly simplifies the complexity of the impulse-response function while maintaining the key features that govern the stochastic gain, the excess-noise and speed properties of the APD.

4.1 Mean impulse response function

Using the coupled integral equations derived in [25], we numerically calculate the mean impulse response function and study its asymptotic behavior. We define $I_e(t,x,s)$, the age-dependent stochastic impulse-response function at time t initiated by an electron injected at location x and with age s. Similarly, $I_h(t,x,s)$ is the stochastic age-dependent impulse-response function at time t, initiated by a hole injected at location x with age s. Let $i_e(t,x,s)$ and $i_h(t,x,s)$ represent the mean quantities of $I_e(t,x,s)$ and $I_h(t,x,s)$, respectively. Using the same recurrent technique used in deriving the recurrence equations for the age-dependent joint PDF shown in Section 3.2, the coupled integral equations for the mean impulse response are found to be [25]

$$i_e(t,x,s) = \frac{qv_e}{w}\left[u(t) - u\left(t - \frac{w-x}{v_e}\right)\right]\int_w^\infty h_e(\xi;x,s)\,\mathrm{d}\xi + \int_x^{w\wedge x+v_e t}\left[2i_e(t-\tau_e,\xi,s+\tau_e) + i_h(t-\tau_e,\xi,s+\tau_e)\right]h_e(\xi;x,s)\,\mathrm{d}\xi \tag{4.1a}$$

$$i_h(t,x,s) = \frac{qv_h}{w}\left[u(t) - u\left(t - \frac{x}{v_h}\right)\right]\int_{-\infty}^0 h_h(\xi;x,s)\,\mathrm{d}\xi + \int_{0\vee x-v_h t}^{x}\left[2i_h(t-\tau_h,\xi,s+\tau_h) + i_e(t-\tau_h,\xi,s+\tau_h)\right]h_h(\xi;x,s)\,\mathrm{d}\xi \tag{4.1b}$$

where $\wedge$ and $\vee$ represents the minimum and the maximum, respectively and the variables τ_e and τ_h are as before the electron and hole transport time from location x to ξ, respectively, as defined in Section 3.2. The probability density functions $h_e(\xi;x,s)$ and $h_h(\xi;x,s)$ were defined in Section 2.3.2.

The two coupled integral equations can be solved numerically using a simple iterative approach. We note that from the definition of the age-dependent stochastic impulse response, $I_h(t,x,s)$, The stochastic impulse-response function for a hole

injected to the multiplication region at location $x = w$ with age s (as the case of Inp APD) is the same as $I_h(t, w, s)$. Thus the mean impulse response function is then obtained using $i(t, s) = \mathsf{E}\left[I_h(t, w, s)\right] = i_h(t, w, s)$.

4.2 Numerical calculation for the mean impulse response

As before, we selected an InGaAs-InP APD receiver with a multiplication layer of width $w = 200$ nm. The reverse sinusoidal biasing period is set to be equal to 5.5 transit times which is equivalent to 60 GHz transmission speed. The electron and hole saturation velocity are assumed as $v_e = v_h = 0.67 \times 10^7$ cm/s. The sinusoidal-biasing parameters were selected as follows: $B = 13$ V, $C = 6$ V, $\psi = 0$.

The calculation of the age-dependent mean impulse response function for a dynamically biased 200-nm InP multiplication layer is shown in Fig. 4.1 for different values of the age variable s. These curves were obtained by solving the coupled integral in (4.1). Unlike the static-bias case, we observe that the APD's impulse response depends on the arrival time (age) of the parent carrier. For example, when the photon is absorbed at $s = 0.3T_b$ where T_b is the optical-pulse window (note that, the optical-pulse window is 5.5 transit time), the mean gain is 85.6 and the corresponding bandwidth is 79.9 GHz. In contrast, for a photon arriving at $s = 0.9T_b$ of the optical-pulse window, the gain is 1.14 and the bandwidth is 135.2 GHz. This is due to the rise in the field initially, where a high gain is built up, followed by a drop in the field causing the shortening of the impulse response as the probability of the avalanche terminating is high. Figure 4.1 shows that the tail of the impulse response can be approximated by a decaying exponential function with a constant average rate. It is clear from the numerical calculations that the average decay rate

is independent of the carrier age, i.e., regardless of the arriving time of the photon with respect to the dynamic electric field the impulse response function decays at the same average rate.

In what follows, we will use the calculated mean impulse response to find the integrated pulse response and its corresponding eye diagram.

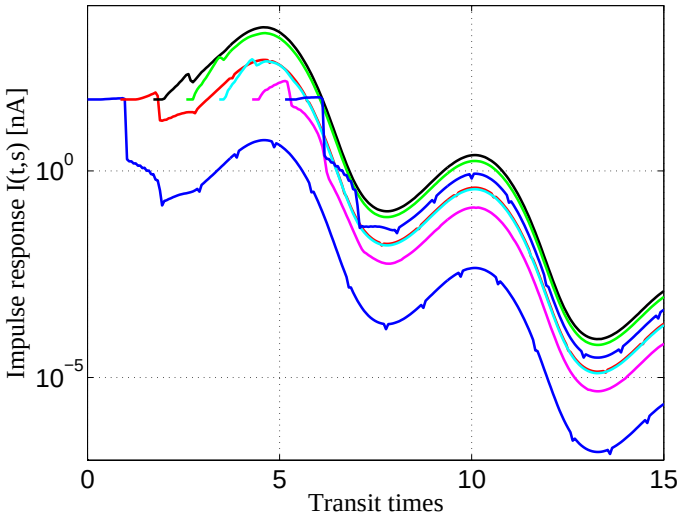

Figure 4.1: Calculated age-dependent impulse response functions of a 200-nm InP APD under 60 GHz sinusoidal dynamic bias. Different curves correspond to different ages (in transit time) of the initiating hole. The dynamic-biasing parameters used are: $B = 13$ V, $C = 6$ V and $\psi = 0$.

4.2.1 The calculated mean pulse response

To see the effect of the dynamic biasing scheme on the ISI, we calculated the mean pulse-response function by integrating the age-dependent impulse responses over the age variable s in the interval $[0, T_b]$. Figure 4.2 shows the calculated mean pulse response of a 200 nm multiplication region InP-based APD, when it is illuminated by a rectangular non-return-to-zero (NRZ) pulse. For simplicity, in this example we assume a uniformly distributed random stream of photons. Two cases are con-

sidered: sinusoidal dynamic bias and a constant reverse bias. In this example the width of the optical pulse is 16.5 ps (consistent with 60-Gb/s NRZ bit stream). The reduction in the tail of the pulse response in the dynamic-bias case is clearly evident compared with that for the constant-bias case. The total mean gain generated by the pulse under dynamic-biasing is 27 and its bandwidth is 80 GHz, giving rise to an average GBP (i.e., the GBP averaged over the age variable s in the interval $[0, T_b]$) of 2,161 GHz, which is compared to 437 GHz in the constant-bias case as pointed out in [25]. This shows that a dynamically biased APD can increase the pulse-response gain-bandwidth product of an APD by a factor of 5. We anticipate even greater improvement when the dynamic bias characteristics are optimized over the peak-to-peak AC value and DC value. Note that the GBP for the constant-bias scheme is larger than that normally reported for a 200-nm InP APD. This is because only buildup-time limitations are considered here and all RC effects are ignored.

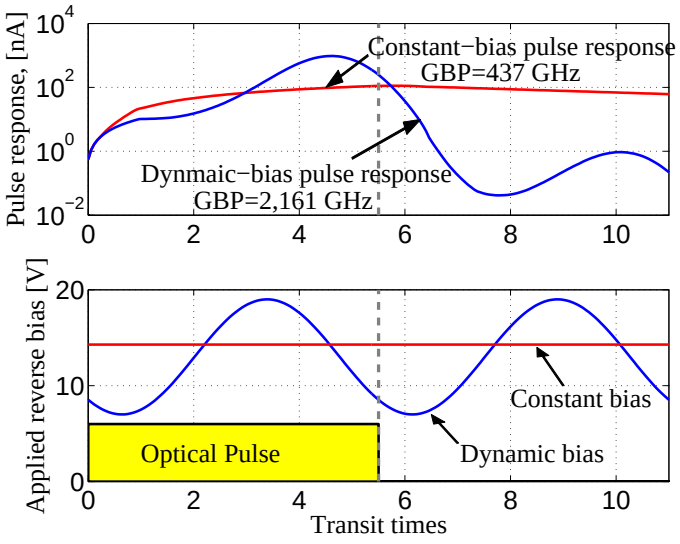

Figure 4.2: Calculated time response to a 16.5-ps rectangular optical pulse of dynamically biased APD, with a sinusoidal-dynamic bias function as shown, and a conventional InP APD. A five-fold enhancement in the GBP is predicted

4.2.2 The calculated eye diagram

By overlaying sweeps of different segments of a long data stream, an eye diagram can be simulated. We consider $2^{13} - 1$ NRZ bits with a pulse width of 25 ps as in a 40-Gb/s NRZ bit stream. Figure 4.3 shows the simulated eye diagram of the 200 nm multiplication region APD, once with the sinusoidal dynamic-field (upper plot) and once with the static reverse bias (lower plot). We observe that in the presence of channel noise, the eye opening of the sinusoidal-bias case is wide open compared to that for the static-bias case. This shows that dynamically biased APD can increase the receiver performance substantially compared to the same APD operated under the conventional static biasing scheme. Note that, the shape of the eye diagram for dynamic bias case is different from that of the conventional OOK NRZ. This result is expected due the nature of dynamic bias APD-based receivers that provide strong avalanche current in the early phase of the optical-pulse window followed by a much weaker impact ionization that terminates the avalanche current with high probability before the start of next bit. This can also be realized in the logarithmic plot of the pulse response depicted in 4.2.

4.3 Photocurrent noise

We now examine the statistics of the electric current, $\mathcal{C}(t)$, produced by an APD operating under dynamic reverse bias generated by a random photoelectron flux with mean ϕ. Note that, the average photon absorption rate can be defined as $\phi = \eta\Phi$, where η is the quantum efficiency of the APD defined as the probability that a single photon incident generates an impulse response and Φ is the photon flux incident on the photodetector. Every photon absorbed that enters the multiplication region generates an impulse response of electric current of charge qG_s and time duration T_s. Therefore, a photon stream incident on an APD results in a stream of electrical

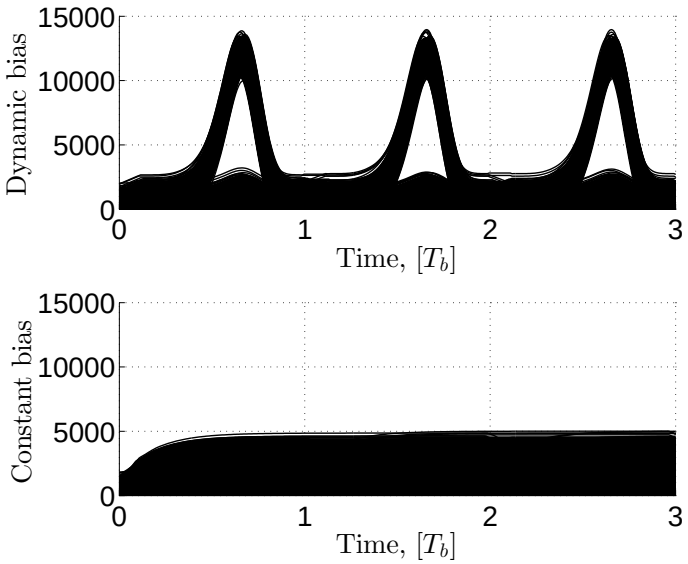

Figure 4.3: The eye diagram of a 200 nm InP dynamically biased APD (upper plot) compared to the traditional biasing APD (lower plot) for an OOK communication system operating at 40 Gb/s.

impulse responses which add together to generate an electric current $\mathcal{C}(t)$. The randomness of the photon stream is transformed into fluctuating electric current. These fluctuations are known as shot noise when the incident photons have Poisson distribution [11]. Moreover, the randomness in the gain generates additional noise characterized by the excess noise factor.

The mean and the variance of the photocurrent generated by an APD has been extensively study it in the literature [11, 61, 62]. However, these results are not applicable when the reverse bias is dynamic. The derivation of the photocurrent mean and variance must be generalized to account for the variation in the electric field.

Assume that a photo-event (absorption of a photon and the creation of an electron-hole pair) generated at time s produces a random impulse response, $I(t, s)$. If the time axis is divided into incremental time intervals Δt, the number of photo-

events in one time-interval follows a Poisson distribution with a mean $\phi\Delta t$. Thus, for a sufficiently small Δt, the Poisson distribution can be approximated by a Binomial distribution where the probability p that a photo-event occurs within an interval is $p = \phi\Delta t$. The electric current is written as

$$\mathcal{C}(t) = \sum_s X_s I(t, s\Delta t), \tag{4.2}$$

where X_s has a value 1 with probability p and 0 otherwise, representing the existence of a photocurrent at the instant $s\Delta t$. The random variables, X_s, are independent with a mean value $\mathsf{E}[X_s] = p$. The mean of the product $X_s X_k$ is p for $s = k$ and p^2 otherwise. The first and second moment of $\mathcal{C}(t)$ become

$$\mathsf{E}[\mathcal{C}(t)] = \sum_s pi(t, s) \tag{4.3}$$

and

$$\begin{aligned}\mathsf{E}\left[\mathcal{C}^2(t)\right] &= \sum_s \sum_k \mathsf{E}[X_s X_k]\,\mathsf{E}[I(t, s\Delta t) I(t, k\Delta t)] \\ &= \sum\sum_{s\neq k} p^2 \mathsf{E}[I(t, s\Delta t)]\,\mathsf{E}[I(t, k\Delta t)] + \sum_s p\mathsf{E}\left[I^2(t, s\Delta t)\right].\end{aligned} \tag{4.4}$$

By substituting $p = \phi\Delta t$ and taking the limit $\Delta t \to 0$, the first and second moment of the photocurrent become

$$\mathsf{E}[\mathcal{C}(t)] = \phi \int_{-\infty}^{\infty} i(t, s) ds = \phi \int_{-\infty}^{t} i(t, s)\,\mathrm{d}s \tag{4.5}$$

and

$$\mathsf{E}\left[\mathcal{C}^2(t)\right] = \left(\phi \int_{-\infty}^{t} i_p(t, s) ds\right)^2 + \phi \int_{-\infty}^{t} i_2(t, s)\,\mathrm{d}s, \tag{4.6}$$

where $i(t, s) = \mathsf{E}[I(t, s)]$ and $i_2(t, s) = \mathsf{E}[I^2(t, s)]$. As a result the variance of $\mathcal{C}(t)$ can be found as follows:

$$\sigma_{\mathcal{C}}^2(t) = \mathsf{E}\left[\mathcal{C}^2(t)\right] - \mathsf{E}\left[\mathcal{C}^2(t)\right]^2 = \phi \int_{-\infty}^{t} i_2(t, s)\,\mathrm{d}s. \tag{4.7}$$

The calculation of the variance of the photocurrent generated by an APD requires knowledge of the second moment of the APD's impulse response $i_2(t,s)$. However, calculation of the second-order statistics of $I(t,s)$ are generally computationally intensive. To overcome this complexity, one approach is to ignore the randomness in the shape of the impulse response function. For example, the variance of the photocurrent was found in [11] by assuming a deterministic shape proportional for the mean impulse response function. Let $\hat{I}(t,s)$ be the simplified impulse response with a deterministic shape such as $\hat{I}(t,s) = G_s h(t-s)$, where G_s is the stochastic gain generated by a photoevent at time s and $h(t)$ is the normalized (with an area q) function that represents the deterministic shape of the impulse response.

Substituting $\hat{I}(t,s)$ in (4.3) and (4.4), the first and second moment of the photocurrent become

$$\mathsf{E}\left[\mathcal{C}(t)\right] = \sum_s p\mathsf{E}\left[G_s\right] h(t - s\Delta t) \tag{4.8}$$

and

$$\mathsf{E}\left[\mathcal{C}^2(t)\right] = \sum\sum_{s\neq k} p^2\mathsf{E}\left[G_s\right]\mathsf{E}\left[G_k\right] h(t-s\Delta t)h(t-k\Delta t) + \sum_s p\mathsf{E}\left[G_s^2\right] h^2(t-s\Delta t). \tag{4.9}$$

As before by taking the limit $\Delta t \to 0$, the simplified variance of the photocurrent can be written as

$$\hat{\sigma}^2(t) = \phi\mathsf{E}\left[G^2(t)\right] * h^2(t), \tag{4.10}$$

where $*$ represents the convolution in t.

4.4 Approximation of the mean impulse response function

Figure 4.1 suggests that the tail of the impulse response can be approximated by a decaying exponential function with a constant average rate, b. It is clear from the numerical calculations that the average decay rate, b, is independent of the carrier age; i.e., regardless of the arriving time of the photon with respect to the dynamic electric field the impulse response function decays at the same average rate. Moreover, the fluctuations in the tail can be ignored because we are interested in the limit of the impulse response, where the average decay rate exponent b dominates the bounded sinusoidal fluctuations, i.e., $e^{-bt+\delta\sin(\omega_b t)} \approx e^{-bt}$ when t is large. With this in mind, we approximate the mean and the second moment of the impulse response as follows:

$$i(t,s) \approx a_s e^{-b(t-s)} \tag{4.11}$$

and

$$i_2(t,s) \approx c_s e^{-b(t-s)}, \tag{4.12}$$

where a_s and c_s are age-dependent coefficients to be determined and b is the average decaying rate of the impulse response (ignoring the fluctuation).

4.4.1 Exploring the parameters a_s and c_s

In this section, we investigate the physical meaning of the parameters a_s and c_s. These parameters can be related to the statistics of the stochastic gain and buildup time. Finding the relation between the impulse response parameters and the age-dependent joint PDF facilitates the derivation of the BER closed-form expressions.

To do so, we consider the area under the mean of the impulse response approximations

$$\int_s^\infty i(t,s)\,\mathrm{d}t \approx \int_s^\infty a_s e^{-b(t-s)}\,\mathrm{d}t = \frac{a_s}{b} \tag{4.13}$$

On the other hand, due to the linearity of the expectation, one could realize that $\int_s^\infty i(t,s)\,\mathrm{d}t$ is equivalent to $\mathsf{E}\left[\int_s^\infty I(t,s)\,\mathrm{d}t\right]$. To evaluate the latter term, $I(t,s)$ can be approximated by a specified shape function. The rationale is to approximate $I(t,s)$ by a function that is parameterized by the age-dependent stochastic gain G_s and the age-dependent stochastic buildup time T_s. An example of such a function is the rectangular–random-duration (RD) with random height qG_s/T_s and random duration T_s, where q is the electronic charge. Note that the area under this function is qG_s. The randomness in the impulse-response function's area represents the gain uncertainty and the randomness in its duration represents the buildup time. This shape significantly simplifies the complexity of the impulse-response function while maintaining the key features that govern the stochastic gain, the excess-noise and speed properties of the APD. Other shapes function may also be considered such as triangular-RD [23]. However for simplicity we will use rectangular-RD approximation. Therefore,

$$\mathsf{E}\left[\int_s^\infty I_p(t,s)\,\mathrm{d}t\right] \approx \mathsf{E}\left[\int_s^\infty q\frac{G_s}{T_s}\left(u(t-s)-u(t-s-T_s)\right)\,\mathrm{d}t\right] \tag{4.14}$$

$$= q\mathsf{E}\left[G_s\right]. \tag{4.15}$$

From (4.13) and (4.15), we can conclude that $a_s = qb\mathsf{E}\left[G_s\right]$. Similarly, the parameter c_s of the second moment, $i_2(t,s)$, can be found as follows:

$$\int_s^\infty i_2(t,s)\,\mathrm{d}t \approx \int_s^\infty c_s e^{-b(t-s)}\,\mathrm{d}t = \frac{c_s}{b}. \tag{4.16}$$

Moreover,

$$\mathsf{E}\left[\int_s^\infty I_p^2(t,s)\,\mathrm{d}t\right] \approx \mathsf{E}\left[\int_s^\infty q^2\frac{G_s^2}{T_s^2}\left(u(t-s)-u(t-s-T_s)\right)\,\mathrm{d}t\right] \tag{4.17}$$

$$= q^2\mathsf{E}\left[\frac{G_s^2}{T_s}\right]. \tag{4.18}$$

As a result, Eq. (4.16) and (4.18) together imply $c_s = q^2 b\mathsf{E}\left[G_s^2/T_s\right]$. Note that the approximation of $I_p(t,s)$ is based on the rectangular parameterized model, which takes into account the stochastic gain, G_s, and the stochastic buildup time, T_s, and the parent carrier age, s. In the next section, We proceed to characterize decaying rate, b, in function of the statistics of the age-dependent joint PDF.

4.4.2 The decaying rate b

We now proceed to characterize the decaying rate factor, b. By comparing the exact and the simplified expression for the photocurrent variance, we can relate the decaying rate to the statistics of the impulse response G_s and T_s.

Note that the dynamic field in the APD multiplication layer is periodic with a period T_b. An initiated carrier with an age s experiences the same electric profile as a carrier with an age $s + kT_b$. The stochastic photocurrent of the receiver output follows a cyclostationary process; the statistical properties of the cyclostationary photocurrent will be periodic in s with a period equal to the dynamic bias period, T_b, including the first and second moment of the impulse response (i.e., $i(t,s) = i(t+kT_b, s+kT_b)$ and $i_2(t,s) = i_2(t+kT_b, s+kT_b)$ for $\forall k \in \mathbb{N}$).

Due to the periodicity in the second moment of the impulse response, the exact photocurrent variance found in (4.7) can be expended as follows:

$$\sigma_C^2(t) = \phi\sum_0^\infty \int_{t-T_b}^t i_2(t+kT_b, s)\,\mathrm{d}s. \tag{4.19}$$

Clearly from (4.7), the photocurrent variance is periodic with the same period as $i_2(t,s)$. Integrating both sides over one period and by flipping the order of integration on the right side, we obtain

$$\int_0^{T_b} \sigma_{\mathcal{C}}^2(t)\,\mathrm{d}t = \phi \int_0^{T_b}\int_s^{\infty} i_2(t,s)\,\mathrm{d}t\,\mathrm{d}s. \tag{4.20}$$

Moreover, a closed-form estimate of the second moment of the APD's impulse-response function can be obtained using the rectangular-RD stochastic models for the impulse-response function introduced in Section 4.4.1. The average photocurrent variance is estimated as follows:

$$\int_0^{T_b} \sigma_{\mathcal{C}}^2(t)\,\mathrm{d}t = \phi q^2 \int_0^{T_b} \mathsf{E}\left[\frac{G_s^2}{T_s}\right]\,\mathrm{d}s. \tag{4.21}$$

Next, we consider the simplified photocurrent variance derived in (4.10). Using the exponential model approximation for the mean impulse response, we evaluate the average simplified photocurrent variance while letting $h(t) = qe^{-bt}$ (as we approximated the shape of the mean impulse response). This leads us to

$$\int_0^{T_b} \hat{\sigma}^2(t)\,\mathrm{d}t = \frac{\phi q^2 b}{2} \int_0^{T_b} \mathsf{E}\left[G_s^2\right]\,\mathrm{d}s. \tag{4.22}$$

Now by comparing the exact and the simplified variance, we relate the decaying rate of the mean impulse response, b, with the statistics of the gain and buildup time as follows:

$$b = \frac{2\int_0^{T_b} \mathsf{E}\left[G_s^2/T_s\right]\,\mathrm{d}s}{\int_0^{T_b} \mathsf{E}\left[G_s^2\right]\,\mathrm{d}s}. \tag{4.23}$$

4.4.3 The approximation result

For the dynamically biased APD, we were able to approximate the statistics of the impulse response function using a rectangular parameterized model as follows:

$$i(t,s) \approx a_s e^{-b(t-s)} \quad \text{and} \quad i_2(t,s) \approx c_s e^{-b(t-s)}, \tag{4.24}$$

where

$$a_s = qb\mathsf{E}\left[G_s\right], \tag{4.25}$$

$$c_s = q^2 b\mathsf{E}\left[G_s^2/T_s\right] \tag{4.26}$$

and

$$b = \frac{2\int_0^{T_b}\mathsf{E}\left[G_s^2/T_s\right]\,\mathrm{d}s}{\int_0^{T_b}\mathsf{E}\left[G_s^2\right]\,\mathrm{d}s}. \tag{4.27}$$

These parameters can be readily evaluated using our knowledge of the age-dependent joint distribution f_{G_s,T_s} obtained in Chapter 3.

We note that for a static-bias case, the dependence on the age variable s will be absent in G_s and T_s, and the parameters a_s, c_s and b of the approximated impulse response statistics collapse to their static-field counterparts reported in [23] [Eqs. (11), (26) and (29)]. In the next section, we use the impulse-response-function approximations described above to determine the receiver performance of an APD operating with a dynamically reversed bias. We particularly investigate the effect of the different bias settings (DC level, peak-to-peak value and phase) on the receiver BER.

4.5 Summary and conclusions

In this chapter, we have determined the asymptotic behavior, and particularly the decay rate, of the mean and variance of the impulse response function of the dynamically biased APD. We approximated the statistics of the impulse response by a simple exponentially decaying function parameterized by the stochastic gain and buildup time. This shape significantly simplifies the complexity of the impulse-response function while maintaining the key features that govern the stochastic gain, the excess-noise and speed properties of the APD.

We also numerically calculated the mean impulse response, the pulse response of an OOK NRZ system and its eye diagram. In [25], Hayat and Ramirez calculated the mean impulse response of a dynamically-biased InP. Their calculations shows that the asymptotic behavior of the tail saturates at a certain value. In this chapter, we recalculated the mean impulse response and we showed that the tail keeps decaying exponentially with an average decaying rate, b, independent of the parent carrier age, s. In the dynamic bias scenario, the tail of the pulse response was significantly reduced compared to the results of those for the constant-bias base. The calculated GBP for dynamically biased APD was found to be 2,161 GHz, which is 5 times larger than the GBP of 437 GHz for the constant bias case. We anticipate even greater improvement when the dynamic bias characteristics are optimized over the peak-to-peak AC value, phase offset and DC value.

Chapter 5

Gaussian Approximation in Analyzing the Performance of Optical Receivers

Before assessing the receiver performance, we need to develop a method to calculate the BER. The analytical calculation of the BER of digital optical receivers that employ APDs is especially challenging due to the presence of ISI and the stochastic nature of avalanche gain and its correlation with the stochastic avalanche buildup time. The BER analysis for a dynamically biased APD have never been reported before. In this chapter, we offer an effective method to approximate the BER with the inclusion of ISI, dead space, Johnsom noise, excess noise, receiver speed, transmission rate for a dynamically biased APD.

5.1 Literature review and contributions

Numerous methods have been developed to approximate the BER. In [81], a procedure was given to numerically compute system performance which uses the nearly exact Webb's approximation of the true Conradi distribution for the APD output. The measured performance of the system was found to be in excellent agreement with the performance predicted. In their model, the ISI was not addressed due to the low transmission speed. However, as it is the case in modern lightwave systems, the transmission rates are large (upwards of 10 Gb/s) and the ISI cannot be neglected. Sun *et al.* [82] developed a method to compute the exact BER based on the moment-generating function (MGF). The effects of ISI as well as the APD's dead space are both included in the analysis. The exact BER was computed by adding the contribution of every photon absorbed by the APD during every bit interval to the receiver output. However, this exact method is computationally expensive and provides no closed-form expression for the BER.

In many cases, a closed-form expression for the BER is required to understand, predict and provide analytical insight for the receiver performance. A closed-form expression for the BER can be found by first conditioning on the past bit pattern; then the BER is calculated by averaging the conditional BER over all possible past bit patterns. This approach, denoted here by the bit-pattern–dependent (PD) approach, was adopted by Ong *et al.* [58, 65] in which the receiver output, conditional on the present and all the past bits, is approximated by a Gaussian random variable. The Gaussian approximation is known to give a good estimate of the BER [66]. On the other hand, to simplify the analysis, another method has been commonly used by conditioning on the current bit while considering the *average* of all possible bit patterns (in place of the individual realizations of bit patterns) to generate the Gaussian distribution of the output [23, 67, 68]. Hence, the receiver output in this approach is bit-pattern–independent (PI), as it depends only on the average past bit

pattern. Due to its simplicity, the PI method has been used to evaluate the APD performance and to give analytical insight for the system behavior in low speed applications. However, the benefit from the simplification comes at the expense of inaccuracy in the BER when ISI is dominant, i.e., when transmission speed is very high as in the OC-192 standard.

This chapter analyzes the closed-form expressions of the BER found using the PI and PD methods and studies their accuracy. To do so, the asymptotic behavior and the analytical bounds of each method are derived. By comparing the results to the numerical computed BER [82], it is found that at high transmission speeds, the PD method can give a much more accurate approximation of the BER than that offered by the PI method. This inaccuracy is negligible for low-speed applications in which the ISI does not have a significant impact on the current bit. Therefore from the asymptotic behavior, we find a photocount threshold that can be used as a decision rule to determine which approach should be used. When the photocount is below the threshold, the PI method can be adopted as a simplified approach. However, after exceeding the photocount threshold, ISI should be properly addressed by conditioning on the entire bit pattern stream as done by the PD approach. The PD method will be used in Chapter 6 to derive close-form expressions for the BER of a dynamically biased APD

5.2 Review of relevant BER models

Consider a typical non-return-to-zero, on-off keying optical communication system incorporating an APD-based integrate-and-dump receiver. When an information bit 1 is transmitted, an optical pulse is transmitted in a time interval of duration T_b; otherwise, no pulse is transmitted. Let B_n denote the input binary sequence representing the binary information in the nth bit ($n = 0$ represents current bit).

Let Γ denote the raw output resulting from the integrate-and-dump receiver (i.e., prior to any decision) [23]. The information (0 or 1) can be detected by comparing Γ to a threshold, θ. Each information bit B_n contributes a term $R_n B_n$ to the receiver output, where R_n is the random variable representing the stochastic receiver output when the nth past bit is a 1 and all other past bits are 0. Thus, the receiver outputs conditioned on the present bit ($B_0 = 0$ or 1), denoted by Γ_0 and Γ_1, respectively, can be expressed as

$$\Gamma_0 = \sum_{n=1}^{\infty} R_n B_n + N \tag{5.1a}$$

and

$$\Gamma_1 = \sum_{n=1}^{\infty} R_n B_n + R_0 + N, \tag{5.1b}$$

where N is the receiver Johnson noise. Note that only the term R_0 conveys information from the current bit. The components R_n, $n \geq 1$, represent the ISI contributions in the receiver output from the earlier bits. Due to the analytical complexity of the exact statistics of R_n, it is customary to model R_n as a Gaussian random variable.

We begin by briefly reviewing the probabilistic model for the conditional receiver outputs, Γ_0 and Γ_1, developed using the PI and PD methods to determine their BERs; these BERs are termed $\mathrm{BER_I}$ and $\mathrm{BER_D}$, respectively. Both the mean and variance of R_n, denoted by μ_n and σ_n^2, respectively, are shown in [58] to be proportional to the average number of photons per bit, n_0. Additionally, they are both exponentially decreasing with the bit order n. More precisely [58],

$$\mu_0 = n_0 \beta_\mu, \tag{5.2a}$$

$$\mu_n = n_0 e^{-\kappa\lambda n} \alpha_\mu \quad (n = 1, 2, \ldots), \tag{5.2b}$$

$$\sigma_0^2 = n_0 \beta_\sigma \tag{5.2c}$$

and

$$\sigma_n^2 = n_0 e^{-\kappa\lambda n} \alpha_\sigma \quad (n = 1, 2, \ldots). \tag{5.2d}$$

The coefficients $\alpha_\mu, \alpha_\sigma, \beta_\mu$ and β_σ are APD-specific system parameters derived in [58] for constant reverse bias as

$$\beta_\mu = \frac{\mathsf{E}[G]}{\kappa\lambda}(\kappa\lambda - 1 + e^{-\kappa\lambda}), \tag{5.3}$$

$$\beta_\sigma = \frac{\mathsf{E}[G]^2 F}{\kappa\lambda}(\kappa\lambda - 2 + 2e^{-\kappa\lambda} + \kappa\lambda e^{-\kappa\lambda}), \tag{5.4}$$

$$\alpha_\mu = \frac{2\mathsf{E}[G]}{\kappa\lambda}(\cosh(\kappa\lambda) - 1) \tag{5.5}$$

and

$$\alpha_\sigma = \frac{\mathsf{E}[G]^2 F}{\kappa\lambda}(e^{-\kappa\lambda} - 1)(1 - \kappa\lambda e^{-\kappa\lambda} - e^{-\kappa\lambda}), \tag{5.6}$$

where brackets represent ensemble average and F is the APD's excess noise factor, defined as $F = \mathsf{E}[G^2]/\mathsf{E}[G]^2$. Sun *et al.* [23] defined the so-called shot-noise-equivalent-bandwidth as $B_{sneq} = \mathsf{E}[G^2/T]/2\mathsf{E}[G]^2 F$, the bandwidth correlation factor as $\kappa = 4B_{sneq}/2\pi B_{3dB}$ and the detector's relative speed as $\lambda = 2\pi B_{3dB} T_b$, where T_b is the bit duration. The ensemble average quantities can be computed using the joint PDF associated with the random variables comprising the APD's stochastic gain, G, and its stochastic avalanche duration time, T, developed in [23]. Note that, these parameters were defined for an APD operating with a constant reverse bias. In the next chapter, we generalize these parameters to include the dynamic biasing approach.

The PI method used in [23] approximates the conditional receiver outputs, Γ_0 and Γ_1, by Gaussian random variables. In particular, $\mathrm{BER_I}$ is computed as [23]

$$\mathrm{BER_I} = \frac{1}{2}\operatorname{erfc}\left(\frac{\mu_{\mathrm{I}|1} - \mu_{\mathrm{I}|0}}{\sqrt{2}\left(\sigma_{\mathrm{I}|0} + \sigma_{\mathrm{I}|1}\right)}\right), \tag{5.7}$$

where $\mu_{\mathrm{I}|0}$ and $\sigma^2_{\mathrm{I}|0}$ denote the mean and variance of the receiver output conditional on the present bit being 0 while assuming the average of all possible patterns, i.e., $B_n = 1/2$ for $n \geq 1$. Moreover, $\mu_{\mathrm{I}|1}$ and $\sigma^2_{\mathrm{I}|1}$ are similar quantities conditional on

the present bit being 1. The expressions for the parameters $\mu_{\mathrm{I}|0}$, $\sigma^2_{\mathrm{I}|0}$, $\mu_{\mathrm{I}|1}$ and $\sigma^2_{\mathrm{I}|1}$ are [23]

$$\mu_{\mathrm{I}|0} = \frac{1}{2}\frac{e^{-\kappa\lambda}}{1-e^{-\kappa\lambda}} n_0 \alpha_\mu, \tag{5.8a}$$

$$\mu_{\mathrm{I}|1} = \mu_{\mathrm{I}|0} + \beta_\mu n_0, \tag{5.8b}$$

$$\sigma^2_{\mathrm{I}|0} = \frac{1}{4}\sum_{n=1}^{\infty}(2\sigma_n^2 + \mu_n^2) + \sigma_N^2 \tag{5.8c}$$

and

$$\sigma^2_{\mathrm{I}|1} = \sigma^2_{\mathrm{I}|0} + n_0\beta_\sigma. \tag{5.8d}$$

The optimal decision threshold, θ that minimizes $\mathrm{BER_I}$ is [16]

$$\theta = \frac{\mu_{\mathrm{I}|1}\sigma_{\mathrm{I}|0} + \mu_{\mathrm{I}|0}\sigma_{\mathrm{I}|1}}{\sigma_{\mathrm{I}|1} + \sigma_{\mathrm{I}|0}}. \tag{5.9}$$

Note that in the PI method, the probability density function of the conditional receiver output has a unimodal distribution.

We next describe the PD method. Instead of assuming a Gaussian PDF for the receiver output conditional on the present bit, Ong *et al.* [58] assume a Gaussian PDF for the receiver output conditional on the present *and the entire past bit stream.* This will lead to a multimodal distribution for the conditional receiver output.

More precisely, for an arbitrary past bit pattern, $I_j \in \{0,1\}^\infty$, the pattern-dependent means and variances of Γ_0 and Γ_1 are given by [58]

$$\mu_{\mathrm{D}|0}(I_j) = \sum_{k=1}^{\infty} u_k(I_j)\mu_k, \tag{5.10a}$$

$$\mu_{\mathrm{D}|1}(I_j) = \mu_{\mathrm{D}|0}(I_j) + \mu_0, \tag{5.10b}$$

$$\sigma^2_{\mathrm{D}|0}(I_j) = \sum_{k=1}^{\infty} u_k(I_j)\sigma_k^2 + \sigma_N^2 \tag{5.10c}$$

and

$$\sigma^2_{\mathrm{D}|1}(I_j) = \sigma^2_{\mathrm{D}|0}(I_j) + \sigma_0^2, \tag{5.10d}$$

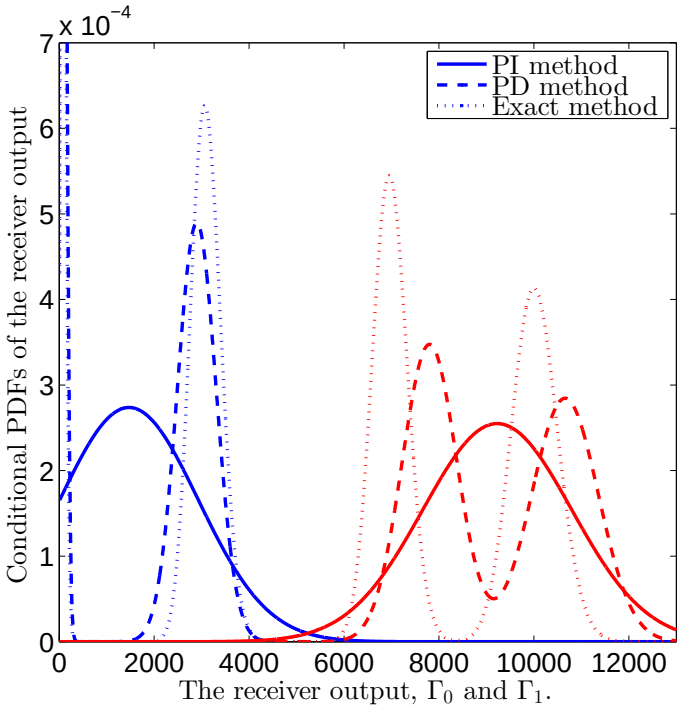

Figure 5.1: PDF of an InP APD receiver output conditioned on the current bit being either 0 (blue curves) or 1 (red curves) for the PI and PD approaches. The exact conditional PDF is also shown for comparison. The average number of photons in a 1 transmitted bit is $n_0 = 1000$.

where $u_k(I_j) = 0$ unless the k-th bit in the pattern I_j is a 1 bit, in which case $u_k(I_j)$ assumes the value 1. To calculate $\mathrm{BER_D}$, Ong *et al.* compute the ensemble average of the pattern-specific BER over all possible past bit patterns: [58]

$$\mathrm{BER_D} = \lim_{L\to\infty} \frac{1}{2^L} \sum_{j=1}^{2^L} \frac{1}{4} \left[\mathrm{erfc}\left(\frac{\theta - \mu_{\mathrm{D}|0}(I_j)}{\sqrt{2}\sigma_{\mathrm{D}|0}(I_j)} \right) + \mathrm{erfc}\left(\frac{\mu_{\mathrm{D}|1}(I_j) - \theta}{\sqrt{2}\sigma_{\mathrm{D}|1}(I_j)} \right) \right], \quad (5.11)$$

where θ is calculated for convenience from (5.9). Note that the optimal threshold, denoted by θ_o, does not have a simple analytical expression in this case because the PDF of the receiver output is a multimodal distribution. However, one can calculate θ_o numerically by finding the intersection point of the conditional PDFs of the receiver output. In the calculations considered in Section 5.4, we evaluate

$\mathrm{BER}_{\mathrm{D,\ opt}}$ using the optimal threshold, θ_o, and compare it to $\mathrm{BER}_{\mathrm{D}}$, which uses the threshold θ.

Figure 5.1 shows an example of the conditional PDFs calculated for an InP-based APD with 100-nm multiplication layer. An electric field of 10.5 kV/cm was assumed in the multiplication layer, corresponding to an average gain of 10.3 and a buildup-time–limited 3-dB bandwidth of 29 GHz. The PDFs of Γ_0 and Γ_1 for the PI and PD approaches are compared to the exact PDFs found in [82]. Figure 5.1 foretells that the PD method yields a better approximation of the exact PDF compared to the PI approach. Also, it is clear from the figure that $\mathrm{BER}_{\mathrm{D}}$ (as well as the exact BER) outperforms $\mathrm{BER}_{\mathrm{I}}$ since the PDFs of the PI method are larger than that for the PD (and the exact) method in the vicinity of the decision threshold, θ.

5.3 Asymptotic analysis of the BER

We now compare $\mathrm{BER}_{\mathrm{I}}$ and $\mathrm{BER}_{\mathrm{D}}$ for large n_0.

Theorem 1. $\lim_{n_0\to\infty} \mathrm{BER}_I$ *is a constant whereas* BER_D *decays exponentially in* n_0. *Moreover, when* n_0 *exceeds the threshold*

$$n_{th} \equiv -\frac{1}{c_2^2} \ln\left[\sqrt{\pi}\,\mathrm{erfc}\left(\frac{\beta_\mu\sqrt{1-e^{-2\kappa\lambda}}}{\sqrt{2}e^{-\kappa\lambda}\alpha_\mu}\right)\right], \tag{5.12}$$

where c_2 *is defined in* (5.17), *then* $\mathrm{BER}_I - \mathrm{BER}_D > r(n_0)$, *where* $r(n_0)$ *is a monotonically increasing positive function converging to* $\lim_{n_0\to\infty} \mathrm{BER}_I$.

Proof. Consider the case for which the current bit is 0; in this case and for large n_0,

$$\sigma_{\mathrm{I}|0}^2 \sim \frac{1}{4}\frac{e^{-2\kappa\lambda}}{1-e^{-2\kappa\lambda}}\alpha_\mu^2 n_0^2. \tag{5.13}$$

Similarly, for the case when the current bit is 1, it can be shown that $\sigma_{\mathrm{I}|1}^2 \sim \sigma_{\mathrm{I}|0}^2$ when n_0 is large. Substituting these results in the error probability found in (5.7),

we obtain

$$\lim_{n_0\to\infty} \mathrm{BER_I} = \frac{1}{2}\,\mathrm{erfc}\left(\frac{\beta_\mu\sqrt{1-e^{-2\kappa\lambda}}}{\sqrt{2}e^{-\kappa\lambda}\alpha_\mu}\right). \tag{5.14}$$

Thus, $\mathrm{BER_I}$ is asymptotically independent of n_0 and it saturates to a predetermined constant.

Next, we find the upper bound, $U(n_0)$, for $\mathrm{BER_D}$ and describe its asymptotic behavior. This is done by considering the worst (maximum error) bit-pattern scenario. Consider the first term in (5.11), which represents the probability of falsely announcing 1 when the current bit is 0. This term is maximized when all the past bits are 1. Similarly, the second term in (5.11), which represents the probability of falsely announcing 0 when the current bit is 1, is maximized when all the past bits are 0. By replacing these worst-case scenarios in (5.11), we obtain the following upper bound for $\mathrm{BER_D}$:

$$\mathrm{BER_D} \le \frac{1}{4}\left[\mathrm{erfc}\left(\frac{\theta-\sum_{n=1}^{\infty}\mu_n}{\sqrt{2\sum_{n=1}^{\infty}\sigma_n^2}}\right)+\mathrm{erfc}\left(\frac{\mu_0-\theta}{\sqrt{2\sum_{n=0}^{\infty}\sigma_n^2}}\right)\right]. \tag{5.15}$$

Using the upper bound $\mathrm{erfc}(x) < \frac{2}{\sqrt{\pi}}\frac{e^{-x^2}}{x+\sqrt{x^2+\frac{4}{\pi}}}$ [83], we further obtain

$$\mathrm{BER_D} < \frac{1}{4\sqrt{\pi}}\left(\frac{e^{-c_1^2 n_0}}{c_1\sqrt{n_0}}+\frac{e^{-c_2^2 n_0}}{c_2\sqrt{n_0}}\right) \equiv U(n_0), \tag{5.16}$$

where c_1 and c_2 are defined as

$$c_1 = \frac{\frac{1}{2}\beta_\mu - \frac{e^{-\kappa\lambda}}{2(1-e^{-\kappa\lambda})}\alpha_\mu}{\sqrt{2\frac{e^{-\kappa\lambda}}{1-e^{-\kappa\lambda}}\alpha_\sigma}} \text{ and } c_2 = \frac{\frac{1}{2}\beta_\mu - \frac{e^{-\kappa\lambda}}{2(1-e^{-\kappa\lambda})}\alpha_\mu}{\sqrt{2\left(\beta_\sigma+\frac{e^{-\kappa\lambda}}{1-e^{-\kappa\lambda}}\alpha_\sigma\right)}}. \tag{5.17}$$

Similarly, to find a lower bound for $\mathrm{BER_D}$, we consider the best (minimum error) past-bit scenarios (a past-bit stream of all 0s when considering the probability of falsely announcing 1 and a past-bit stream of all 1s when considering the probability

of falsely announcing 0). By using these best-case scenarios in conjunction with the lower bound $\text{erfc}(x) > \frac{2}{\sqrt{\pi}} \frac{e^{-x^2}}{x+\sqrt{x^2+2}}$ [83], it can be shown that

$$\text{BER}_{\text{D}} > \frac{1}{4\sqrt{\pi}} \frac{e^{-c_0^2 n_0}}{c_0 \sqrt{n_0}}, \tag{5.18}$$

where $c_0 = {}^{\beta_\mu}/_{2\sqrt{2\beta_\sigma}}$. Therefore, unlike BER_{I}, BER_{D} decays exponentially with respect to the average photon count n_0 since its upper and lower bounds decay exponentially in n_0.

Next, consider the intersection point between $\lim_{n_0 \to \infty} \text{BER}_{\text{I}}$ and $U(n_0)$, which can be approximated for large n_0 using

$$n_{th} \equiv -\frac{1}{c_2^2} \ln \left[\sqrt{\pi}\, \text{erfc} \left(\frac{\beta_\mu \sqrt{1 - e^{-2\kappa\lambda}}}{\sqrt{2} e^{-\kappa\lambda} \alpha_\mu} \right) \right]. \tag{5.19}$$

Note that when $n_0 > n_{th}$, $\text{BER}_{\text{I}} > \text{BER}_{\text{D}}$; furthermore, $\text{BER}_{\text{I}} - \text{BER}_{\text{D}} > r(n_0)$ where $r(n_0) = \lim_{n_0 \to \infty} \text{BER}_{\text{I}} - U(n_0)$. Clearly, $r(n_0)$ is a monotonically increasing function in n_0 with $\lim_{n_0 \to \infty} r(n_0) = \lim_{n_0 \to \infty} \text{BER}_{\text{I}}$.

□

5.4 Numerical results

In our calculations, we selected an InP-based APD receiver with a 100-nm multiplication layer and an electric field of 10.5 kV/cm. The system parameters, calculated numerically using the renewal theory approach [23], are $\alpha_\mu = 97.49$, $\alpha_\sigma = 5.5 \times 10^3$, $\beta_\mu = 7.76$ and $\beta_\sigma = 325.4$. The behavior of BER_{I}, BER_{D} and $\text{BER}_{\text{D, opt}}$, are shown in Fig. 5.2 and Fig. 5.3 for two transmission rates, 10 GHz and 30 GHz. We compare the results to the exact BER calculated using the MGF approach [82]. The numerical results suggest that at low transmission rates, the PI method gives a good estimate of the BER. However, at 30 Gb/s, ISI becomes crucial to the BER and

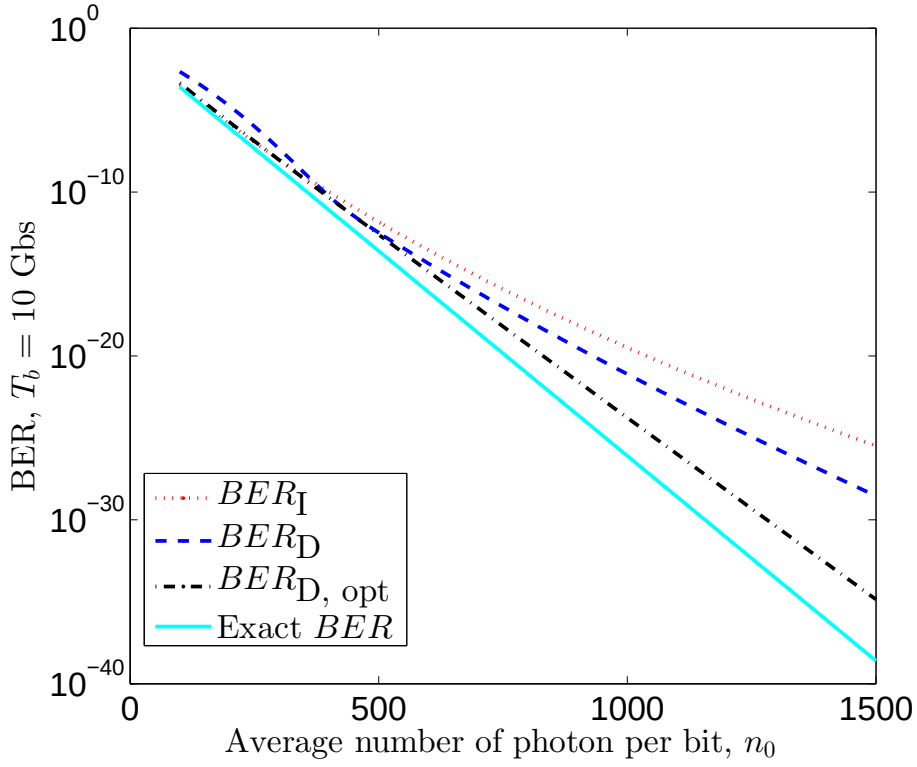

Figure 5.2: The BER of an InP-based optical receiver at a transmission rate of 10 Gb/s using the two approximation methods compared to the exact BER. In the PD method, the optimal threshold, θ_o, was considered in addition to the suboptimal threshold, θ.

the PI method deviates from the exact BER and saturates at high optical powers as the asymptotic analysis predicted. On the other hand, for the PD method, both $\mathrm{BER_D}$ and $\mathrm{BER_{D,\ opt}}$ decay exponentially and follow the exact BER. Therefore, we conclude that the PD method offers a better approximation to the exact BER than the PI method at high transmission rates.

The asymptotic analysis found in Section 5.3 is included in Fig. 5.3. The intersection point of the asymptotic lines, $n_{th} \approx 1500$, which can also be found from (5.12), guarantees that $\mathrm{BER_I} - \mathrm{BER_D} > r(n_0)$ when $n_0 > n_{th}$. Figure 5.4 illustrates $\mathrm{BER_I} - \mathrm{BER_D}$ at different transmission speeds. It is observed that the dis-

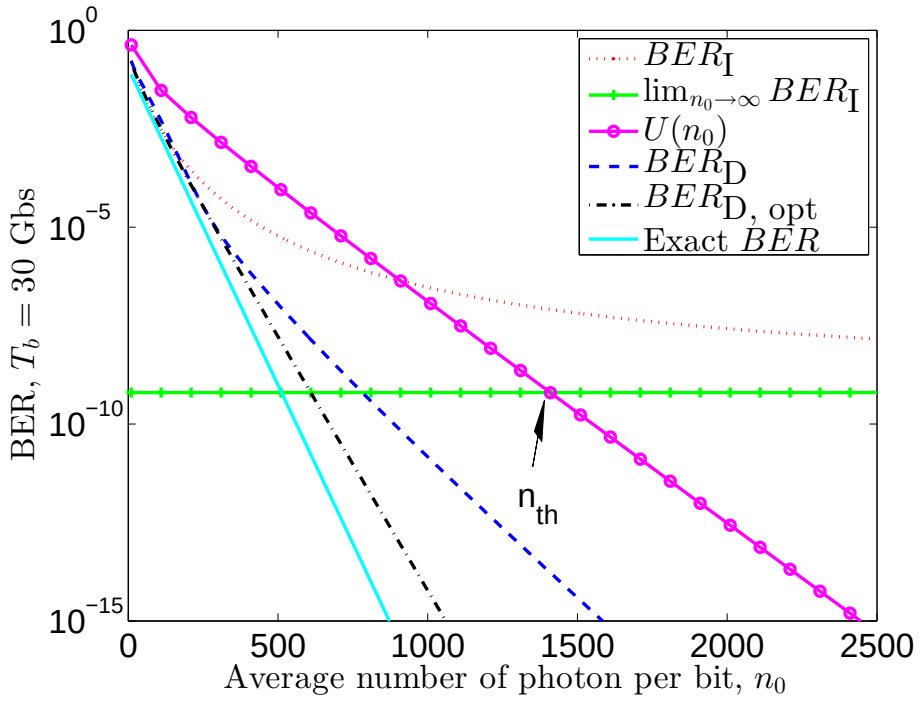

Figure 5.3: The BER of an InP-based optical receiver at a transmission rate of 30 Gb/s using the two approximation methods compared to the exact BER. In the PD method, the optimal threshold, θ_o, was considered in addition to the suboptimal threshold, θ.

crepancy between $\mathrm{BER_I}$ and $\mathrm{BER_D}$ widens with the transmission rate. At lower transmission rates such as 10 Gb/s, where ISI is not severe, the PI and PD methods are almost equivalent. However, at higher transmission rates, e.g., $R = 30$ Gb/s, $\mathrm{BER_I} - \mathrm{BER_D} = 2.9 \times 10^{-7}$ when $n_0 = 1000$, and $\mathrm{BER_I} - \mathrm{BER_D} = 6.6 \times 10^{-8}$ when $n_0 = 1500$.

5.5 Summary and conclusions

This chapter provides a rigorous comparison of two commonly used BER approximations for APD-based optical receivers. The analysis has been supported with

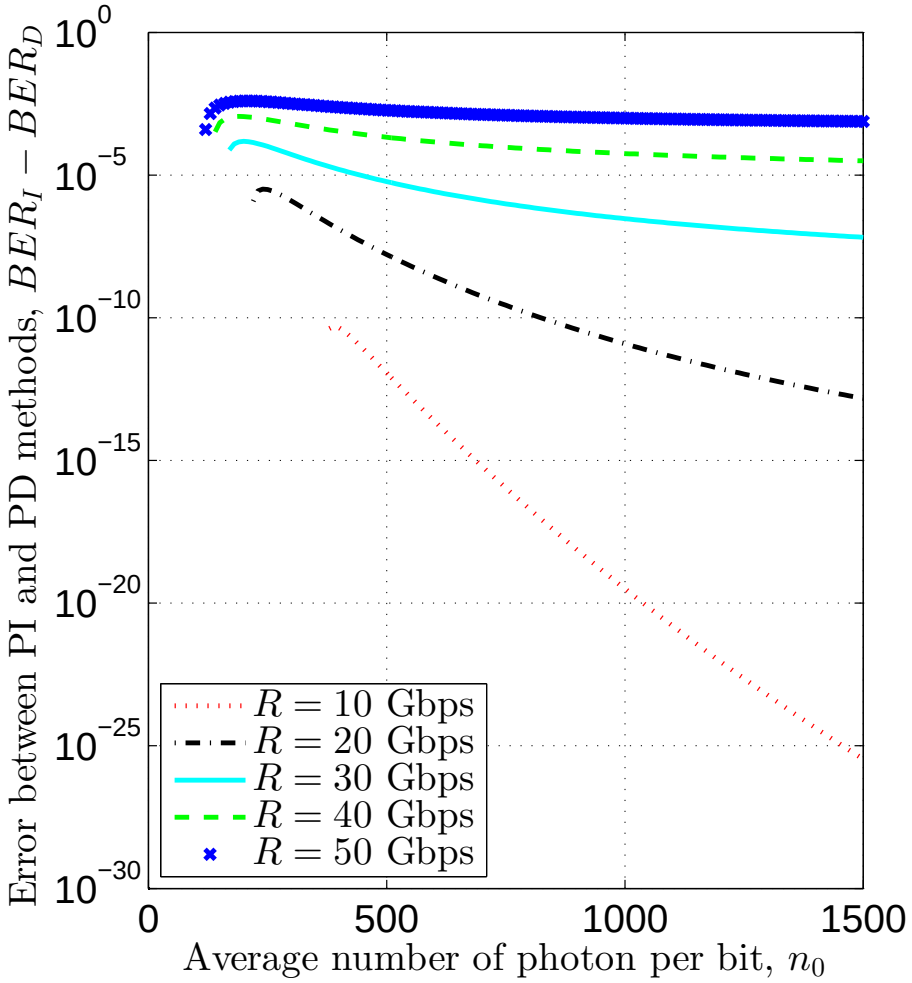

Figure 5.4: The discrepancy, $\mathrm{BER_I} - \mathrm{BER_D}$, between the PI and PD approximation methods for different transmission rates.

examples and compared to the numerical BER found using the MGF approach. When ISI is dominant, the PI method overestimates the BER substantially and the PD method should be used instead. The BER of the PD method decreases exponentially with the optical energy in each bit while the BER computed using the simplified PI method saturates to a constant as the optical energy per bit increases. A closed-form expression was found for a threshold value, n_{th}, for the average number of photons per 1 bit beyond which the PD method should be used instead of

the PI method. As an example, the numerical calculations show that the BER of an optical receiver utilizing InP APD with a 100 nm multiplication layer, cannot be approximated with the PI method when the system speed exceeds 20 Gb/s.

Chapter 6

Performance Analysis of a Dynamically Biased APD Receiver

In this chapter, we develop for the first time closed-form expression for the BER of an APD-based receiver operating under dynamic biasing. Since we are particularly interested in the performance at high transmission speeds, it is important to clearly identify ISI and carefully model it using the tools discussed in Chapter 5. We will use the PD method where we consider an arbitrary past bit pattern of length L bits and calculate the mean and the variance of the photocurrent and the receiver output conditional on the value of the current bit. This is done by adding up the contributions from each of the ISI terms from the past bits in the pattern. Next, by averaging over all possible past bit-patterns, we determine the average BER. The BER is then used to calculate the receiver sensitivity. To enable that, we develop expressions for the statistics of the integrate-and-dump receiver output. We investigate the effect of the dynamic reverse bias on the performance of an APD-based receiver in a direct-detection OOK optical communication system. The analysis developed here offer a closed form expressions for the mean and variance of the receiver's output, with well-defined parameters that capture ISI, Johnson noise, excess noise, detector speed

and transmission speed. These expressions will be further generalized to include the band-to-band tunneling effect in Chapter 7.

6.1 Output of an integrate-and-dump receiver

Consider a modulated optical photon stream with a bit duration T_b. The photocurrent generated by APD-based receiver operated under dynamic bias is denoted by $\mathcal{C}(t)$. Let the time axis be divided into time intervals Δt. Consider the scenario for which the nth past bit is a "1" bit and all other past bits are "0"bits (including the present bit). More precisely, if we assume that the nth past bit extends from $-nT_b$ to $-(n-1)T_b$, then the photocurrent generated by the photons that had arrived in the nth bit, for $n = 1, 2, \cdots$, is

$$\mathcal{C}_n(t) = \sum_{-nT_b \le s\Delta t < -(n-1)T_b} X_s I(t, s\Delta t), \tag{6.1}$$

where, as before, X_s has a value 1 with probability $p = \phi\Delta t$ and 0 otherwise.

The photocurrent is fed into a bit integrator synchronized with the optical stream. The resultant output is used to detect the information modulated with the incident optical stream. Let Γ_n be the integrate-and-dump receiver output when $\mathcal{C}_n(t)$ is the receiver photocurrent. The integral of the nth bit photocurrent over the bit duration T_b is therefore

$$\Gamma_n = \int_0^{T_b} \mathcal{C}_n(t)\,\mathrm{d}t = \int_0^{T_b} \sum_{-nT_b \le s\Delta t < -(n-1)T_b} X_s I(t, s\Delta t)\,\mathrm{d}t. \tag{6.2}$$

By taking the limit $\Delta \to 0$, the mean value of the receiver output can be calculated by

$$\mathsf{E}\left[\Gamma_n\right] = \phi \int_0^{T_b} \int_{-nT_b}^{-(n-1)T_b} i(t, s)\,\mathrm{d}s\,\mathrm{d}t, \tag{6.3}$$

where $i(t, s)$ is the mean of the impulse response $I(t, s)$.

It was shown earlier that the mean impulse response can be approximated by an exponential decaying function of the form $i(t,s) = a_s e^{-b(t-s)}$, where a_s and b are be found using the rectangular-RD approach as described in Section 4.4.1. Note that, a_s and c_s are in function of the statistics of the buildup time and gain buildup time and gain statistics. Unlike the static case, the statistics of the buildup time and gain of an APD operating under dynamic reverse bias will vary cyclically with time with a period equal to the dynamic field period. therefore, a_s is periodic in s with a period equal to bit duration and to the dynamic reverse voltage period T_b. Using the Fourier series expansion, a_s can be rewritten as follows:

$$a_s = \sum_{k=-\infty}^{\infty} A_k e^{j2\pi k f_b s}, \tag{6.4}$$

where f_b is the transmission rate ($f_b = 1/T_b$) and A_k are the fourier series coefficient defined as $A_k = 1/T_b \int_0^{T_b} a_s e^{-j2\pi k f_b s}\,\mathrm{d}s$. Thus, the mean of the nth bit photocurrent output becomes

$$\mu_n = \mathsf{E}\left[\Gamma_n\right] = \frac{\phi e^{-nbT_b}}{b}\left(e^{bT_b} + e^{-bT_b} - 2\right)\sum_{k=-\infty}^{\infty} \frac{A_k}{j2\pi k f_b + b} \qquad \text{for } n = 1, 2, \cdots. \tag{6.5}$$

To calculate the variance of Γ_n, we utilize the cyclostationary stochastic photocurrent analysis shown in Section 4.3. This yields us to

$$\sigma_n^2 = \phi \int_0^{T_b}\int_0^{T_b}\int_{-nT_b}^{-(n-1)T_b} R_I(t_1, t_2, s)\,\mathrm{d}s\,\mathrm{d}t_1\,\mathrm{d}t_2 \qquad \text{for } n = 1, 2, \cdots, \tag{6.6}$$

where $R_I(t_1, t_2, s)$ is the autocorrelation function of the impulse response $I(t,s)$, defined as $R_I(t_1, t_2, s) = \mathsf{E}\left[I(t_1, s)I(t_2, s)\right]$.

Using the rectangular-RD model, we can approximate the autocorrelation function by

$$R_I(t_1, t_2, s) = \mathsf{E}\left[\frac{G_s}{T_s}u(t_1 - s)u(t_1 - s - T_s) \times \frac{G_s}{T_s}u(t_2 - s)u(t_2 - s - T_s)\right], \tag{6.7}$$

where $u(t)$ is the unit step function. Note that the right hand side is zero unless $T_s \geq (t_1 \vee t_2) - s$, where the notation $t_1 \vee t_2$ denotes the maximum between t_1 and t_2.

Therefore, using the joint probability density function of G_s and T_s we can evaluate the autocorrelation function as follows:

$$R_I(t_1, t_2, s) = \sum_{m=1}^{\infty} \int_{(t_1 \vee t_2)-s}^{\infty} \frac{m^2}{\tau^2} \frac{\partial}{\partial \tau} f_{G_s,T_s}(m, \tau, s)\, \mathrm{d}\tau, \tag{6.8}$$

Moreover when $t_1 = t_2 = t$, the autocorrelation function collapses to the second moment of the impulse response function and becomes

$$R_I(t, t, s) = \mathsf{E}\left[I^2(t, s)\right] = \sum_{m=1}^{\infty} \int_{t-s}^{\infty} \frac{m^2}{\tau^2} \frac{\partial}{\partial \tau} f_{G_s,T_s}(m, \tau, s)\, \mathrm{d}\tau. \tag{6.9}$$

Therefore, using the second moment approximation $i_2(t, s) = c_s e^{-b(t-s)}$, the autocorrelation will have a similar behavior and it can be approximated by

$$R_I(t_1, t_2, s) = c_s e^{-b[(t_1 \vee t_2)-s]}. \tag{6.10}$$

As before, due to the periodicity of c_s in s, the autocorrelation function can be decomposed into sum of complex exponentials functions, i.e., $c_s = \sum_{k=-\infty}^{\infty} C_k e^{j2\pi k f_b s}$, and C_k are the Fourier series coefficients with $C_k = 1/T_b \int_0^{T_b} c_s e^{-j2\pi k f_b s}\, \mathrm{d}s$. Finally, we substitute the autocorrelation function approximation in σ_n^2 to get

$$\sigma_n^2 = \frac{2\phi}{b^2} e^{-nbT_b} \left(e^{bT_b} - 1\right) \left(1 - e^{-bT_b} - bT_b e^{-bT_b}\right) \sum_{k=-\infty}^{\infty} \frac{C_k}{b + j2\pi k f_b} \quad \text{for } n = 1, 2, \cdots. \tag{6.11}$$

In what follow, we consider the PD method described in Chapter 5, which dictates that the receiver output, conditional on the state of the present bit and the entire past bit stream, I_j, is a Gaussian random variable. We then compute the BER conditional on the entire past bit stream, and then average the resulting pattern-specific BERs over all possible past bit patterns and obtain the overall average BER.

Consider an arbitrary past bit-pattern, I_j, of length L representing the transmitted information. It is known that the avalanche duration, T_s, is finite almost surely

as long as the electric field is below the avalanche breakdown condition (as in our case). Therefore, the bit-length parameter, L , can be chosen to be sufficiently large to capture all the previous bits that has significant impacts on the current output. An appropriate value of L can be determined by trial and error. To calculate the mean of the receiver output for the bit pattern I_j when the present bit is zero, we add up the contributions from each non-zero past bits in the pattern, this yields the expression

$$\mu_{\Gamma|0}(I_j) = \sum_{n=1}^{2^L} u_n(I_j)\mu_n, \tag{6.12}$$

where $u_n(I_j)$ is 1 when the nth bit in the pattern I_j is a "1" bit and 0 otherwise.

Similarly, one can calculate the variance of the receiver output associated with the pattern I_j while conditioning on the first bit being 0 bit by adding up the contributions from the non-zero past bits as well as contribution from Johnson noise and obtain

$$\sigma^2_{\Gamma|0}(I_j) = \sum_{n=1}^{2^L} u_n(I_j)\sigma_n^2 + \sigma_J^2. \tag{6.13}$$

The statistics of the receiver output when the present bit is 1 is found by adding to $\mu_{\Gamma|0}$ and $\sigma^2_{\Gamma|0}$ the contributions from the photons in the present bit. The contribution to the mean of the receiver output from the photons available in the present bit (for $n = 0$) is

$$\begin{aligned}\mu_0 &= \phi \int_0^{T_b} \int_0^t i(t,s)\,\mathrm{d}s\,\mathrm{d}t \\ &= \phi\frac{A_0}{b^2}\left(bT_b - 1 + e^{-bT_b}\right) + \phi \sum_{\substack{k=-\infty \\ k\neq 0}}^{\infty} \frac{A_k}{b\left(j2\pi k f_b + b\right)}\left(e^{bT_b} - 1\right).\end{aligned} \tag{6.14}$$

The contribution to the variance of the receiver output from the photons available

in the present bit is

$$\begin{aligned}\sigma_0^2 &= \phi \int_0^{T_b} \int_0^{T_b} \int_0^{t_1 \wedge t_2} R_I(t_1, t_2, s)\, \mathrm{d}s\, \mathrm{d}t_1\, \mathrm{d}t_2 \\ &= \phi \frac{2C_0}{b^3} \left[bT_b + bT_b e^{-bT_b} + 2e^{-bT_b} - 2 \right] + \\ &\quad \phi \sum_{\substack{k=-\infty \\ k \neq 0}}^{\infty} \frac{C_k}{b + j2\pi f_b k} \left[\frac{2e^{-bT_b} - 2}{b(b + j2\pi f_b k)} + 2\frac{bT_b e^{-bT_b} + e^{-bT_b} - 1}{b^2} \right]. \end{aligned} \tag{6.15}$$

When we combine these components (μ_0 and σ_0^2) with the contribution from the previous bits (μ_n and σ_n^2 for $n = 1, 2, \cdots$), we obtain the mean and the variance of the receiver output associated with the pattern I_j conditioning on the present bit being 1, i.e.,

$$\mu_{\Gamma|1}(I_j) = \mu_{\Gamma|0}(I_j) + \mu_0 \tag{6.16}$$

and

$$\sigma_{\Gamma|1}^2(I_j) = \sigma_{\Gamma|0}^2(I_j) + \sigma_0^2. \tag{6.17}$$

A common approximation for the receiver output is the Gaussian distribution. By conditioning on the transmitted bit, the conditional probability for a specific pattern I_j, is therefore

$$f_0(x, I_j) = \frac{1}{\sigma_{\Gamma|0}(I_j)\sqrt{2\pi}} \exp\left\{ -\frac{(x - \mu_{\Gamma|0}(I_j))^2}{2\sigma_{\Gamma|0}^2(I_j)} \right\} \tag{6.18}$$

and

$$f_1(x, I_j) = \frac{1}{\sigma_{\Gamma|1}(I_j)\sqrt{2\pi}} \exp\left\{ -\frac{(x - \mu_{\Gamma|1}(I_j))^2}{2\sigma_{\Gamma|1}^2(I_j)} \right\}. \tag{6.19}$$

Next, for every pattern, I_j, we calculate the pattern-specific BER as follows:

$$\mathrm{BER}(I_j) = \frac{1}{4} \left[\mathrm{erfc}\left(\frac{\theta - \mu_{\Gamma|0}(I_j)}{\sigma_{\Gamma|0}\sqrt{2}} \right) + \mathrm{erfc}\left(\frac{\mu_{\Gamma|1}(I_j) - \theta}{\sigma_{\Gamma|1}\sqrt{2}} \right) \right], \tag{6.20}$$

where θ is the decision threshold. In practice, θ is optimized to minimize the overall BER. In the next section, we show an efficient method to determine θ.

By assuming an equiprobable distribution on the bits priors, the overall BER is calculated by averaging over all possible bit patterns. More precisely,

$$\mathrm{BER} = \frac{1}{2^L} \sum_{j=1}^{2^L} \mathrm{BER}(I_j). \tag{6.21}$$

6.2 The decision threshold, θ

The derivation of the BER expressions involves the computation of the decision threshold, θ, i.e., the optimized threshold that minimizes the overall BER. To the best of our knowledge, there is no analytical expression for the optimal decision threshold when the BER is of the form defined in (6.21), since it is impossible to obtain analytically. However, the optimal decision threshold can be obtained numerically by finding the maximum likelihood based on the conditional PDFs of the receiver output obtained as follows:

$$f_0(x) = \sum_{j=1}^{2^L} f_0(x, I_j) = \sum_{j=1}^{2^L} \frac{1}{\sigma_{\Gamma|0}(I_j)\sqrt{2\pi}} \exp\left\{ -\frac{(x - \mu_{\Gamma|0}(I_j))^2}{2\sigma^2_{\Gamma|0}(I_j)} \right\} \tag{6.22a}$$

and

$$f_1(x) = \sum_{j=1}^{2^L} f_1(x, I_j) = \sum_{j=1}^{2^L} \frac{1}{\sigma_{\Gamma|1}(I_j)\sqrt{2\pi}} \exp\left\{ -\frac{(x - \mu_{\Gamma|1}(I_j))^2}{2\sigma^2_{\Gamma|1}(I_j)} \right\}. \tag{6.22b}$$

The optimal decision threshold can be approximated by considering the average past bit patter, $\hat{I} = \{1/2, \cdots, 1/2\}$ instead of the actual past bit-pattern I_j [24, 58]. As a result, the PDFs of the receiver output conditioned on the present bit defined in (6.22) is simplified to a Gaussian distribution with mean $\mu_{\Gamma|i}(\hat{I})$ and variance $\sigma_{\Gamma|i}(\hat{I})$ where $i \in \{0, 1\}$. However, this method oversimplifies the conditional PDFs and deviates from the optimal decision threshold when the ISI is dominant.

A better approximation for the optimal decision threshold is found by investigating the first derivative of the BER. The derivative of the BER with respect to the decision threshold follows immediately from the definition of the error function. To find the minimum BER, we set $\frac{\mathrm{dBER}}{\mathrm{d}\theta} = 0$. As a result,

$$\sum_{j=1}^{2^L} e^{-\frac{\left(\mu_{\Gamma|1}(I_j)-\theta\right)^2}{2\sigma^2_{\Gamma|1}(I_j)}} / \sigma_{\Gamma|1}(I_j) = \sum_{j=1}^{2^L} e^{-\frac{\left(\theta-\mu_{\Gamma|0}(I_j)\right)^2}{2\sigma^2_{\Gamma|0}(I_j)}} / \sigma_{\Gamma|0}(I_j). \tag{6.23}$$

However, the obtained result cannot be solved analytically. Let $\overline{I} = \arg\max_{I_j} \mu_{\Gamma|0}(I_j)$ and $\underline{I} = \arg\min_{I_j} \mu_{\Gamma|1}(I_j)$. It is clear that, the left hand side of (6.23) is dominated by the exponent $\left(\mu_{\Gamma|1}(\underline{I}) - \theta\right)^2 / 2\sigma^2_{\Gamma|1}(\underline{I})$ and the right hand side is dominated by $\left(\theta - \mu_{\Gamma|0}(\overline{I})\right)^2 / 2\sigma^2_{\Gamma|0}(\overline{I})$. Thus by equating the dominant terms, the decision threshold $\hat{\theta}$ can be approximated as follows:

$$\hat{\theta} = \frac{\sigma_{\Gamma|0}(\overline{I})\mu_{\Gamma|1}(\underline{I}) + \sigma_{\Gamma|1}(\underline{I})\mu_{\Gamma|0}(\overline{I})}{\sigma_{\Gamma|0}(\overline{I}) + \sigma_{\Gamma|1}(\underline{I})}. \tag{6.24}$$

6.3 The algorithm to compute the BER

In this section, we describe the algorithm to calculate the overall BER. We first select a sufficiently large bit length parameter, L. We then compute the nth bit statistics in the receiver output as described in (6.5) and (6.11) for $n = 1, 2, \cdots, L$. Next, we consider all the 2^L possible bit pattern I_j. For each I_j, we calculate the pattern specific mean, $\mu_{\Gamma|0}(I_j)$, and variance, $\sigma_{\Gamma|0}(I_j)$, of the integrate-and-dump receiver output when the present bit is "0" using (6.12) and (6.13), respectively. To find the receiver output statistics when the present bit is "1," we add the mean μ_0 [Eq. (6.14)] and the variance σ_0 [Eq. (6.15)] to $\mu_{\Gamma|0}(I_j)$ and $\sigma_{\Gamma|0}(I_j)$ found earlier. The pattern-specific BER can be then calculated using the decision threshold, θ and the statistics of the receiver output $\mu_{\Gamma|0}$, $\mu_{\Gamma|1}$, $\sigma_{\Gamma|0}$ and $\sigma_{\Gamma|1}$ following (6.20). Finally, the overall BER is computed by averaging over all possible bit patters. A flowchart is presented in Fig. 6.1 to describe the model to compute the overall BER.

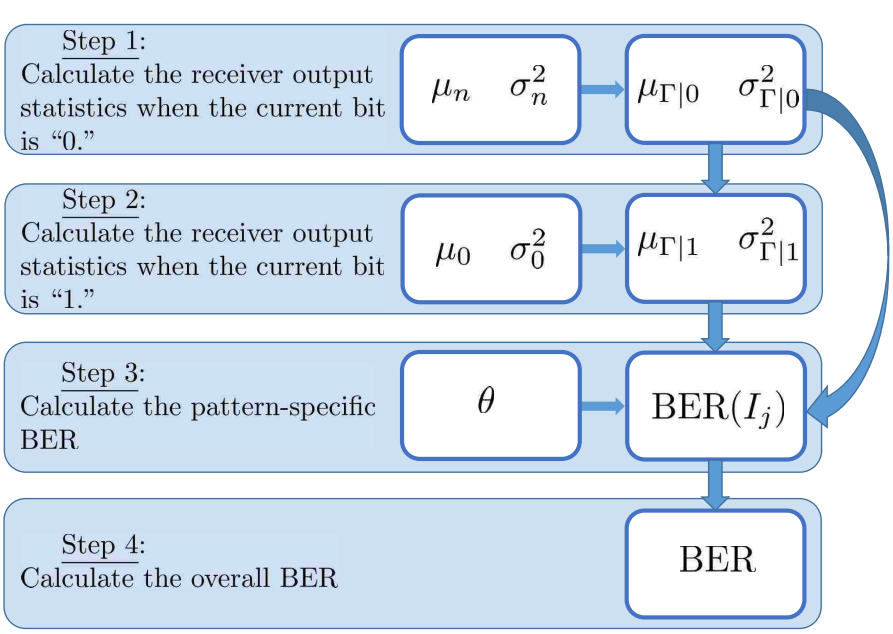

Figure 6.1: A flowchart describing the steps to calculate the BER of a dynamically biased APD using the PD method.

6.4 BER and receiver-sensitivity results under dynamic biasing

We will use the algorithm described above to derive the sinusoidal dynamic-biasing parameters comprising the peak-to-peak voltage, time-delay offset and DC value for optimal BER and receiver sensitivity. Of particular interest is for us to understand the behavior of the receiver sensitivity when the peak-to-peak voltage and DC value (assuming that the frequency is set at the bit-stream frequency) of the dynamic bias are near the boundary of the breakdown condition. Recall that the essence of dynamic biasing is to promote very strong impact ionization in the early phase of an optical information bit while suppressing the ionizations near the end of the bit. We hypothesize that this can be best achieved by setting the DC level of the

dynamic bias just below breakdown, so that the high cycle of a suitably leveled AC component results in very strong ionization for a limited time, followed by a low field cycle during which the ionization is very weak.

As before, we consider an InP-based APD with 200 nm multiplication layer. The transmission rate is 60 Gb/s. From the statistical analysis of the gain and buildup time derived in Chapter 3, we calculate all the parameters of the model, which are summarized in Table 6.1. Note that the statistics of the stochastic gain, G_s, and buildup time, T_s, are averaged over all possible arrival ages of the incident photon, s. The field-dependent nonlocalized ionization coefficients and the ionization threshold energies for InP are obtained from Table 2.1 and 2.2, respectively. As holes impact ionize more readily than electrons in InP, the calculations used avalanche statistics due to pure hole injection into the InP avalanche region, as realized in practice by separate absorption multiplication InGaAs/InP APDs.

Table 6.1: Avalanche Process Statistics of an InP APD

$\mathsf{E}[G_s]$	27.46	$\mathsf{E}[G_s^2]$	3.689×10^3
$\mathsf{E}\left[\frac{G_s^2}{T_s}\right]$	2.915×10^{14}	b	1.580×10^{11}
A_0	4.402×10^{-18}	C_0	7.482×10^{-24}

As for the benefits of dynamic biasing on the BER, our numerical calculation predicts an improvement by a factor of 10^6. For example, as shown in Fig. 6.2, assuming an average of 600 photons per pulse, our calculations show that the BER is 0.2 when using the traditional static biasing scheme at a transmission speed 60 Gb/s, which is way beyond the speed of this APD. On the other hand, if we use a dynamic biasing (DC level=13V, 12V peak-to-peak AC component with the sinusoids lagging the bit by 0.73 bit period), then the BER associated with the same APD operated at 60 Gb/s can be reduced astonishingly to 10^{-6}. These parameters were chosen, in part, so that the static and dynamic biasing schemes are equivalent from the average

multiplication gain perspective. The average gain in our example is approximately 26 for all the peak-to-peak reverse bias voltages in Fig. 6.2. With that said, it is important to note that the benefit of sinusoidal basing is dependent upon the time offset between the optical pulse and the dynamic bias, as Fig. 6.2 shows. On the other hand, note that the optimal performance is robust with respect to errors in the offset if such errors occur in the implementation stage of the dynamic biasing. For example, an error of ±13% from the optimal phase lagging (between 0.6 and 0.86 bit period) guarantees a BER less than 10^{-5} for InP-based receiver operating under dynamic bias with 12V peak-to-peak at 60 Gb/s. With that said, it is important to note that the benefit of sinusoidal basing is dependent upon the time offset between the optical pulse and the dynamic bias, as Fig. 6.2 shows. Fortunately, the optimal performance appears to be robust with respect to errors in the offset if such errors occur in the implementation stage of the dynamic biasing. For example, an error of ±13% from the optimal phase lagging (between 0.6 and 0.86 bit period) guarantees a BER less than 10^{-5} for the receiver operating under dynamic bias with a 12V peak-to-peak bias swing.

The BER calculated in Fig. 6.2 uses the approximated threshold $\hat{\theta}$ described earlier. However, the optimal BER can be found numerically using the conditional PDFs of the receiver output. Figure 6.3 compares the approximated decision threshold $\hat{\theta}$ with the numerical optimized BER. The results show that the BER found using the approximated decision threshold, $\hat{\theta}$, has almost the same performance as the optimized BER in the region of interest (when the phase is optimized). The bottom plot of Fig. 6.3 shows the percentage error between the BER found using the approximated threshold $\hat{\theta}$ with the optimal BER found numerically. It turns out that the approximated threshold, $\hat{\theta}$, overestimates the BER by an error less than 1% when operating within ±13% from the optimal phase lagging as compared to the numerical threshold, θ.

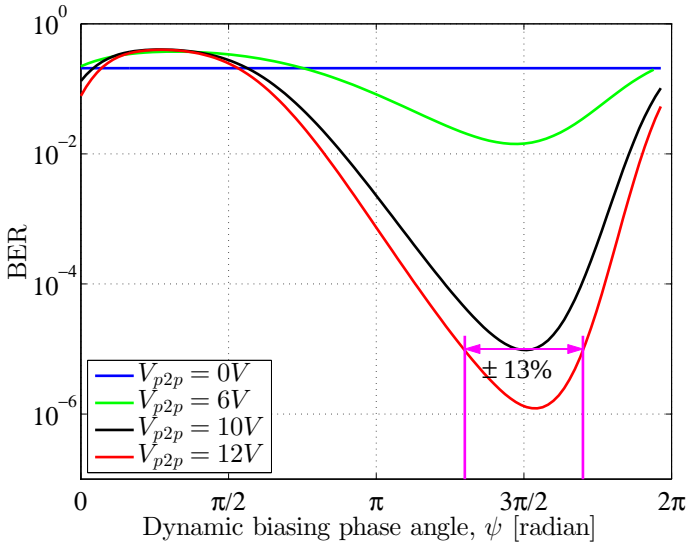

Figure 6.2: The error probability of an InP-based APD with 200nm multiplication width investigated for different reverse bias peak-to-peak. The average gain in all cases is around 26.

We also examined the receiver sensitivity, defined as the minimum optical power (or average number of photons per bit) needed to achieve a BER of 10^{-12}. Sensitivity-versus-gain curves were calculated for different peak-to-peak bias swings. The results are shown in Fig. 6.4 for a transmission speed of 60 Gb/s. The key observation is that by increasing the peak-to-peak voltage, the optimum sensitivity is reduced dramatically. Indeed, our calculations predict a reverse dynamic biasing can improve the receiver sensitivity -20 dBm at an optimal gain of approximately 47 for a 60 Gb/s system when the peak-to-peak voltage is 12V.

Note that, as the peak-to-peak voltage increases, the optimal gain increases while providing a lower sensitivity due to the reduced avalanched buildup time caused by the dynamic nature of the reverse bias. In addition, we observe that by increasing the peak-to-peak voltage, the sensitivity to the optimal-gain values decreases. For instance, at 6 V peak-to-peak, the optimal gain region is around 12. However, as we increase the peak-to-peak voltage to 12, the receiver sensitivity becomes resilient to

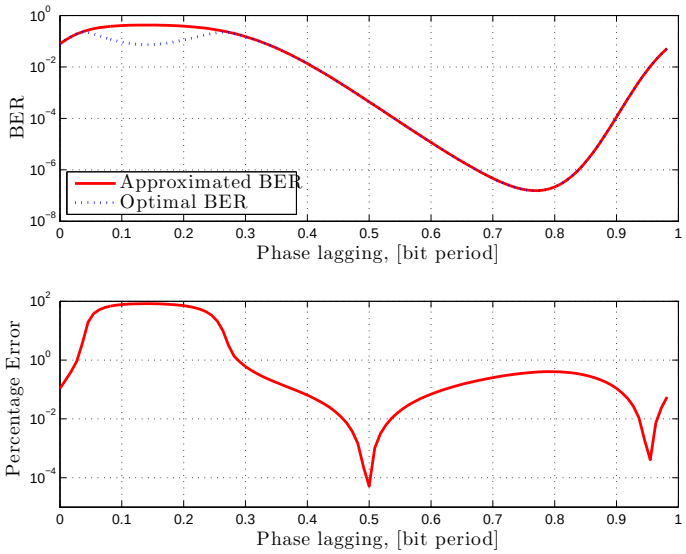

Figure 6.3: The BER for an InP-InGaAs APD with a 200-nm multiplication region and assuming an average of 500 photons per pulse. The reverse bias is set to be $V = 13 + 6\sin(2\pi f_b t)V$. The average gain is 26. The top plot compares the approximated BER found using the approximated decision threshold $\hat{\theta}$ with the optimal BER that uses the optimal detection rule that maximize the likelihood ratio. The bottom plot illustrates the percentage error between the two BERs.

the optimal gain. For example, the receiver sensitivity is less than -20 dBm when the average gain is between 30 and 70. This too is a benefit of the dynamic-biasing scheme, which offers substantial increase in the avalanche gain while maintaining a short avalanche buildup time. It is worth to mention that this device cannot operate with the conventional (static) reverse bias with such transmission speeds. The calculated BER for the static reverse bias at 60 Gb/s was in the range of 10^{-1} even for large input power (sensitivity > 0 dBm).

The analysis in this chapter ignores the tunneling current caused by the high electric field in the multiplication region. However, generalizing the receiver output statistics to include the tunneling effects can be carried out in a straightforward fashion. Of course, in practice, the benefits of the dynamic biased will be reduced when

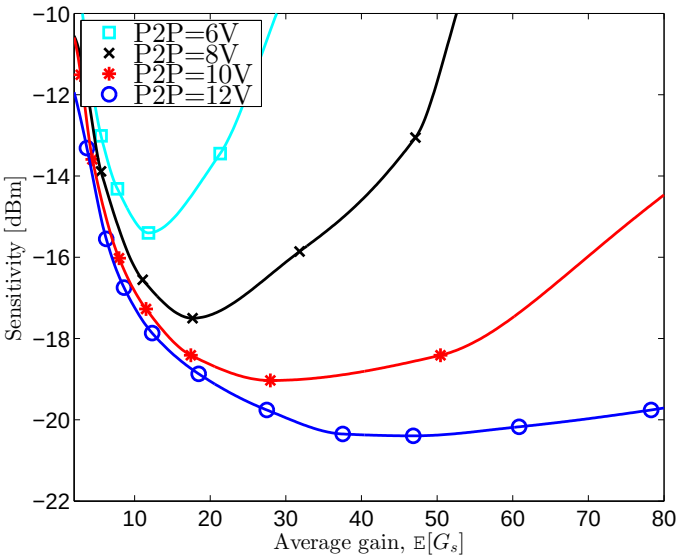

Figure 6.4: Receiver sensitivity versus gain for the dynamically biased InP APDs investigated for a 60 Gb/s transmission system and for different peak-to-peak reverse bias voltage.

the tunneling current becomes dominant. In the following chapter, we generalize the model to include the tunneling effect and realistic values of Johnson noise

6.5 Summary and conclusions

In this chapter, we have developed a method to predict the performance of APD-based receivers operating under dynamic biasing that is synchronized with the incoming bit stream. To do this, we used the statistical correlation between the stochastic gain the stochastic avalanche buildup time in dynamically biased APDs derived in Chapter 3. We incorporated these results with modified point-process analysis that accommodate the dynamic nature of the APD's bias to derive compact expressions for the output of an integrate-and-dump receiver in an OOK direct-detection system. The results drawn here are based on the PD method described in Chapter 5 and in-

clude the effects of ISI, dead-space, Johnson noise, receiver speed and transmission data rate. The closed-form expressions for APD receiver output operating under dynamic reverse biased can be used to properly select the DC level, peak-to-peak value and phase of a dynamic reverse bias to yield the optimal receiver sensitivity. We also proposed an efficient method to approximate a closed form expression for decision threshold of OOK direct detection system. The approximated threshold was in a perfect agreement with the exact decision threshold found numerically.

The calculations have shown that dynamic biasing operating at the optimal settings improves the receiver performance beyond its traditional limits inherited from the notoriously long buildup times of InP APD under conventional static biasing. Indeed, our calculations predicted a reverse dynamic biasing can improve the receiver sensitivity for InP APDs with 200 nm multiplication region from 0 dBm to -20 dBm at an optimal gain of approximately 47 for a 60 Gb/s system when the peak-to-peak voltage is set to 12V compared to the conventional static reverse bias.

Chapter 7

Optimization of InP APDs Operating Under Dynamic Reverse Bias

In this Chapter, we use the results presented in Chapter 6 to rigorously solve the optimization problem over the sinusoidal dynamic-biasing parameters (peak-to-peak voltage, time-delay offset and DC value) for an InP-based APD. The model uses the compact expressions for the mean and variance of the receiver's output that include the effect of ISI, detector speed relative to the transmission speed, and the complex correlation between the APD's gain and buildup time and generalize it to capture the effect of the dark current and realistic Johnson noise. The results conducted here enable us to identify the optimal dynamic reverse bias voltage for InP-based APD for use at a prescribed digital transmission speed. Our generalized model, consider the three factors that govern the sensitivity of APD optical receivers: Avalanche noise, stochastic avalanche buildup time and dark current.

The sensitivity formulation developed here can be used as a guide in designing dy-

namically biased APD-based receivers for specific system performance requirements well beyond the limits previously known under the traditional constant-bias setting.

7.1 Generalization of the model to include multiplied tunneling current

The tunneling dominates the dark current at high voltages. The un-multiplied band-to-band tunneling current, I_{tun}, is given for direct gap semiconductors by [58, 84–86]

$$I_{\text{tun}} = \gamma A \exp\left(-\frac{2\pi\Theta\sqrt{m_0\epsilon_g^3}}{q\hbar E(t)}\right), \tag{7.1}$$

where m_0 is the free electron mass, q is the electron charge, $E(t)$ is the dynamic electric field, A is the device area, ϵ_g is the direct energy band gap, and $\hbar$ is Planck's constant. The parameter Θ is dimensionless quantity given by $\Theta = \sigma_T\sqrt{m^*/m_0}$ where m^* is the effective mass of the electron and σ_T is the tunneling fitting parameter that depends on the detailed shape of the tunneling barrier. For an InP APD, a good fits to the tunneling current densities were obtained with values of σ_T between 1.16 and 1.20 [8]. The prefactor γ depends on the initial and final states of the tunneling carrier, and for band-to-band tunneling $\gamma = (2m^*)^0.5q^3E(t)V/\hbar\epsilon_g^0.5$ where V is the applied reverse voltage. The parameters used to find the InP-APD dark current, I_{tun}, are extracted from [7] and they are listed for convenience in Table 7.1.

m_0	9.109×10^{-31} Kg	$\hbar$	6.626×10^{-34} J.s
m^*	$0.08m_0$ Kg	ϵ_g	1.35 eV
q	1.602×10^{-19} C	σ_T	1.16

Table 7.1: Parameters used to find the InP-APD dark current, I_{tun} [7].

The dark carriers generation rate is given by $\phi_{\text{tun}} = I_{\text{tun}}/q$ and has Poisson statistics. Therefore, the effect of dark carriers on the integrate-and-dump receiver

output can be treated as photo-generated carriers. However, the dark carriers exist independently of the status of the optical signal, whereas the photocarrier generation is modulated by a random stream of binary random variables. Therefore, we model the dark current as a constant photon stream incident on the APD with a photon flux ϕ_{tun} photons per second.

We begin by deriving the effect of the dark carrier on the mean of the integrate-and-dump receiver output. The mean of the integrated dark current output can be calculated by

$$\mu_{\text{tunn}} = \phi \int_0^{T_b} \int_{-\infty}^{t} i_p(t,s)\,\mathrm{d}s\,\mathrm{d}t. \tag{7.2}$$

By substituting the mean impulse response, $i_p(t,s)$, by its decaying exponential approximation, we can obtain the effect of the dark-current on the mean of the receiver output as follows:

$$\mu_{\text{tunn}} = \phi A_0 T_b / b. \tag{7.3}$$

Adding the effect of the dark-current on the mean receiver output, we obtain the new expression for $\mu_{\Gamma|0}(I_j)$

$$\mu_{\Gamma|0}(I_j) = \sum_{n=1}^{2^L} u_n(I_j)\mu_n + \mu_{\text{tunn}}. \tag{7.4}$$

The expression for $\mu_{\Gamma|1}(I_j)$ is identical in form to that shown in (6.16) with the proviso that $\mu_{\Gamma|0}(I_j)$ is now represented by (7.4) and not by (6.12).

The derivation of a new expression for $\sigma^2_{\Gamma|0}(I_j)$ requires to obtain the variance of the receiver output assuming a constant optical power that extends from the infinitive past to the end of the present bit

$$\sigma^2_{\text{tunn}} = \int_0^{T_b} \int_0^{T_b} \int_{-\infty}^{t_1 \wedge t_2} R_{I_p}(t_1, t_2, s)\phi(s)\,\mathrm{d}s\,\mathrm{d}t_1\,\mathrm{d}t_2. \tag{7.5}$$

As before, by approximating the autocorrelation function using the second moment of the impulse response function, we calculate the variance of the photocurrent as

follows:

$$\sigma_{\text{tunn}}^2 = \phi\frac{2C_0}{b^2}\left(T_b - \frac{1}{b}(1-e^{-\gamma T_b})\right) - \phi\sum_{\substack{k=-\infty \\ k\neq 0}}^{\infty}\frac{2C_k}{b(b+j2\pi k f_0)^2}\left(1-e^{-bT_b}\right). \quad (7.6)$$

After adding the effect of the dark current, we obtain the new expression for $\sigma_{\Gamma|0}^2(I_j)$

$$\sigma_{\Gamma|0}^2(I_j) = \sum_{n=1}^{2^L} u_n(I_j)\sigma_n^2 + \sigma_{\text{tunn}}^2 + \sigma_J^2. \quad (7.7)$$

The expression for $\sigma_{\Gamma|1}(I_j)$ is identical in form to that shown in (6.17) with the proviso that $\sigma_{\Gamma|0}(I_j)$ is now represented by (7.7) and not by (6.13).

7.2 Estimating the Johnson noise in InP APD

In order to obtain the Johnson noise level, we investigated TIAs for 2.5-100 Gb/s operation. The input noise current density, i_n, and 3-dB bandwidth, B_{TIA}, of TIAs as a function of transmission speed was roughly approximated by Ong and *et al.* in [58]. The average functions of i_n and B_{TIA} were found by fitting linearly several TIAs modules fabricated and published for different transmission speed. The fit yielded the equation

$$i_n = 4.81\times 10^{-10}R_b + 5.87 \quad \text{pA}/\sqrt{\text{Hz}}. \quad (7.8)$$

The average B_{TIA} against transmission speed is given by

$$B_{\text{TIA}} = 0.91R_b. \quad (7.9)$$

To verify these results, we compared the averaged i_n and B_{TIA} functions with prior published TIA [87–91]. These parameters were also compared to commercial TIA modules manufactured by Applied Micro Circuit, Maxim Integrated Products, Sumitomo Electric, Analog Devices, TriQuint Semiconductor and Texas Instruments.

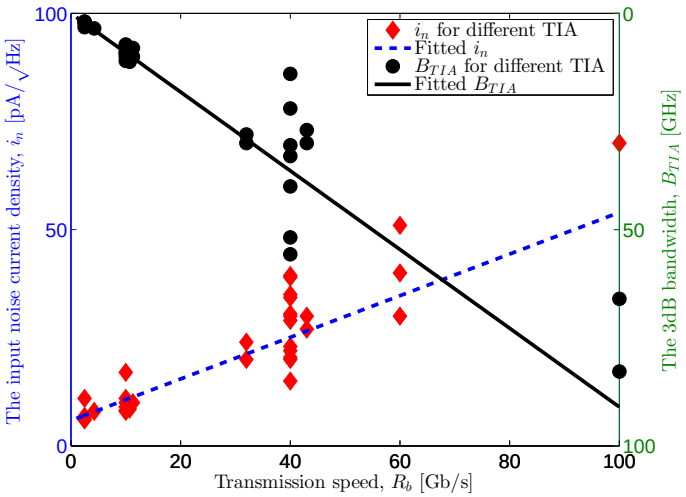

Figure 7.1: A survey on prior TIA modules input current noise, i_n, (diamonds) and 3-dB bandwidth high cut-off frequency, B_{TIA}, (circles) compared with the averaged fitted lines as a function of the transmission speed R_b. it is clear that the linearly fitted functions described in (7.8) and (7.9) match closely all the prior TIA modules.

The input noise current density, i_n, and 3-dB bandwidth, B_{TIA}, of each TIA obtained is depicted in Fig. 7.1. As the result shows, the linearly fitted functions of i_n and B_{TIA} roughly approximate all the prior TIA modules. Using these fitted i_n and B_{TIA} values, we can obtain the average Johnson noise levels, σ_J , as a function of transmission speed using the formula

$$\sigma_J = i_n \sqrt{B_{\text{TIA}} T_b}. \tag{7.10}$$

All the results to follow are generated using the generalized model that includes both dark current and realistic Johnson noise for InP-based APD receivers. For convenience, the procedure to calculate the overall BER is summarized in Algorithm 1.

Algorithm 1 Procedure to calculate the generalized BER

$\sigma_J = i_n\sqrt{B_{\text{TIA}}}T_b$

$\mu_{\text{tunn}} = \phi A_0 T_b/b$

$\sigma^2_{\text{tunn}} = \phi\frac{2C_0}{b^2}\left(T_b - \frac{1}{b}(1-e^{-\gamma T_b})\right) - \phi\sum_{\substack{k=-\infty\\k\neq 0}}^{\infty}\frac{2C_k}{b(b+j2\pi k f_0)^2}\left(1-e^{-bT_b}\right)$

for $n = 1$ to L **do**

$\mu_n = \frac{\phi e^{-nbT_b}}{b}\left(e^{bT_b}+e^{-bT_b}-2\right)\sum_{k=-\infty}^{\infty}\frac{A_k}{j2\pi k f_b+b}$

$\sigma^2_n = \frac{2\phi}{b^2}e^{-nbT_b}\left(e^{bT_b}-1\right)\left(1-e^{-bT_b}-bT_b e^{-bT_b}\right)\sum_{k=-\infty}^{\infty}\frac{C_k}{b+j2\pi k f_b}$

end for

for $j = 1$ to 2^L **do**

$\mu_{\Gamma|0}(I_j) = \sum_{n=1}^{2^L} u_n(I_j)\mu_n + \mu_{\text{tunn}}$

$\sigma^2_{\Gamma|0}(I_j) = \sum_{n=1}^{2^L} u_n(I_j)\sigma^2_n + \sigma^2_{\text{tunn}} + \sigma^2_J$

$\mu_{\Gamma|1}(I_j) = \mu_{\Gamma|0}(I_j) + \mu_0$

$\sigma^2_{\Gamma|1}(I_j) = \sigma^2_{\Gamma|0}(I_j) + \sigma^2_0$

$\text{BER}(I_j) = \frac{1}{4}\left[\text{erfc}\left(\frac{\theta-\mu_{\Gamma|0}(I_j)}{\sigma_{\Gamma|0}\sqrt{2}}\right) + \text{erfc}\left(\frac{\mu_{\Gamma|1}(I_j)-\theta}{\sigma_{\Gamma|1}\sqrt{2}}\right)\right]$

end for$\text{BER} = \frac{1}{2^L}\sum_{j=1}^{2^L}\text{BER}(I_j)$

7.3 Numerical calculations

To optimize the dynamic biasing of an InP APD, the joint PDF of the gain and avalanche duration is obtained from the model described in 3. The field-dependent nonlocalized ionization coefficients and the ionization threshold energies for InP are obtained from [8] and they are reiterated for convenience Table 7.2. The electron and hole saturation velocities are assumed as 6.7×10^6 cm/s. With the joint PDF at hand, we calculate all the parameters of the model, which are $a(s)$, $c(s)$ and b and the Fourier series coefficients A_k and C_k.

	A [cm^{-1}]	B [V/cm]	m	E_{th} [eV]
Electron	1.41×10^6	1.69×10^6	1.23	2.80
Hole	2.11×10^6	1.77×10^6	1.15	3.00

Table 7.2: Ionization parameters for InP [8]

7.3.1 Optimum dynamic reverse bias for a given transmission speed

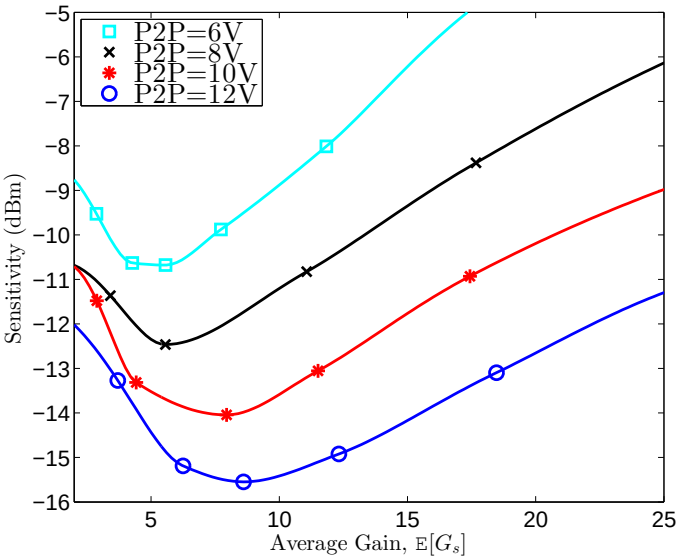

Figure 7.2: Receiver sensitivity versus gain for the dynamically biased InP APDs investigated for a 60 Gb/s transmission system and for different peak-to-peak reverse bias voltage with the inclusion of dark currents and a realistic Johnson noise.

The theoretical investigation was conducted on a 25μm-radius InP p-i-n diodes, with avalanche-region widths, $w = 200$ nm and a quantum efficiency $\eta = 0.85$ [92]. Dynamic reverse bias voltage was applied with different peak-to-peak voltages and different DC voltages.

We examine the receiver sensitivity versus gain curves for the InP APD with the inclusion of dark currents and realistic Johnson noise. The results are compared in

Fig. 7.2 at a transmission speed of 60 Gb/s. The results in Fig. 7.2 are optimized over the delay, ψ, between the dynamic reverse voltage and bit stream. For each peak-to-peak voltage, there is an optimal average gain that offers minimum receiver sensitivity. The key observation is with the inclusion of the dark current, the calculations predict higher sensitivity values with lower average gain than those calculated in Chapter 6 when the dark current was excluded. This result is expected since the dark current exponentially increases with the reverse bias voltage. Therefore, by increasing the peak-to-peak voltage, the average dark current increases exponentially and dominates the enhancement caused by the dynamic reverse bias on ISI, or more precisely on the buildup time. Indeed, our calculations show that the receiver sensitivity for InP APDs increases from -20 dBm at an optimal gain of approximately 47 to a sensitivity of -15 dBm at an optimal gain of 8 when the peak-to-peak voltage is set to 12V.

We can also realize that the optimum receiver sensitivity decreases while increasing peak-to-peak voltage. With this expected result, we are able to predict the optimal operation gain for a specific peak-to-peak voltage. This plot allows us to realistically identify an InP-APD optimum dynamic reverse bias for a given transmission speed, thereby yielding the optimized sensitivity for a given transmission speed.

7.3.2 Optimum avalanche width for a given dynamic reverse bias

To optimize over the avalanche width, we investigate a series of 25 μm-radius InP APD operating under reverse dynamic bias with avalanche-region widths, w, ranging from 0.16 to 0.5 μm. Sensitivity versus gain curves were calculated for the diodes and the results are compared in Fig. 7.4 at a transmission speed of 60 Gb/s. For

each diode, there exists an optimum mean gain that achieves the lowest sensitivity. With the inclusion of both ISI and dark current, this result enables us to make a correct prediction of the optimal operation gain for each multiplication width. As the device width decreases, the electric field increases, resulting in increased dark current, as shown in Fig. 7.4 for $w = 160$ for instance. On the other hand, for a thick multiplication region with the conventional static reverse bias, the APD's bandwidth decreases, which causes an increase in the ISI. Thereby causing an elevation in the sensitivity. However, due to the dynamic reverse bias, the ISI is reduced which enable us to increase the avalanche width to avoid dark current without affecting the device speed.

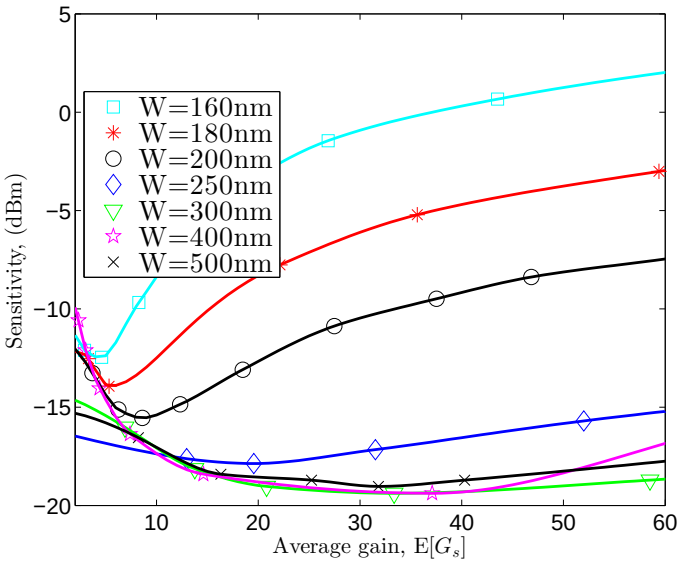

Figure 7.3: Receiver sensitivity versus gain for the dynamically biased InP APDs investigated for a 60 Gb/s transmission system and a peak-to-peak reverse voltage of 12 V. The calculations conducted here include the dark currents and Johnson noise

For clarity, in Fig. 7.3 we plot the lowest sensitivity for each device and corresponding optimal mean gain both as functions of the avalanche-region width; this plot allows us to identify the optimum avalanche width for a given transmission speed operating under dynamic reverse bias. Our calculations predict an optimum

avalanche width of 400 nm for InP APDs, yielding a lowest sensitivity of -19 dBm at an optimal gain of approximately 36 for a 60 Gb/s system operating with a dynamic reverse bias with peak-to-peak voltage of 12 V. It is clear for this result that the dynamic reverse voltage reduce the effect of ISI in slow APDs (thick multiplication region) making the difference between the optimal diode ($w = 400$ nm) and the "slow" diodes ($w = 500$ nm, for instance) negligible. We end this section by making important observations when tunneling current is included in the analysis. We point out that in the presence of the dynamic reverse voltage the restriction on the multiplication layer width is relaxed, as normally done to increase the APD speed, which causes a substantial reduction in the tunneling current.

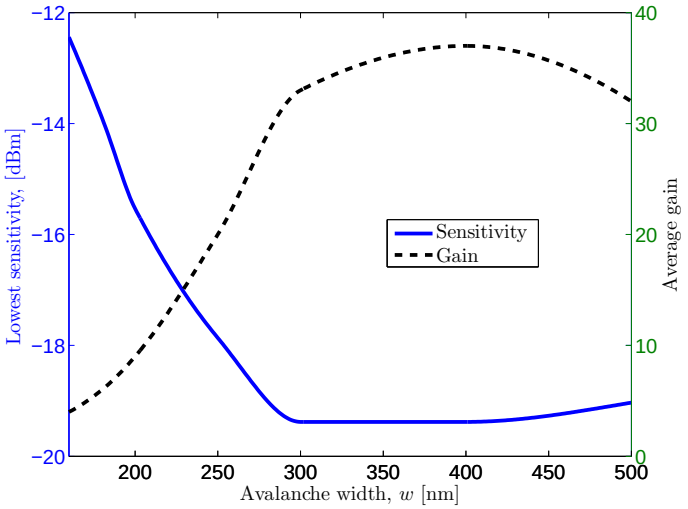

Figure 7.4: Lowest sensitivity (solid line, left axis) and its corresponding optimal mean gain (dashed line, right axis) versus InP APD avalanche width for a 60 Gb/s transmission system operating under dynamic reverse bias with a peak-to-peak voltage fo 12V.

7.4 Summary and conclusions

We have generalized the APD-based receiver model to include tunneling current and used it for the purpose of optimization of the dynamic reverse voltage for best receiver sensitivity for an arbitrarily prescribed transmission speed. The model offers compact analytical expressions for the mean and the variance of the output of the integrate-and-dump APD-based receiver that capture dark current and Johnson noise. It turns out that with the dynamic biasing scheme we can relax the stringent requirements of the width of the multiplication region, as normally done to enhance the APD speed. This, in turn, reduces the electric field in the multiplication region, which reduces tunneling current.

Optimizing the dynamic reverse bias of InP receivers showed that for a 60 Gb/s system, an optimal width of 400 nm is predicted, yielding a minimum sensitivity of -19 dBm at an optimal gain of approximately 35. As device width decreases below its optimum value, increased tunneling current results in increasing receiver sensitivity. On the other hand, as device width increases above its optimum, the device bandwidth slightly decreases due to the dynamic reverse bias nature that aims to suppress the buildup time.

Chapter 8

Future Work

In this dissertation, we tackled multiple challenging problems regarding modeling and analyzing a dynamically biased APD and the rigorous predicting the sensitivity including tunneling current and realistic Johnson noise of an InP-based APD receiver. We developed the first theory for the joint buildup-time and gain statistics for avalanche multiplication under dynamic reverse bias. We also developed a theory for filtered shot noise under dynamic biasing, which addresses rigorously the statistics of the APD photocurrent (mean, variance, autocorrelation function, etc.). This is used in turn to derive analytical expressions for the statistics of the photocurrent of dynamically based APDs. Moreover, we extract exact expressions for the receiver bit-error rate and receiver sensitivity in an OOK setting. The sensitivity analysis of the dynamically biased APD-based receiver include the effect of ISI and dark current, receiver speed relative to the transmission rate as well as trans-impedance amplifier noise used in the pre-amplification stage of receivers. In addition to the multiple problems addressed in this dissertation, a number of interesting problems remain for future work. In this chapter, we present an overview of future research problem in this area.

Demonstration of the dynamically biased APD technology

One of the key feature of dynamically biased APD technology is that it is essentially APD-agnostic; that is, it can be used to improve the GBP of any APD that has a poor buildup-time performance. Hence, the performance of any APD system can be remarkably improved with modest cost. The next step is to implement a complete dynamically APD optical transceiver (transmitter and receiver) system including high-speed measurement equipment, a high-speed dynamic bias generator, feedback clock/data recovery, transmitter, and receiver circuitry. A proof of concept of the dynamically biased APD technology using an off-the-shelf APD can be demonstrated. One of the challenges in implementing dynamically biased APD is that the applied dynamic bias signal may contaminate the photocurrent resulting from the incoming optical pulse because of the APD's parasitic capacitance. The harmonics frequency of the dynamic bias can be eliminated using a bandpass filters. Hence further work should be done to implement the dynamic biasing APD. Dynamic Photonics Inc. is currently pursuing the demonstration and commercialization of the dynamic biased APD technology [93].

Spatial and temporal coupling of impact ionization

The coupling between spatial (via spatial doping and material engineering) and temporal modulation of impact ionization may open the door to a totally new research area where impact ionization can be tuned to (or away from) certain optical signals. In other words, the spatial and temporal coupling of impact ionization could results in optical (bandpass or notch) filters just as photonic bandgaps and filtering by means of photonic crystals are the result of the coupling between periodic structures (a spatial property) and waves.

The reverse bias waveform shape

The theory developed in this dissertation can be applied to any dynamically biased reverse voltage. In the numerical analysis, we considered the sinusoidal dynamic reverse voltage as a proof the concept. Further analysis on different waveform shape are interesting problems to be investigates. Several waveform can be considered such as rectangular waveform, sawtooth, or trapezoid. In addition to the previous optimization parameters, the receiver performance can be optimized further by adjusting the duty cycle, for instance.

Characterization of breakdown conditions under dynamic fields

The dynamic bias scheme radically changes the way we characterize breakdown condition in devices. Traditionally, breakdown in APDs is characterized by a single quantity, namely the reverse bias for which the avalanche pulse (resulting from a parent carrier triggering the avalanche process) is self-sustained. This simplistic characterization is not adequate when the electric field is allowed to be dynamic. For dynamic biasing, breakdown condition amounts to regions in the three dimensional parameter space comprising the DC level, AC level, and frequency of the sinusoid. The joint PDF of the stochastic gain and buildup time, $f_{G_s,T_s}(m,t;s)$, developed in Chapter 3, can be utilized to identify regions of the three-dimensional space comprising the three biasing parameters (the DC level, the peak-to-peak value, and the frequency of the dynamic bias), for which breakdown occurs.

References

[1] C. H. Tan, J. S. Ng, S. Xie, and J. P. R. David, "Potential materials for avalanche photodiodes operating above 10 Gb/s," in *4th International Conference on Computers and Devices for Communication (CODEC2009)*, 2009, pp. 1–6.

[2] B. L. Kasper and J. C. Campbell, "Multigigabit-per-second avalanche photodiode lightwave receivers," *Journal of Lightwave Technology*, vol. 5, no. 10, pp. 1351–1364, 1987.

[3] M. M. Hayat, J. P. David, S. Krishna, L. F. Lester, D. A. Ramirez, and P. Zarkesh-Ha, "Impact ionization devices under dynamic electric fields," U.S. Patent Provisional Application 61/456,455, November 04, 2011, attorney docket No. 1863.098US1.

[4] X. Li, X. Zheng, S. Wang, F. Ma, and J. C. Campbell, "Calculation of gain and noise with dead space for gaas and $Al_xGa_{1-x}As$ avalanche photodiode," *IEEE Transactions on Electron Devices*, vol. 49, no. 7, pp. 1112–1117, 2002.

[5] J. P. R. David and C. H. Tan, "Material considerations for avalanche photodiodes," *IEEE Journal of Selected Topics in Quantum Electronics*, vol. 14, no. 4, pp. 998–1009, 2008.

[6] M. A. Saleh, M. M. Hayat, B. E. A. Saleh, and M. C. Teich, "Dead-space-based theory correctly predicts excess noise factor for thin GaAs and AlGaAs avalanche photodiodes," *IEEE Transactions on Electron Devices*, vol. 47, no. 3, pp. 625–633, 2000.

[7] S. M. Sze and K. K. Ng, *Physics of Semiconductor Devices*, 3rd ed. Hoboken, NJ: Wiley-Interscience, 2006.

[8] L. J. J. Tan, J. S. Ng, C. H. Tan, and J. P. R. David, "Avalanche noise characteristics in submicron InP diodes," *IEEE Journal of Quantum Electronics*, vol. 44, no. 4, pp. 378–382, 2008.

[9] A. Momtaz, J. Cao, M. Caresosa, A. Hairapetian, D. Chung, K. Vakilian, M. Green, W.-G. Tan, K.-C. Jen, I. Fujimori, and Y. Cai, "A fully integrated SONET OC-48 transceiver in standard CMOS," *IEEE Journal of Solid-State Circuits*, vol. 36, no. 12, pp. 1964–1973, 2001.

[10] J. Cao, M. Green, A. Momtaz, K. Vakilian, D. Chung, K.-C. Jen, M. Caresosa, X. Wang, W.-G. Tan, Y. Cai, I. Fujimori, and A. Hairapetian, "OC-192 transmitter and receiver in standard 0.18-μm CMOS," *IEEE Journal of Solid-State Circuits*, vol. 37, no. 12, pp. 1768–1780, 2002.

[11] B. E. A. Saleh and M. C. Teich, "Semiconductor photon detectors," in *Fundamentals of Photonics*. New York: John Wiley & Sons, Inc., 1991, ch. 17, pp. 644–695.

[12] Y. S. Wang, S.-J. Chang, C. L. Tsai, M.-C. Wu, Y. Chiou, S. P. Chang, and W. Lin, "10-Gb/s planar InGaAs P-I-N photodetectors," *IEEE Sensors Journal*, vol. 10, no. 10, pp. 1559–1563, 2010.

[13] S. H. Hsu, Y. J. Chen, and H. Z. You, "10 GHz high-speed optical interconnection," *Electronics Letters*, vol. 46, no. 2, pp. 149–150, 2010.

[14] M. Bitter, R. Bauknecht, W. Hunziker, and H. Melchior, "Monolithic InGaAs-InP p-i-n/HBT 40-Gb/s optical receiver module," *IEEE Photonics Technology Letters*, vol. 12, no. 1, pp. 74–76, Jan. 2000.

[15] D. Huber, R. Bauknecht, C. Bergamaschi, M. Bitter, A. Huber, T. Morf, A. Neiger, M. Rohner, I. Schnyder, V. Schwarz, and A. Jackel, "InP-InGaAs single HBT technology for photoreceiver OEIC's at 40 Gb/s and beyond," *Journal of Lightwave Technology*, vol. 18, no. 7, pp. 992–1000, July 2000.

[16] G. P. Agrawal, *Fiber-Optic Communication Systems*, 3rd ed. New York: Wiley-Interscience, 2002.

[17] J. C. Livas, E. A. Swanson, S. R. Chinn, E. S. Kintzer, R. S. Bondurant, and D. J. DiGiovanni, "A one-watt, 10-Gb/s high-sensitivity optical communication system," *IEEE Photonics Technology Letters*, vol. 7, no. 5, pp. 579–581, 1995.

[18] Y. B. Lu, P. L. Chu, A. Alphones, and P. Shum, "A 105-nm ultrawide-band gain-flattened amplifier combining C- and L-band dual-core EDFAs in a parallel configuration," *IEEE Photonics Technology Letters*, vol. 16, no. 7, pp. 1640–1642, July 2004.

[19] C. Bornholdt, J. Slovak, and B. Sartorius, "Semiconductor-based all-optical 3r regenerator demonstrated at 40 Gbit/s," *Electronics Letters*, vol. 40, no. 3, pp. 192–194, Feb. 2004.

[20] S. D. Personick, "Receiver design for digital fiber-optic communication systems, parts I and II," *The Bell System Technical Journal*, vol. 52, no. 6, pp. 843–886, Jul./Aug. 1973.

[21] R. G. Smith and S. D. Personick, "Receiver design for optical fiber communications systems," in *Semiconductor Devices for Optical Communication.* New York: Springer-Verlag, 1980, ch. 4.

[22] S. R. Forrest, "Sensitivity of avalanche photodector receivers for high-bit-rate long-wavelength optical communication systems," in *Semiconductor and Semimetals.* Orlando, FL: Academic, 1985, vol. 22, ch. 4.

[23] P. Sun, M. M. Hayat, B. E. A. Saleh, and M. C. Teich, "Statistical correlation of gain and buildup time in APDs and its effects on receiver performance," *Journal of Lightwave Technology*, vol. 24, no. 2, pp. 755–768, Feb. 2006.

[24] D. S. G. Ong, J. S. Ng, J. P. R. David, M. M. Hayat, and P. Sun, "Optimization of InP APDs for high-speed lightwave systems," in *20th International Conference on Indium Phosphide and Related Materials, (IPRM 2008)*, Versailles, France, May 2008.

[25] M. M. Hayat and D. A. Ramirez, "Multiplication theory for dynamically biased avalanche photodiodes: new limits for gain bandwidth product," *Opt. Express*, vol. 20, no. 7, pp. 8024–8040, Mar 2012. [Online]. Available: http://www.opticsexpress.org/abstract.cfm?URI=oe-20-7-8024

[26] H. Melchior, A. R. Hartman, D. P. Schinke, and T. E. Seidel, "Atlanta fiber system experiment: Planar epitaxial silicon avalanche photodiode," *Bell System Technical Journal*, vol. 57, no. 6, pp. 1791–1807, 1978. [Online]. Available: http://dx.doi.org/10.1002/j.1538-7305.1978.tb02127.x

[27] J. C. Campbell, "Recent advances in telecommunications avalanche photodiodes," *Journal of Lightwave Technology*, vol. 25, no. 1, pp. 109–121, 2007.

[28] K. Taguchi, T. Torikai, Y. Sugimoto, K. Makita, and H. Ishihara, "Planar-structure InP," *Journal of Lightwave Technology.*

[29] G. Hasnain, W. Bi, S. Song, J. Anderson, N. Moll, C.-Y. Su, J. N. Hollenhorst, N. Baynes, I. Athroll, S. Amos, and R. Ash, "Buried-mesa avalanche photodiodes," *IEEE Journal of Quantum Electronics*, vol. 34, no. 12, pp. 2321–2326, Dec. 1998.

[30] J. C. Campbell, A. G. Dentai, W. S. Holden, and B. L. Kasper, "High-speed InP/InGaAsP/InGaAs avalanche photodiodes," in *International Electron Devices Meeting*, vol. 29, 1983, pp. 464–467.

[31] E. Ishimura, S. Funaba, Y. Tanaka, T. Aoyagi, T. Nishimura, and E. Omura, "High efficiency 10 Gb/s InP/InGaAs avalanche photodiodes with distributed bragg reflector," in *27th European Conference on Optical Communication (ECOC2001).*, vol. 4, Amsterdam, Netherlands, Oct. 2001, pp. 554–555 vol.4.

[32] B. F. Levine, R. N. Sacks, J. Ko, M. Jazwiecki, J. A. Valdmanis, D. Gunther, and J. H. Meier, "A new planar InGaAs-InAlAs avalanche photodiode," *IEEE Photonics Technology Letters*, vol. 18, no. 18, pp. 1898–1900, Sep. 2006.

[33] N. Yasuoka, H. Kuwatsuka, M. Makiuchi, T. Uchida, and A. Yasaki, "Large multiplication-bandwidth products in APDs with a thin inp multiplication layer," in *The 16th Annual Meeting of the IEEE Lasers and Electro-Optics Society. (LEOS 2003)*, vol. 2, 2003, pp. 999–1000.

[34] G. S. Kinsey, J. C. Campbell, and A. G. Dentai, "Waveguide avalanche photodiode operating at 1.55 μm with a gain-bandwidth product of 320 GHz," *IEEE Photonics Technology Letters*, vol. 13, no. 8, pp. 842–844, 2001.

[35] H. Nie, K. A. Anselm, C. Hu, S. S. Murtaza, B. G. Streetman, and J. C. Campbell, "High-speed resonant-cavity separate absorption and multiplication avalanche photodiodes with 130 GHz gain-bandwidth product," *Applied Physics Letters*, vol. 70, no. 2, pp. 161–163, 1997.

[36] Y. L. Goh, D. J. Massey, A. R. J. Marshall, J. S. Ng, C. H. Tan, M. Hopkinson, and J. P. R. David, "Excess noise and avalanche multiplication in InAlAs," in *19th Annual Meeting of the IEEE Lasers and Electro-Optics Society, (LEOS 2006)*, 2006, pp. 787–788.

[37] J. C. Campbell, H. Nie, C. Lenox, G. Kinsey, P. Yuan, J. Holmes, A. L., and B. G. Streetman, "High-speed, low-noise avalanche photodiodes," in *Optical Fiber Communication Conference*, vol. 4, 2000, pp. 114–116 vol.4.

[38] Y. L. Goh, A. R. J. Marshall, D. J. Massey, J. S. Ng, C. H. Tan, M. Hopkinson, J. P. R. David, S. K. Jones, C. C. Button, and S. M. Pinches, "Excess avalanche noise in $In_{0.52}Al_{0.48}As$," *IEEE Journal of Quantum Electronics*, vol. 43, no. 6, pp. 503–507, 2007.

[39] G. S. Kinsey, R. Sidhu, J. Holmes, A. L., J. C. Campbell, and A. G. Dentai, "High-speed waveguide avalanche photodetectors," in *Device Research Conference*, 2001, pp. 149–150.

[40] C. Y. Park, K. S. Hyun, S. K. Kang, M. K. Song, T. Y. Yoon, H. M. Kim, H. M. Park, S.-C. Park, Y. H. Lee, C. Lee, and J. B. Yoo, "High-performance InGaAs/Inp avalanche photodiode for a 2.5 gb/s optical receiver," *Optical and*

Quantum Electronics, vol. 27, no. 5, pp. 553–559, 1995. [Online]. Available: http://dx.doi.org/10.1007/BF00563597

[41] M. A. Itzler, C. S. Wang, S. McCoy, N. Codd, and N. Komaba, "Planar bulk InP avalanche photodiode design for 2.5 and 10 Gb/s applications," in *24th European Conference on Optical Communication*, vol. 1, 1998, pp. 59–60 vol.1.

[42] T. Torikai and K. Makita, "40-Gbps high-sensitive waveguide photodetectors," *Proc. SPIE*, vol. 6020, pp. 602 024–1–602 024–8, 2005.

[43] Y. Kang, H.-D. Liu, M. Morse, M. J. Paniccia, M. Zadka, S. Litski, G. Sarid, A. Pauchard, Y.-H. Kuo, H.-W. Chen, W. S. Zaoui, J. E. Bowers, A. Beling, D. C. McIntosh, X. Zheng, and J. C. Campbell, "Monolithic germanium/silicon avalanche photodiodes with 340 GHz gain-bandwidth product," *Nature Photonics*, vol. 3, pp. 59–63, Jan. 2009.

[44] W. S. Zaoui, H.-W. Chen, J. E. Bowers, Y. Kang, M. Morse, M. J. Paniccia, A. Pauchard, and J. C. Campbell, "Frequency response and bandwidth enhancement in Ge/Si avalanche photodiodes with over 840 GHz gain-bandwidth-product," *Opt. Express*, vol. 17, no. 15, pp. 12 641–12 649, Jul 2009. [Online]. Available: http://www.opticsexpress.org/abstract.cfm?URI=oe-17-15-12641

[45] P. Sun, M. M. Hayat, J. C. Campbell, B. E. A. Saleh, and M. C. Teich, "Correlation between gain and buildup-time fluctuations in ultrafast avalanche photodiodes and its effect on receiver sensitivity," in *Optical Fiber Communication Conference. Technical Digest. OFC/NFOEC*, vol. 1, Mar. 2005.

[46] N. Namekata, S. Adachi, and S. Inoue, "1.5 GHz single-photon detection at telecommunication wavelengths using sinusoidally gated ingaas/inp avalanche photodiode," *Opt. Express*, vol. 17, no. 8, pp. 6275–6282, Apr 2009.

[47] J. Zhang, P. Eraerds, N. Walenta, C. Barreiro, R. Thew, and H. Zbinden, "2.23 GHz gating InGaAs/InP single-photon avalanche diode for quantum key distribution," *Proc. SPIE*, vol. 7681, pp. 76 810Z1–76 810Z8, Feb. 2010.

[48] Z. Lu, W. Sun, J. Campbell, X. Jiang, and M. A. Itzler, "Single photon detection with sine gated dual InGaAs/InP avalanche diodes," in *IEEE Photonics Conference (IPC2012)*, Burlingame, CA, Sep. 2012, pp. 98–99.

[49] D. C. Herbert and E. T. R. Chidley, "Very low noise avalanche detection," *IEEE Transactions on Electron Devices*, vol. 48, no. 7, pp. 1475–1477, Jul 2001.

[50] M. M. Hayat, B. E. A. Saleh, and M. C. Teich, "Effect of dead space on gain and noise of double-carrier-multiplication avalanche photodiodes," *IEEE Transactions on Electron Devices*, vol. 39, no. 3, pp. 546–552, 1992.

[51] M. M. Hayat, O.-H. Kwon, Y. Pan, P. Sotirelis, J. C. Campbell, B. E. A. Saleh, and M. C. Teich, "Gain-bandwidth characteristics of thin avalanche photodiodes," *IEEE Transactions on Electron Devices*, vol. 49, no. 5, pp. 770–781, 2002.

[52] M. M. Hayat, W. L. Sargeant, and B. E. A. Saleh, "Effect of dead space on gain and noise in Si and GaAs avalanche photodiodes," *IEEE Journal of Quantum Electronics*, vol. 28, no. 5, pp. 1360–1365, 1992.

[53] M. A. Saleh, M. M. Hayat, P. P. Sotirelis, A. L. Holmes, J. C. Campbell, B. E. A. Saleh, and M. C. Teich, "Impact-ionization and noise characteristics of thin III-V avalanche photodiodes," *IEEE Transactions on Electron Devices*, vol. 48, no. 12, pp. 2722–2731, 2001.

[54] M. M. Hayat and B. E. A. Saleh, "Statistical properties of the impulse response function of double-carrier multiplication avalanche photodiodes including the effect of dead space," *Journal of Lightwave Technology*, vol. 10, no. 10, pp. 1415–1425, 1992.

[55] M. M. Hayat and G. Dong, "A new approach for computing the bandwidth statistics of avalanche photodiodes," *IEEE Transactions on Electron Devices*, vol. 47, no. 6, pp. 1273–1279, 2000.

[56] M. M. Hayat, O.-H. Kwon, S. Wang, J. C. Campbell, B. E. A. Saleh, and M. C. Teich, "Boundary effects on multiplication noise in thin heterostructure avalanche photodiodes: theory and experiment [$Al_{0.6}Ga_{0.4}As$/GaAs]," *IEEE Transactions on Electron Devices*, vol. 49, no. 12, pp. 2114–2123, Dec. 2002.

[57] R. J. Mcintyre, "Multiplication noise in uniform avalanche diodes," *IEEE Transactions on Electron Devices*, vol. 13, no. 1, pp. 164–168, 1966.

[58] D. S. G. Ong, J. S. Ng, M. M. Hayat, P. Sun, and J. P. R. David, "Optimization of InP APDs for high-speed lightwave systems," *Journal of Lightwave Technology*, vol. 27, no. 15, pp. 3294–3302, Aug. 2009.

[59] G. El-Howayek and M. M. Hayat, "Error probabilities for optical receivers that employ dynamically biased avalanche photodiodes," *IEEE Transactions on Commmunications*, Dec. 2014, [In review].

[60] D. Snyder and M. Miller, *Random Point Processes in Time and Space*. New York, NY: Springer-Verlag, 1991.

[61] N. Sorensen and R. M. Gagliardi, "Performance of optical receivers with avalanche photodetection," *IEEE Transactions on Communications,*, vol. 27, no. 9, pp. 1315–1321, 1979.

[62] E. Gramsch, "Noise characteristics of avalanche photodiode arrays of the bevel-edge type," *IEEE Transactions on Electron Devices*, vol. 45, no. 7, pp. 1587–1594, 1998.

[63] D. J. Daley and D. Vere-Jones, *An introduction to the theory of point processes*, 2nd ed., J. Gani, C. C. Heyde, and T. G. Kurtz, Eds. New York, NY: Springer, 2003.

[64] C. H. Tan, P. J. Hambleton, J. P. R. David, R. C. Tozer, and G. J. Rees, "Calculation of APD impulse response using a space- and time-dependent ionization probability distribution function," *Journal of Lightwave Technology*, vol. 21, no. 1, pp. 155–159, 2003.

[65] D. S. G. Ong, M. M. Hayat, J. P. R. David, and J. S. Ng, "Sensitivity of high-speed lightwave system receivers using InAlAs avalanche photodiodes," *IEEE Photonics Technology Letters*, vol. 23, no. 4, pp. 233–235, 2011.

[66] S. D. Personick, P. Balaban, J. Bobsin, and P. Kumar, "A detailed comparison of four approaches to the calculation of the sensitivity of optical fiber system receivers," *IEEE Transactions on Communications*, vol. 25, no. 5, pp. 541–548, May 1977.

[67] J. B. Abshire, "Performance of OOK and low-order PPM modulations in optical communications when using APD-based receivers," *IEEE Transactions on Communications*, vol. 32, no. 10, pp. 1140–1143, Oct. 1984.

[68] H. M. H. Shalaby, "Effect of thermal noise and APD noise on the performance of OPPM-CDMA receivers," *Journal of Lightwave Technology*, vol. 18, no. 7, pp. 905–914, July 2000.

[69] G. El-Howayek, C. Zhang, Y. Li, J. S. Ng, J. P. R. David, and M. M. Hayat, "On the use of gaussian approximation in analyzing the performance of optical receivers," *IEEE Photonics Journal*, vol. 6, no. 1, pp. 1–8, 2014.

[70] R. Van Overstraeten and H. De Man, "Measurement of the ionization rates in diffused silicon p-n junctions," *Solid-State Electronics*, vol. 13, no. 5, pp. 583 – 608, 1970.

[71] J. C. Campbell, W. S. Holden, G. J. Qua, and A. G. Dentai, "Frequency response of InP/InGaAsP/InGaAs avalanche photodiodes with separate absorption "grading" and multiplication regions," *IEEE Journal of Quantum Electronics*, vol. 21, no. 11, pp. 1743–1746, Nov. 1985.

[72] B. E. A. Saleh, M. M. Hayat, and M. C. Teich, "Effect of dead space on the excess noise factor and time response of avalanche photodiodes," *IEEE Transactions on Electron Devices*, vol. 37, no. 9, pp. 1976–1984, Sep. 1990.

[73] C. Hu, K. A. Anselm, B. G. Streetman, and J. C. Campbell, "Noise characteristics of thin multiplication region GaAs avalanche photodiodes," *Applied Physics Letters*, vol. 69, no. 24, pp. 3734–3736, Dec. 1996.

[74] K. A. Anselm, P. Yuan, C. Hu, C. Lenox, H. Nie, G. Kinsey, J. C. Campbell, and B. G. Streetman, "Characteristics of GaAs and AlGaAs homojunction avalanche photodiodes with thin multiplication regions," *Applied Physics Letters*, vol. 71, no. 26, pp. 3883–3885, Dec. 1997.

[75] D. S. Ong, K. F. Li, G. J. Rees, G. M. Dunn, J. P. R. David, and P. N. Robson, "A monte carlo investigation of multiplication noise in thin p+ -i-n+ gaas avalanche photodiodes," *IEEE Transactions on Electron Devices*, vol. 45, no. 8, pp. 1804–1810, Aug. 1998.

[76] K. Li, D. Ong, J. David, G. Rees, R. Tozer, P. Robson, and R. Grey, "Avalanche multiplication noise characteristics in thin GaAs p^+-i-n^+ diodes," *IEEE Transactions on Electron Devices*, vol. 45, no. 10, pp. 2102–2107, Oct. 1998.

[77] P. Yuan, K. A. Anselm, C. Hu, H. Nie, C. Lenox, A. L. Holmes, B. G. Streetman, J. C. Campbell, and R. J. McIntyre, "A new look at impact ionization-part II: Gain and noise in short avalanche photodiodes," *IEEE Transactions on Electron Devices*, vol. 46, no. 8, pp. 1632–1639, Aug. 1999.

[78] P. Yuan, C. C. Hansing, K. A. Anselm, C. V. Lenox, H. Nie, J. Holmes, A. L., B. G. Streetman, and J. C. Campbell, "Impact ionization characteristics of III-V semiconductors for a wide range of multiplication region thicknesses," *IEEE Journal of Quantum Electronics*, vol. 36, no. 2, pp. 198–204, Feb. 2000.

[79] G. El-Howayek and M. M. Hayat, "Method for performance analysis and optimization of APD optical receivers operating under dynamic reverse bias," in *IEEE Photonics Conference*, Bellevue, WA, Sep. 2013.

[80] R. M. Gray and J. W. Goodman, *Fourier Transforms: An Introduction for Engineers*. New York: Kluwer Academic Press, 1995.

[81] F. Davidson and X. Sun, "Gaussian approximation versus nearly exact performance analysis of optical communication systems with PPM signaling and APD receivers," *IEEE Transactions on Communications*, vol. 36, no. 11, pp. 1185–1192, 1988.

[82] P. Sun, M. M. Hayat, and A. K. Das, "Bit error rates for ultrafast APD based optical receivers: exact and large deviation based asymptotic approaches," *IEEE Transactions on Communications*, vol. 57, no. 9, pp. 2763–2770, Sep. 2009.

[83] L. C. Andrews, *Special Functions of Mathematics for Engineers*, 2nd ed., ser. SPIE Press monograph. SPIE Optical Engineerin Press, 1992.

[84] S. R. Forrest, "Performance of $In_xGa_{1-x}As_yP_{1-y}$ photodiodes with dark current limited by diffusion, generation recombination, and tunneling," *IEEE Journal of Quantum Electronics*, vol. 17, no. 2, pp. 217–226, Feb. 1981.

[85] S. R. Forrest, R. F. Leheny, R. E. Nahory, and M. A. Pollack, "$In_{0.53}Ga_{0.47}As$ photodiodes with dark current limited by generation-recombination and tunneling," *Applied Physics Letters*, vol. 37, no. 3, pp. 322–325, Aug. 1980.

[86] J. L. Moll, *Physics of semiconductors*. New York: McGraw-Hill, 1964.

[87] J. Kim and J. F. Buckwalter, "Bandwidth enhancement with low group-delay variation for a 40-Gb/s transimpedance amplifier," *IEEE Transactions on Circuits and Systems I: Regular Papers*, vol. 57, no. 8, pp. 1964–1972, Aug. 2010.

[88] C.-F. Liao and S.-I. Liu, "40 Gb/s transimpedance-AGC amplifier and CDR circuit for broadband data receivers in 90 nm CMOS," *IEEE Journal of Solid-State Circuits*, vol. 43, no. 3, pp. 642–655, Mar. 2008.

[89] J.-D. Jin and S. Hsu, "A 40-Gb/s transimpedance amplifier in 0.18-μm CMOS technology," *IEEE Journal of Solid-State Circuits*, vol. 43, no. 6, pp. 1449–1457, June 2008.

[90] M. N. Ahmed, J. Chong, and D. S. Ha, "A 100 Gb/s transimpedance amplifier in 65 nm CMOS technology for optical communications," in *IEEE International Symposium on Circuits and Systems (ISCAS)*, June 2014, pp. 1885–1888.

[91] T. Takemoto, F. Yuki, H. Yamashita, S. Tsuji, T. Saito, and S. Nishimura, "A 25 Gb/s $\times$ 4-channel 74 mW/ch transimpedance amplifier in 65 nm CMOS," in *IEEE Custom Integrated Circuits Conference (CICC 2010)*, Sep. 2010, pp. 1–4.

[92] W. R. Clark, K. Vaccaro, W. D. Waters, C. L. Gribbon, and B. D. Krejca, "Determination of quantum efficiency in $In_{0.53}$ $Ga_{0.47}As$-InP-based APDs," *Journal of Lightwave Technology*, vol. 32, no. 24, pp. 4178–4182, Dec. 2014.

[93] M. M. Hayat, P. Zarkesh-Ha, X. Zheng, G. El-Howayek, and R. Efroymson, "First demonstration of dynamically biased APDs for improved high-speed direct-detection communication," in *Optical Fiber Communication Conference and Exhibit*, Los Angeles, CA, March 2015.